1-1-2006

Particle image velocimetry study of an axial cooling fan and the interaction of downstream obstructions

Paul J. Melzer
Iowa State University

Particle image velocimetry study of an axial cooling fan and the interaction of downstream obstructions

by

Paul J. Melzer

A thesis submitted to the graduate faculty

in partial fulfillment of the requirements for the degree of

MASTER OF SCIENCE

Major: Mechanical Engineering

Program of Study Committee:
Michael G. Olsen, Major Professor
J. Adin Mann III
Frederick L. Haan

Iowa State University

Ames, Iowa

2006

Graduate College
Iowa State University

This is to certify that the master's thesis of

Paul J. Melzer

has met the thesis requirements of Iowa State University

Signatures have been redacted for privacy

TABLE OF CONTENTS

LIST OF FIGURES

LIST OF TABLES

ABSTRACT

The issue of noise generation in tractors is a problem of great interest to the farm equipment industry, both in the United States and in Europe. Legislation regulating noise generation is becoming increasingly restrictive and necessitates that companies continuously work to improve the noise performance of their products if they are to remain competitive. One of the main sources for sound generation in an engine is the cooling unit. The cooling unit consists of both the radiator and cooling fan.

To gain insight into strategies for noise reduction, particle image velocimetery (PIV) was used to study the airflow in an engine cooling package with an axial cooling fan. The flow field was investigated upstream and downstream of the fan. Data was collected at five different fan positions as one blade passed. Two different engine speeds, two different shroud types, and two different engine block spacings were examined to find their impact on the flow field.

Velocity (m/s) was collected using PIV. Momentum (N-s) and turbulent kinetic energy (TKE) (1/s) data was calculated using the velocity data. This data was used to identify what impact each parameter had on the flow field. It was found that the engine block spacing had the biggest impact on both the upstream and downstream velocity flow fields. In the upstream flow, the vortex increased in size when the engine spacing was decreased. This decrease in engine spacing affected the downstream flow field by increasing the amount of airflow off the fan blade. The shroud type had an affect on the strength of the secondary vortex in the upstream flow field. It was found that the higher the fan speed, the higher the velocity of the flow field and strength of the vortices was.

CHAPTER 1. INTRODUCTION

The issue of noise generation in tractors is a problem of great interest to the farm equipment industry, both in the United States and in Europe. As cities grow larger and expand into the surrounding countryside, the distances between residential homes, commercial sites, and farms is becoming smaller. To prevent complaints from citizens and businesses situated near farms, many governments have begun to place severe restrictions on the amount of noise tractors can generate. Legislation regulating noise generation is becoming increasingly restrictive and necessitates that companies continuously work to improve the noise performance of their products if they are to remain competitive.

One of the main sources for sound generation in an engine is the cooling unit. In a previous experiment, the noise levels were studied with regard to changes made in the fan power and air flow [15]. The cooling unit consists of both the radiator and cooling fan. One design requirement for the fan is that it must pull enough air through the radiator to keep the engine from overheating. As tractors get more powerful and more luxuries are added (air conditioning in the cab for example) the cooling load increases and a larger capacity radiator must be used. As the radiator increases in cooling capacity, the fan must in turn pull more air through the radiator. Perhaps the simplest way to increase air flow through the radiator is to increase the fan speed. However, doing this can greatly increase the noise level generated by the fan.

Despite the increasing importance of noise generation as a design consideration, designers of engine cooling packages have until recently taken a rather cavalier approach to noise generation. For example, when designing a new tractor, a company will typically just

use the noise data from the previous tractor model as a guide to how noisy the new tractor will be. This is often inaccurate because small changes in the location of the engine/fan geometry can make big differences in the noise level without the designer realizing it until the unit is being tested. This can make designing quiet engine/fan geometries a costly trial and error exercise. Part of this difficulty arises from the lack of accurate, easy to use noise prediction models in the software marketplace. Some noise prediction software has come onto the market in recent years, but this software can be highly unreliable in complex flows such as flow in a cooling compartment. Computational fluid dynamic (CFD) programs have been able to model these flows with some accuracy, but incorporating the CFD results into noise generation models has proven extremely difficult.

As mentioned earlier, previous experiments were conducted to determine the main sources of the noise generation with the same setup used in the present study [15]. In these experiments, a major component of the overall noise generation was found to be tone noise. Because tone noise is periodic in nature and often closely coupled to the underlying fluid mechanics, it was decided that looking at the airflow around the fan could be beneficial to generating more accurate prediction models. Accordingly, particle image velocity (PIV), a whole-field velocity measurement technique, was chosen as the method to gather the velocity field data. For each particular flow field investigated with PIV, the amount of noise generated was also measured. Such a coupled technique is helpful because if a known flow field pattern is predicted either in a CFD model or experimentally measured velocity fields of a new engine setup, the noise that would be generated by it would also then be known.

To obtain high-resolution velocity field data, experiments were conducted in a test section previously constructed for use in collecting the sound data [15]. In doing this, the

sound data could easily be correlated to the velocity data because the same test parameters would be used. Then, the presence of large structures in the flow field could be identified and used to validate new noise prediction models.

The following thesis is organized as follows. In Chapter Two a literature review is presented to examine previous experiments on this subject. Chapter Three discusses how the experiment is set up and conducted. Chapter Four contains the results gathered from the experiment and analysis of the results. Chapter Five presents the conclusions and recommendations for future work.

CHAPTER 2. LITERATURE REVIEW

This chapter contains a review of literature on noise measurements and velocity measurements near a fan. Literature about noise measurements will be briefly discussed first, followed by the velocity measurements.

2.1 Noise Measurement Literature

In previous experimental and theoretical studies of fan noise generation, it was found that developing noise prediction models for fans is feasible; however, these models rely on many simplifying assumptions, and thus most are only accurate when used with very basic fan geometries and no secondary noise sources [1]. Even these rather simple models can be useful in system design. For example, Roth et al. [1] used their model to conclude that to make the fan operation quieter, the most important parameters to adjust are the fan radius, the chord width, and the rotational speed.

With the addition of an object (such as the engine block) near the fan, the flow becomes much more complex, thus making noise prediction even more difficult. Perhaps the easiest way to predict the noise in this type of circumstance is to understand which characteristics of the flow are affected by interaction with the object and thus affect the noise level [2]. In these instances, one of the biggest contributors is momentum fluctuation due to fluid-structure interaction. Noise is generated due to the density differences in the air caused by these fluctuations. These density differences are so small that from a fluid dynamic standpoint, the flow is still incompressible. Another component of noise is the interaction of

the vortices created by the fan with solid surfaces (or the fan itself). In modeling fan flows near objects, the size, strength, and location of these vortices are keys to predicting noise.

It is not only obstructions downstream of the fan that can effect noise generation. Maaloum et al. [3] found that the upstream environment of the flow field also was important to the noise level generated by the fan. Small disturbances in the upstream flow increased the broadband noise while larger eddies affected the tonal noise. It was also shown that a contoured duct had a big impact on the upstream flow field.

In 2004, Maaloum et al. [4] presented a methodology for estimating noise based on the unsteady pressure field on the fan blade surface. The potential flow near the fan blade was calculated using an unsteady inlet velocity field. This was used to predict tonal noise away from the fan using the Ffowcs Williams and Hawkings (FW-H) equation [4]. It was found that the potential calculation did not give good noise prediction in a quantitative way, but it could be used to find trends in noise generation based on changes to the fan geometry. Also, they suggested that the potential flow calculation should only be used where the fan is not greatly influenced by the surrounding geometry.

2.2 Velocity Measurement Review

There are many different methodologies for measuring velocity, and each of these has at one time or another been used to study the flowfield generated by axial fans. These methodologies include pitot tubes, hot film anemometry, laser Doppler velocimetry (LDV) , and particle image velocimetry (PIV) to name a few. Each of these methodologies has inherent advantages and disadvantages. Pitot tubes are inexpensive and very easy to use, but they only yield pointwise mean velocity data, and thus provide no information about the

turbulent nature of the flow. Moreover, Pitot tubes can also be intrusive, as they require placing a physical probe into the flowfield. Both hot film anemometry and LDV are pointwise measuring methods that are improvements to the use of pitot tubes in that they provide instantaneous velocity data, and thus can be used to quantify the turbulence in the flowfield. However, being pointwise techniques, neither is particularly useful for investigating large scale vortices. Also, a hot-film probe must be physically placed in the flowfield, and thus can be intrusive.

PIV, on the other hand, can be used to investigate the instantaneous turbulent structure over the entire flow field. Because of this capability, PIV was chosen as the technique to measure the velocity fields in the experiments presented in this thesis. PIV is a non-intrusive, whole field velocity measurement technique that was developed in the late 1980s and early 1990s [5]. Although initially a very difficult and time consuming technique to implement, its usage has become more widespread as digital cameras have become less expensive and computing power has increased. Lawson discusses advantages and disadvantages to PIV and many other laser techniques used to visualize aerospace flows [6]. Even from its earliest days, PIV has proven to be a useful tool in investigating axial fan flows. A brief summary of some experimental measurements of the velocity fields around axial fans is presented below.

In 1986, Kawaguchi analyzed velocity distributions around an axial flow fan using spark trace and smoke wire methods [7]. A drum camera was used to obtain the images for this experiment. The chamber downstream of the fan was a cube with sides of 1 meter. An axial cross section of the fan was examined. Two fan types were examined to correlate the flow around the wing with the fan efficiency. Also the tip vortex was examined using a Pitot

tube. The result of this experiment was the quantification of the effect of the tip vortex on the total fan noise.

Morris et al. obtained axial, radial and tangential components of velocity of an automotive cooling fan using hot wire anemometry [8]. This experiment was performed with boundaries similar to an automotive engine compartment, instead of a circular duct. No obstructions simulating an engine block were placed in front of the fan however. The purpose of this experiment was to show this unique set up could be used to photograph tuft visualizations.

An experiment on an automotive cooling fan was preformed using PIV in 1999 by Zahn et al. [9]. However, this experiment focused on the flow between the radiator and the fan. As the air left the radiator, a von Karman vortex street was observed due to vortex shedding around the tubes in the radiator. An axial view of the fan blade was examined to find the nature of the flow near the fan blades. It was found that as the air approached the fan, its velocity increased. The velocity vectors also pointed to the gaps between blades. Four different blade positions were examined and it was found to be a pulsating flow. The flow between blades was found to be twisted much like laminar flow around airfoils.

Estevadeordal et al. used PIV to examine the flow field near the blade of an axial flow fan in 2000 [10]. These experiments were performed in a circular duct, and velocity fields were measured in an axial cross section of the fan blade. Experimental data were compared with computational fluid dynamics (CFD) results. There was found to be general agreement between the PIV and CFD results for the large flow structures. However, it was found that blade passage velocity magnitudes were under predicted by the CFD code due to its inability to resolve viscous effects.

A Particle Dynamic Analyzer was used in an experiment preformed by Du et al. in 2002 [11] (PDA is a measurement technique related to LDV that can provide particle size information in addition to velocity data). This apparatus was used to measure the three dimensional velocity of an axial flow fan. This experiment also looked at the tip clearance and axial cross section of the fan blade. A strong counterclockwise separation vortex was observed on the suction side of the fan blade. The purpose of this experiment was to show that the flow field could be measured using PDA.

An experiment using three dimensional LDV was preformed by Lee et al. in 2003, but this was done on a forward swept fan [12]. The measurements were taken in a circular duct. This experiment focused mainly on tip leakage and determining how close the CFD codes were to modeling this area. It was found that in comparison to the LDV measurements, the computed results predicted the tip region at a reliable level

Yoon and Lee examined the flow field behind a forward swept axial fan using a stereoscopic PIV system [13]. However, the fluid in this experiment was water, not air. Water was used because the perspective error is less with water then it is with air. The region examined was in front of the fan, and data were obtained at four phases in the fan rotation. It was found that the out of plane component was closely related to the vortices shed from the blade tip. The phase averaged images also showed the periodic nature of the flow field.

Lee et al. used particle tracking velocimetry (PTV) to examine the flow field of a forward swept axial fan in 2003 [14]. These results were phase averaged and showed the periodic nature of the flow. Two fields of view were examined, which were the axial and

radial planes of view. It was observed that strong counterclockwise vortices were shed from the trailing edge of the fan.

Previous experiments have generally only been conducted with an axial fan with nothing impeding the flow. In this experiment, a mock engine block was placed in downstream of the fan. This was done to study how a downstream obstruction would affect the flow near the fan. This is critical to understand because downstream obstructions occur in almost every real life cooling fan flows.

CHAPTER 3. EXPERIMENTAL SETUP

To study the flow in an engine compartment in a John Deere tractor, an experimental system capable of simulating the air flow in the compartment and measuring the velocity fields within the compartment was needed. The experimental technique chosen for this study was particle image velocimetry (PIV), a whole-field, optically based velocity measurement technique. As previously stated, PIV has the advantage over pointwise velocity measurement techniques in that using PIV it is possible to measure an entire plane of instantaneous velocity vectors, and thus large scale turbulent structures can be identified and studied. This experimental capability is especially important in the study of flow and noise generation in the engine compartment of the John Deere tractor, since it is believed that the periodic behavior of large scale turbulent structures is responsible for much of the tone noise observed during operation of the engine.

Because PIV is an optically based technique, the mock engine compartment had to be carefully constructed with these types of measurements in mind. Moreover, the PIV experimental system had to be designed to meet the technical challenges presented by this particular problem, such as the seeding of a highly three-dimensional air flow, and the triggering of the system to a particular fan position. With these challenges in mind, the following sections describe the mock engine compartment constructed for the research and the PIV system used to collect the velocity field data.

3.1 Equipment

The experiment was performed in the anechoic chamber located in the Acoustics Laboratory of Iowa State University, Room 0316 of Howe Hall. The experiment was preformed in the anechoic chamber for two reasons. First, sound measurements were previously taken of the same setup for a previous experiment [15], thus detailed sound power measurements already exist for a number of geometries and run conditions for the mock engine.

Another advantage of using the anechoic chamber is that it made it easy to control the seeding for the PIV measurements. In PIV, the flow is seeded with small tracer particles that must be small enough to accurately follow any velocity gradients, but large enough that they scatter sufficient laser light to be visible in the flow images captured by the CCD camera. For this particular experiment, 1 μm olive oil droplets were chosen as the seed particles. Previous experiments have shown olive oil droplets to be an excellent choice for seeding air flows [5]. The particles were generated using a LaVision VZ seeder atomizer whose baffle insured a constant particle size of less than 1 micrometer.

The anechoic chamber was not initially designed with PIV experiments in mind, and thus some modifications had to be made to the chamber to make the PIV measurements possible. The anechoic chamber measured 4.2 m x 4.2 m but the sound absorbing insulation stuck out 45.7 cm, making the working space in the room of 3.76 m x 3.76 m. A metal grid made up the floor of the chamber above the sound absorbing insulation. This grid was 55.2 cm above the floor of the chamber. Some of the sound absorbing insulation on the floor of the chamber and part of the metal grid had to be removed to make space for the PIV

equipment. However, the relatively small amount of insulation removed did not significantly affect the anechoic properties of the chamber.

A fan and a radiator unit provided by John Deere were enclosed along with a mock engine block inside a Plexiglas box. Plexiglas was chosen as the box material, because it was essential for the PIV experiments that optical access be available to the inside of the mock engine chamber. The box was roughly the same size as an engine compartment on a John Deere tractor. Figure 3.1 shows the front view of this compartment. The frame of the box was constructed out of Unistrut. The Unistrut both gave the box structural support to withstand any vibrations due to the fan operation, and also allowed the box to be firmly anchored to the anechoic chamber floor. Wood was then attached to the Unistrut and provided the attachment surface for the radiator and Plexiglas. Foam strips were glued to the wood to provide a seal between the wood and Plexiglas. This seal prevented air leaks and ensured the pressure in the box was the same as it would be inside an actual engine compartment. The front of the box consisted of triple stacked radiator which also represented the air intake point. The back of the box was made of wood while Plexiglas was used for the top and sides of the box. The bottom of the box was left open and thus used as the air removal point. This compartment measured 76.2 cm deep, 80 cm wide and 105.4 cm tall and rested 73.6 cm above the floor (Fig. 1). An electric motor behind the box supplied the power to the fan through a shaft. This motor was enclosed in a wooden box lined with sound absorbing material. The shaft ran out of the motor box and into the back of the test section box. The engine was capable of running at speeds up to 1200 rpm, and the speed was regulated by a Baldor adjustable speed drive controller located near the computer. A pulley system doubled the rpm output of the engine to the fan axle. The mock engine block was

built so the shaft could run through it also. The fan used had 7 blades. The fan was enclosed by a Plexiglas shroud that was attached to the radiator. Two different kind of shrouds were examined, 50% and 100% immersion. The Plexiglas allowed the optical access to the area between the radiator and the engine. The shrouds were a box type, meaning that the shroud extended from the radiator straight out toward the fan with only a hole cut in the front face for the fan to enter the shroud. This is shown in Fig. 3.2. The mock engine block was constructed of wood. Attached to the back of it was Unistrut that ran out the back of the box. This Unistrut had several holes in it that corresponded to different distances between the front face of the engine block and the fan blade. Brackets were attached to the back of the box and the Unistrut was then screwed into those brackets once the proper distance was chosen. Pulleys of different diameters could be attached to the front face of the mock engine block in several positions. This provided different geometries to examine other then the flat front face of the mock engine block. The pulleys were also made of wood.

A laser and optics were placed next to the fan/mock engine. These were placed on an optical breadboard from Newport Corp. The optical breadboard was supported by scissor jacks that were placed on another table made of wood. This setup will allow for future experiments to examine different planes in the flow field. The laser used was a Nd:YAG laser from New Wave, model Gemini 15. It has two laser heads that produce a double pulse that can be separated by as small of a time separation as necessary. The maximum operating frequency of the lasers is 15 Hz and the maximum power output is 120 mJ. A fast frame transfer rate CCD camera was used (LaVision Flowmaster 3S) which had a resolution of 1280 x 1024 pixels and pixel size of 6.7 x 6.7 μm. This camera can capture 8 images a second, or up 4 image pairs. A Sigma AF-MF zoom lens was attached to the camera which

could magnify the image up to 5.6 times. The camera was placed 1.34 m above the laser sheet. This was necessary for a couple reasons. First, the camera needed to be far enough away to be able to view the whole flow field and secondly, the rail system needed to be high enough so it wouldn't block the door to the chamber. An overhead rail system was installed to let a camera move to view different positions in the flow field. The rail system was made of Unistrut and was attached to the walls of the anechoic chamber. The rail system had an H frame design. Two rails spanned the room running parallel with each other. Another two beams connected those beams and provided the mount for the rail the camera was mounted to. This system let the camera move in both the x and y directions relative to the flow field. The camera and lasers were triggered by a signal generator on the axle of the fan to make sure the fan was in the same position every time a picture was taken. The shaft encoder was a VTL 13 D7-20 transmissive optoswitch made by Perkin Elmer Optoelectronics. The optical equipment used was from Newport Corp. The mirror was 50.4 mm in diameter and was constructed specifically to reflect the high-energy 532 nm laser light at a 45° angle of incidence. Two cylindrical lenses were used, one for the engine block at a spacing of 2.5" and the other for the engine block at a spacing of 0.5". The two cylindrical lenses were a -12.7 mm focal length for the 0.5" spacing and -25.4 mm focal length for the 2.5" spacing. A 0.5 m focal length converging lens was used to reduce the sheets thickness at the region of interest. These lenses had an antireflective coating called AR.14 in the Newport catalog. This coating was chosen because its reflectance for 532 nm laser beam was the minimal in the available antireflective coating range. These lenses shape the beam into a thin, flat sheet as it enters the test section.

Olive oil seed particles were produced by a LaVision VZ seeder atomizer whose baffle insured a constant particle size of less than 1 micrometer, small enough to follow the flow field and big enough to scatter light to the camera. This seeder was powered by a small air compressor that was also located in the anechoic chamber.

The software package used to gather the PIV data was LaVision's DaVis program. This program also tied the camera, lasers, and trigger together so the timing would be correct. The computer was located outside of the anechoic chamber and the wires connecting it to the camera, lasers, and trigger were run through a small opening in the side of the chamber.

3.2 PIV procedure

A typical PIV setup is shown in Figure 3.3. The laser was placed on the optical breadboard along with the sheet forming lenses as shown in Fig. 3.4. This formed a horizontal laser sheet that entered the flow field just below the fan axle (the laser sheet was not placed in the plane of the fan axle because this caused errors due to light reflections off the axle). The laser sheet must be kept the proper thickness is important to ensure useful images. If the laser sheet is too thin the particles could move out of the plane of the laser, thus making the images useless. However, if the laser sheet is too thick, a seed particle could move a great distance in the out of plane direction and the resulting velocity vectors would be inaccurate. Through trial and error the optimum thickness was found to be 2 mm. The atomizer introduced particles to the flow field on the upstream side of the radiator. The atomizer and air compressor were inside the chamber but were controlled by an outlet outside the chamber. The atomizer was run for 2 minutes before the fan was started and for 30 seconds bursts every 3 minutes after that to maintain proper seeding in the flow field. The

flow advected the particles through the radiator and through the fan. Once near the fan, the camera took two images of the visible particles that formed one image set of the flow field. The camera took the images looking down on the flow field as the fan blade was moving up through the laser sheet. This process was repeated for the area between the fan and mock engine block as well.

PIV was used to analyze the flow through the fan at several different fan/mock engine block configurations which included two different distances between the fan and the engine block, two fan speeds and the shroud types. The configurations used are listed in Table 1. At each of these parameters, data were taken at five different blade positions.

Eliminating reflections off the Plexiglas sides and shroud was necessary to obtain quality PIV images. The easiest way to do this is to paint the surfaces that are reflecting light flat black. This is because black absorbs the most light and flat paint absorbs more light then glossy. Typically the bottom and side surfaces give the most problems, so those were addressed first. The bottom of the shroud was painted to absorb light scattering down and reflecting back to the camera. The Plexiglas wall opposite to where the laser was entering the chamber, a black piece of construction paper was attached to the inside surface. This prevented the laser light from reflecting back and increasing the laser sheet thickness. The mock engine block was also painted for the same reasons. After removing those reflections the PIV images were found to be of a good quality to work with.

The images were then broken into interrogation regions of 32x32 pixels with a 50% overlap of the region so that the final vector spacing was 16x16 pixels. An example of the data is shown in Fig. 3.5. The upstream and downstream data sets are shown in their proper positions relative to each other. The shroud, mock engine block and fan are also shown. The

arrows represent the velocity at that point and the color scale makes it easier to read. The values for the color scale are in meters per second.

In the next chapter, the data for the various configurations and fan speeds will be presented and discussed.

Table 1 Experimental setups

Fan Speed	Shroud Type	Fan distance from engine block
1800 rpm	50% immersed	2.5 inches
2200rpm	100% immersed	0.5 inches

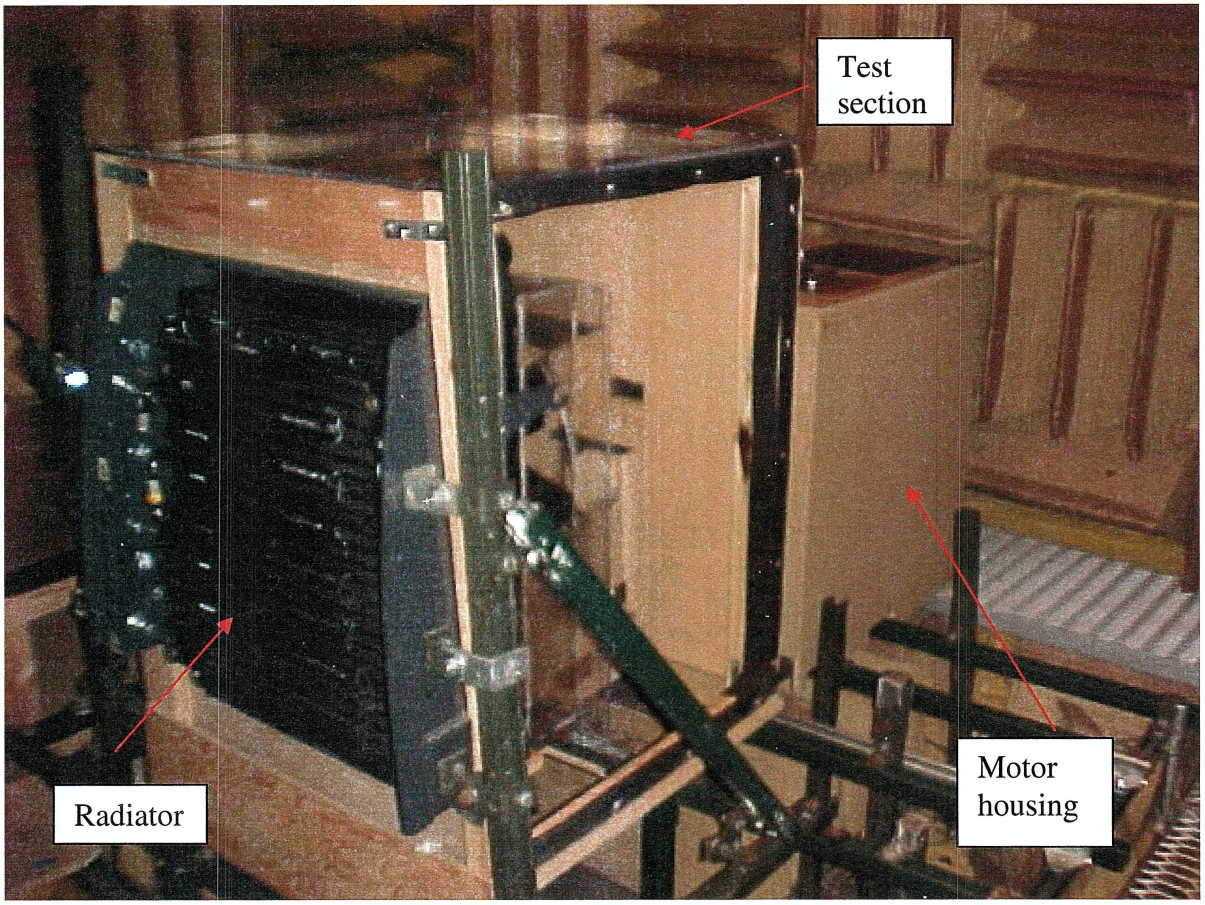

Figure 3.1 Front view of radiator and test section

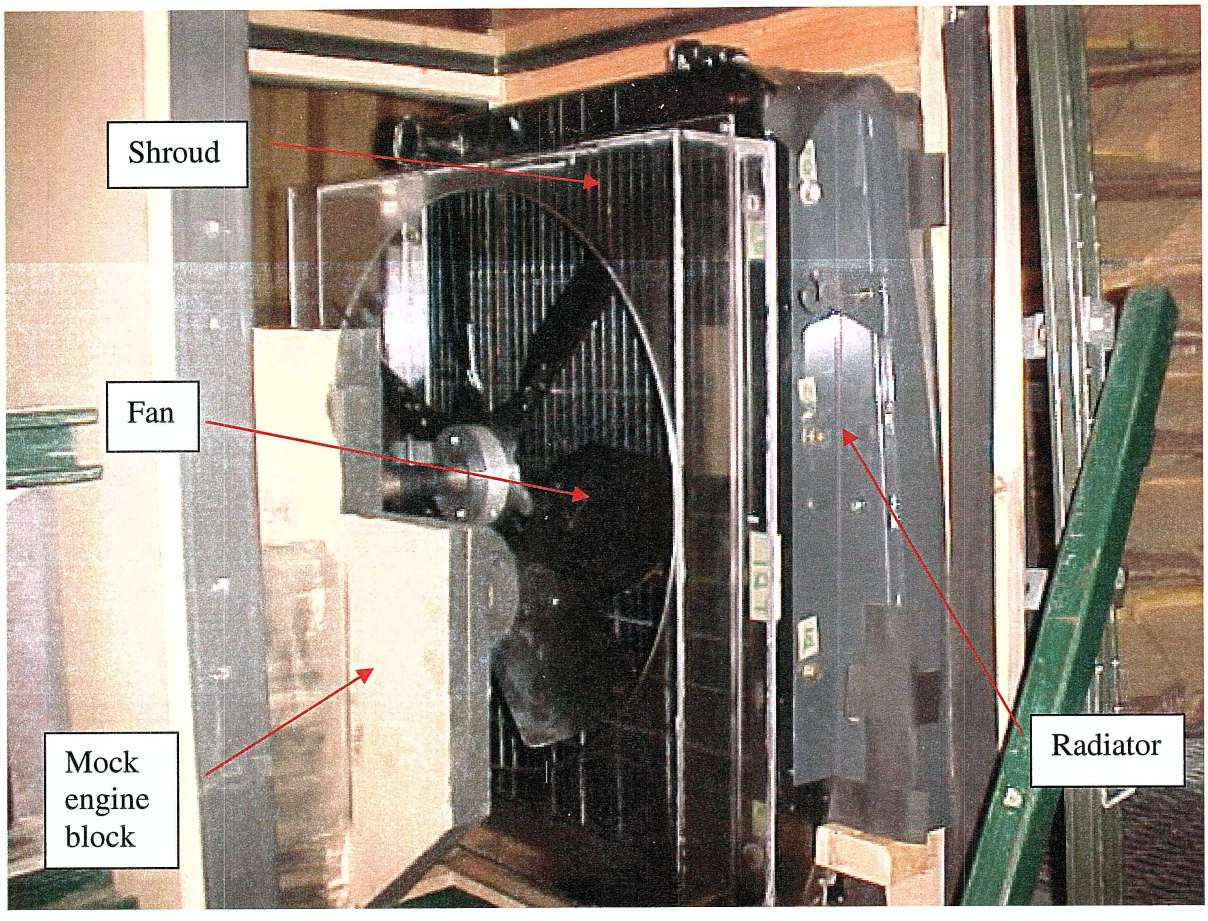

Figure 3.2 Back view of fan, shroud and radiator

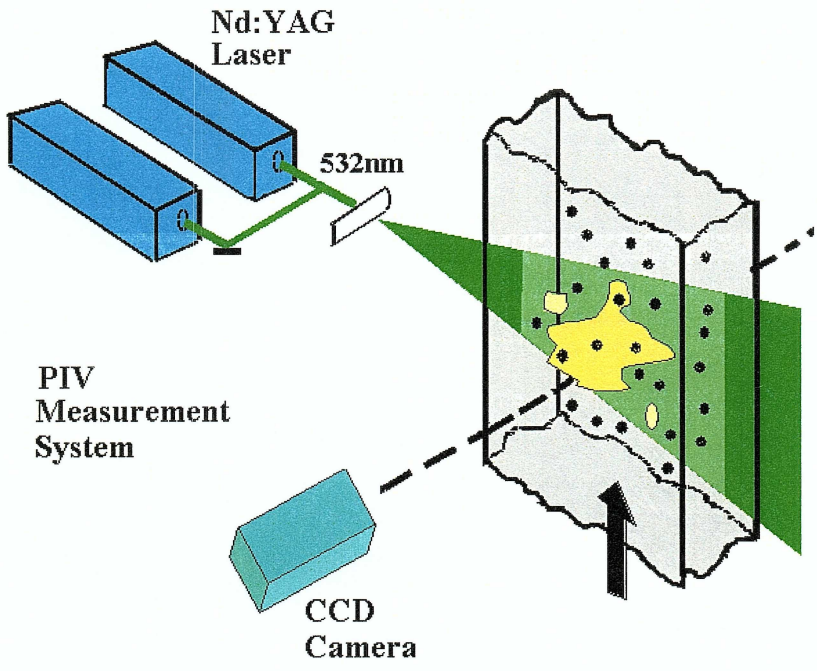

Figure 3.3 Typical PIV setup

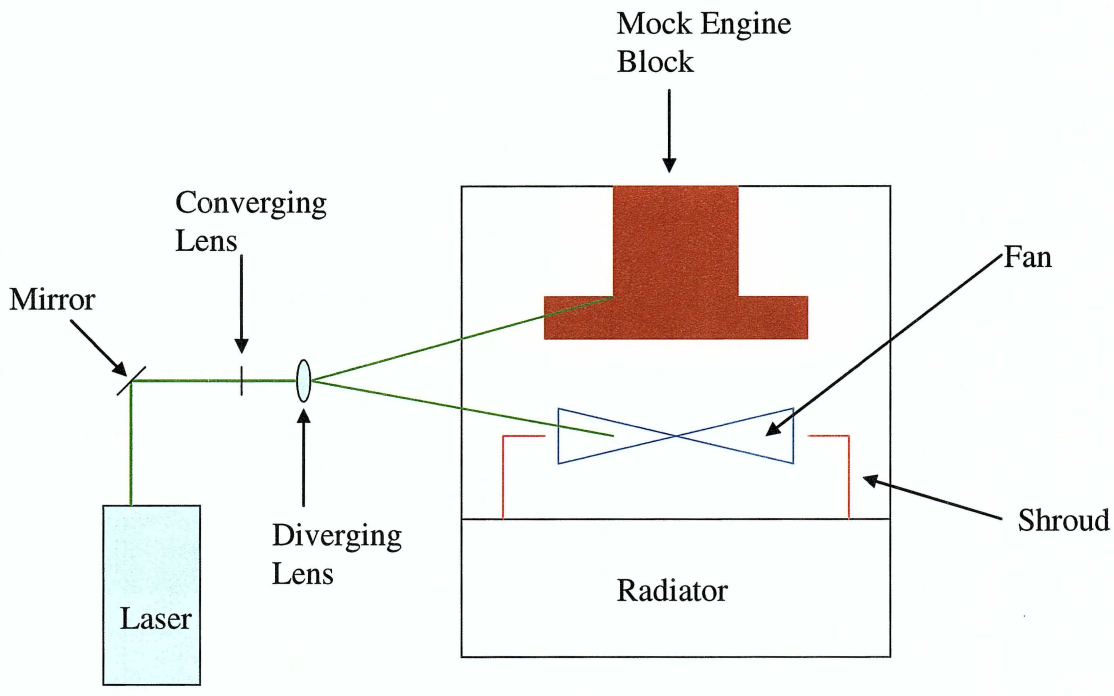

Figure 3.4 Overhead view of PIV setup for experiment

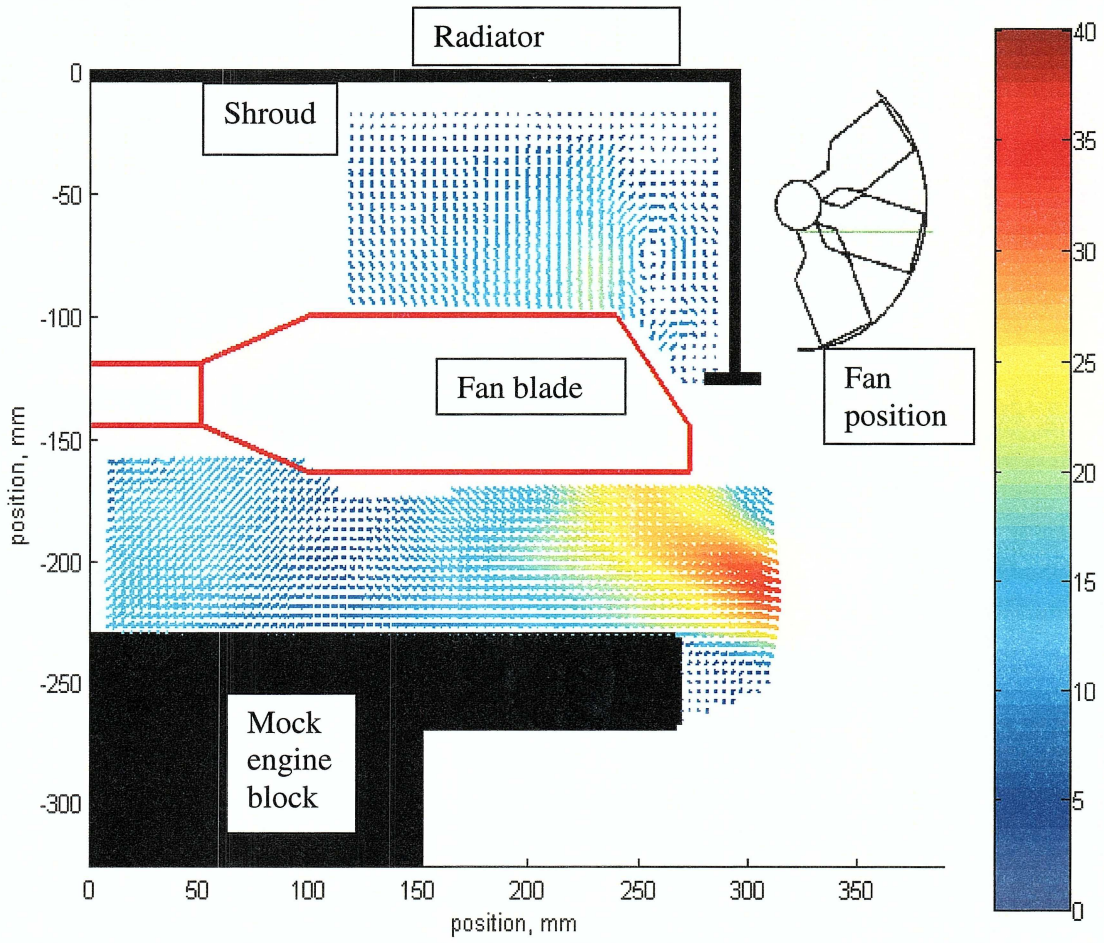

Figure 3.5 Example of velocity image obtained in experiment

CHAPTER 4. RESULTS AND DISCUSSION

4.1 Introduction

In this chapter the data from the various cases that were examined during the sets of experiments will be presented. The chapter has been organized such that comparisons can be made between fan speeds, engine block positions, and shroud types.

4.2 Velocity images

4.2.1 Instantaneous images

Each data set is made up of 2000 images. These images were averaged together to get an overall idea of what is happening at each location. Because the flow is highly turbulent, a large number of images are needed to ensure a good statistical average which is needed when calculating the turbulent kinetic energy. Figure 4.1 shows three instantaneous images taken at 1800rpm, 50% shroud immersion, and 0.5" engine block spacing. These images show the velocity field before the image was postprocessed to eliminate bad vectors. Each of the three images shows the same basic velocity field, the main difference being the difference in the airflow off the fan blade. This difference shows that the flow is not steady and is turbulent as expected. Note the presence of some "spurious" velocity vectors in some regions of the flow field. A small number of erroneous vectors will always occur in instantaneous PIV velocity vector fields. These spurious vectors can be removed and replaced by interpolation.

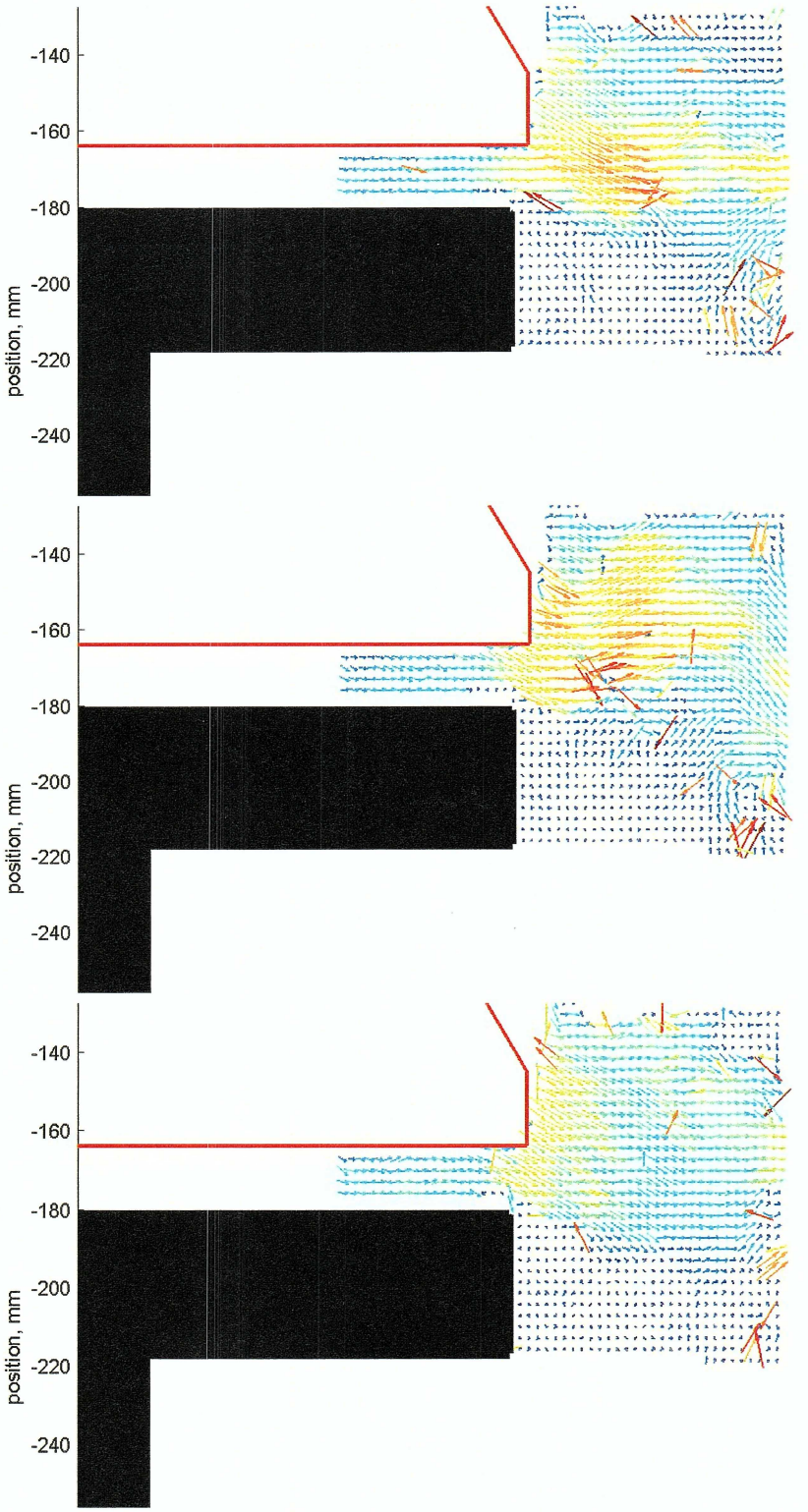

Figure 4.1 Three instantaneous images taken at 1800-50-0.5-3

4.2.2 Average images

In order to provide a general description of the flow for each case investigated, ensemble averages of the instantaneous velocity fields were calculated for each case. The ensemble averages provide a description of how the velocity field is evolving with varying blade position in a mean sense. The letters (a) – (e) on the figures correspond to the fan position in degrees.

4.2.2.1 1800 rpm, 100% shroud and engine block 2.5" away from fan

The image set in Fig. 4.1 shows the ensemble-averaged velocity field at 1800 rpm with the 100% shroud in place and the engine block 2.5" away from the fan for five different fan blade positions. This figure is actually a composite of two different ensemble-averaged velocity fields, one upstream of the fan and one downstream of the fan. These two ensemble-averaged velocity fields could be spliced together because they were calculated from velocity fields triggered to the same fan blade position. The velocity vectors in Fig. 4.2 are color coded corresponding to the magnitude of velocity. Figure 4.3 is a close up of the region of the flowfield containing the vortex. In this figure, the velocity vectors have been overlaid on the vorticity field.

Figure 4.2 (a) shows the velocity field with a fan blade parallel to the laser sheet. The laser sheet is aligned such that the sheet measures the velocity field downstream of the trailing edge of the fan blade. In the sequence of vector fields shown in Figs. 4.2 (a)-(e), the fan is rotating out of the plane depicted in figures and towards the observer. The small schematic of the fan shown in the upper-right-hand corner of each of the images shows the fan blade position relative to the laser sheet for each velocity field presented. This sequence

of velocity fields clearly shows the pulsatile nature of the flowfield both upstream and downstream of the fan. For the fan blade position shown in Fig. 4.3 (a), the velocity downstream is at a relative minimum. At the fan rotates through the blade positions shown in Figs. 4.2 (a)-(e), the velocity magnitudes downstream of the fan increase until a maximum is reached for the fan blade position depicted in Fig. 4.3 (e).

Another interesting feature of the flow downstream of the fan is that both the magnitude and direction of flow vary with radial distance from the axle of the fan. Near the axis, the flow downstream of the fan is actually drawn back *towards* the fan. Farther from the blade axis, the flow reverses direction and is forced away from the fan. Velocity then increases with increasing distance from the fan axis, until the maximum velocity is reached near the fan blade tips. The flow leaves the fan blade at about a 45 degree angle and continues to travel in that direction until the flow reaches the engine block. When it hits the engine block, it travels only in the radial direction. After the high velocity region of the flow moved past the engine block, it continued to move almost entirely in the radial direction.

One of the factors that will be investigated in this study is how changing the shroud immersion affects the flowfield. The shroud is important because it controls how the airflow leaves the fan in the axial and radial directions. The higher the percentage of the shroud containment, the lower the amount of air that enters the downstream region in the radial direction. With a box shroud, the air that leaves the fan blade inside the shroud re-circulates in the upstream region. With a 100% shroud in place, all the air leaving the tip of the blade is inside the shroud, thus the only air leaving the fan blade is moving parallel to the axis.

Another key feature of the flowfield is a vortex located upstream of the fan, as seen both in Figs. 4.2 and in more detail in Fig. 4.3. Notice that for this set of experimental

parameters, (rotation speed, shroud immersion, and engine spacing), this vortex remains nearly stationary as the fan is rotated. Also, as can be seen in the vorticity data shown in Fig. 4.3, the vortex strength is about 750 1/s. A smaller vortex is also seen near the fan blade tip in images (b)-(e). This vortex has a maximum strength of about 1500 1/s in image (b). This small vortex is important because it could contribute to the tone noise of the fan. Because it is near the tip of the fan blade, it could be "chopped" as the fan blade passes it, thus creating a tonal noise.

4.2.2.2 2200 rpm, 100% shroud and engine block 2.5" away from fan

The sequence of velocity fields shown in Figs, 4.4 (a)-(e) shows the average velocity field at 2200 rpm with the 100% shroud in place and the engine block 2.5" away from the fan. That is, it is for the same experimental conditions as the sequence shown in Figs. 4.2 (a)-(e), except that the fan rotational speed has been increased. The flow downstream of the fan blade shows the same general features as at 1800 rpm, except that the velocities for all fan blade positions are greater. Near the axis of the fan, the flow downstream of the fan blades is towards the fan, with the flow direction changing to away from the fan at a similar radial distance as in the 1800 rpm case. The flow velocities also increase steadily as the fan blade rotates from the position shown in Fig. 4.4 (a) to the position shown in Fig. 4.4 (e). As for the flow at 1800 rpm, the flow leaves the fan blade at about a 45 degree angle and continues to travel in that direction until the flow reaches the engine block. When it hits the engine block, it travels only in the radial direction. After the high velocity region of the flow moved past the engine block, it continued to move almost entirely in the radial direction.

A close-up of the upstream vortex for this set of experimental conditions is shown in Fig. 4.5. The vortex upstream of the fan is stronger (2000 1/s) then the one formed at 1800 rpm, but is still predominantly stationary. The small vortex near the fan blade tip is still visible in images (b), (d), and (e). It probably is exists in image (c) but the data was unreadable where the vortex would be. The strength of this vortex was the same as the 1800 rpm case, with the maximum being about 1500 1/s in image (b). Again, this vortex is important because it could contribute to the tone noise of the fan the same way as in the previous case.

4.2.2.3 1800 rpm, 50% shroud and engine block 2.5" away from fan

The sequence of velocity fields shown in Figs, 4.6 (a)-(e) shows the average velocity field at 1800 rpm with the 50% shroud in place and the engine block 2.5" away from the fan. That is, it is for the same experimental conditions as the sequence shown in Figs. 4.2 (a)-(e), except that the shroud size has been decreased. Downstream of the fan, the area of high velocity has moved more toward the tip of the fan then in the cases with the 100% shroud in place. Once again, the flow leaves the fan blade at about a 45 degree angle and continues to travel in that direction until the flow reaches the engine block. After impinging on the engine block, the flow travels only in the radial direction, and after the high velocity region of the flow moved past the engine block, it continued to move almost entirely in the radial direction. In images (a)-(c), a region of high velocity air is seen moving away from the fan blade, again clearly showing the pulsatile nature of the flowfield in these images.

In Figs, 4.7 (a)-(e), a close up view of the upstream vortex is shown. Notice that for this set of experimental parameters, (rotation speed, shroud immersion, and engine spacing),

this vortex remains nearly stationary in the radial direction but moved upwards in the axial direction as the fan rotated. Also, as can be seen in the vorticity data shown in Fig. 4.7, the vortex strength varies with fan position. The vortex starts with strength of 1300 1/s in image (a), increases to 2000 1/s in image (c), and then decreases back to 1300 1/s in image (e). A smaller vortex is also seen forming near the fan blade tip in image (c), and fully formed in images (d) and (e). This vortex has a maximum strength of about 1500 1/s in image (e).

4.2.2.4 2200 rpm, 50% shroud and engine block 2.5" away from fan

The sequence of velocity fields shown in Figs, 4.8 (a)-(d) shows the average velocity field at 2200 rpm with the 50% shroud in place and the engine block 2.5" away from the fan. That is, it is for the same experimental conditions as the sequence shown in Figs. 4.6 (a)-(d), except that the fan rotational speed has been increased. The flow downstream of the fan blade shows the same general features as at 1800 rpm, except that the velocities for all fan blade positions are greater. On the downstream side of the fan, the velocity is not uniform as it leaves the fan blade. A much higher velocity region is seen near the fan tip, and after the fan passes, this region moves downstream with a lower velocity region behind it. As in the previously described cases, the flow leaves the fan blade at about a 45 degree angle and continues to travel in that direction until the flow reaches the engine block.

In Figs, 4.9(a)-(e), a close up view of the upstream vortex is shown. Just as for the same shroud and engine spacing with 1800 rpm, this vortex remains nearly stationary in the radial direction but moves upwards in the axial direction as the fan rotated. Also, as can be seen in the vorticity data shown in Fig. 4.9, the vortex strength varies with fan position. Image (a) shows the vortex at 1500 1/s and (b) shows it weakens to 1300 1/s. It then

increases in strength to 2000 1/s in images (c)-(e). Because the vortex forms at a different fan position then the 1800 rpm case, it means the vortex is forming at a different rate then the vortex in the 1800 rpm case. This could be an important consideration for tonal noise.

4.2.2.5 1800 rpm, 100% shroud and engine block 0.5" away from fan

The sequence of velocity fields shown in Figs, 4.10 (a)-(e) shows the average velocity field at 1800 rpm with the 100% shroud in place and the engine block 0.5" away from the fan. That is, it is for the same experimental conditions as the sequence shown in Figs. 4.2 (a)-(e), except that the engine block spacing has been decreased. A small jet of high velocity air leaves the fan blade in images (a) and (b). This jet decreases velocity in images (c)-(e). After the air moves past the engine block, it continued to move mostly in the radial direction.

In Figs, 4.11(a)-(e), a close up view of the upstream vortex is shown. Notice that for this set of experimental parameters, (rotation speed, shroud immersion, and engine spacing), this vortex remains nearly stationary, as was in the 1800 rpm, 100% shroud, 2.5" engine block spacing case. The difference between those two cases is the size of the vortex. With the engine block at the 0.5" spacing, the vortex measures about 100 mm in diameter, compared to only 50 mm in diameter when the engine block was at the 2.5" spacing. The strength of this large vortex is around 800 1/s. As the images move from (a) to (e), there is a small area of higher vorticity that is moving counterclockwise in the vortex that is around 1200 1/s. There is no small vortex near the fan blade tip.

4.2.2.6 2200 rpm, 100% shroud and engine block 0.5" away from fan

The sequence of velocity fields shown in Figs, 4.12 (a)-(e) shows the average velocity field at 2200 rpm with the 100% shroud in place and the engine block 0.5" away from the fan (i.e. for the same experimental conditions as the sequence shown in Figs. 4.10 (a)-(e), except that the fan speed has been increased). The flow downstream of the fan blade shows the same general features as at 1800 rpm, except that the velocities for all fan blade positions are greater. A small jet of high velocity air leaves the fan blade in images (a) and (b). This jet decreases velocity in images (c)-(e). The maximum velocity in this setup was around 45 m/s, as opposed to only around 40 m/s in all other setups. After the air moves past the engine block, it continued to move mostly in the radial direction.

In Figs, 4.13(a)-(e), a close up view of the upstream vortex is shown. Notice that for this set of experimental parameters, this vortex remains nearly stationary, just as it was in the 2200 rpm, 100% shroud, 2.5" engine block spacing case. The difference between those two cases is the size of the vortex. With the engine block at the 0.5" spacing, the vortex measures about 100 mm in diameter, compared to only 50 mm in diameter when the engine block was at the 2.5" spacing. The strength of this large vortex is around 900 1/s. As the images move from (a) to (e), there is a small area of higher vorticity that is moving counterclockwise in the vortex that is around 1300 1/s. Again, there is no small vortex near the fan blade tip.

4.2.2.7 1800 rpm, 50% shroud and engine block 0.5" away from fan

The sequence of velocity fields shown in Figs, 4.14 (a)-(e) shows the average velocity field at 1800 rpm with the 50% shroud in place and the engine block 0.5" away from the fan (i.e. for the same experimental conditions as the sequence shown in Figs. 4.10 (a)-(e), except that the shroud size has been decreased). In this series a high velocity region of air is formed

near the fan and moves away as the fan passes. This is probably the best example of the pulsatile nature of the downstream flowfield. This high velocity region is much larger then in previous setups, going from the edge of the shroud to the edge of the engine block.

In Figs, 4.15(a)-(e), a close up view of the upstream vortex is shown. Notice that for this set of experimental parameters, this vortex remains nearly stationary, as opposed to the 1800 rpm, 50% shroud, 2.5" engine block spacing case, which moved in the axial direction. Another difference between those two cases is the strength of the vortex. With the engine block at the 0.5" spacing, the vortex has a 750 1/s and did not change in strength as the fan blade passed. The size of the vortex was nearly the same is in the 2.5" spacing case, but much smaller then the other 0.5" cases. There is a small vortex near the tip of the fan blade, similar to those present in the 2.5" cases.

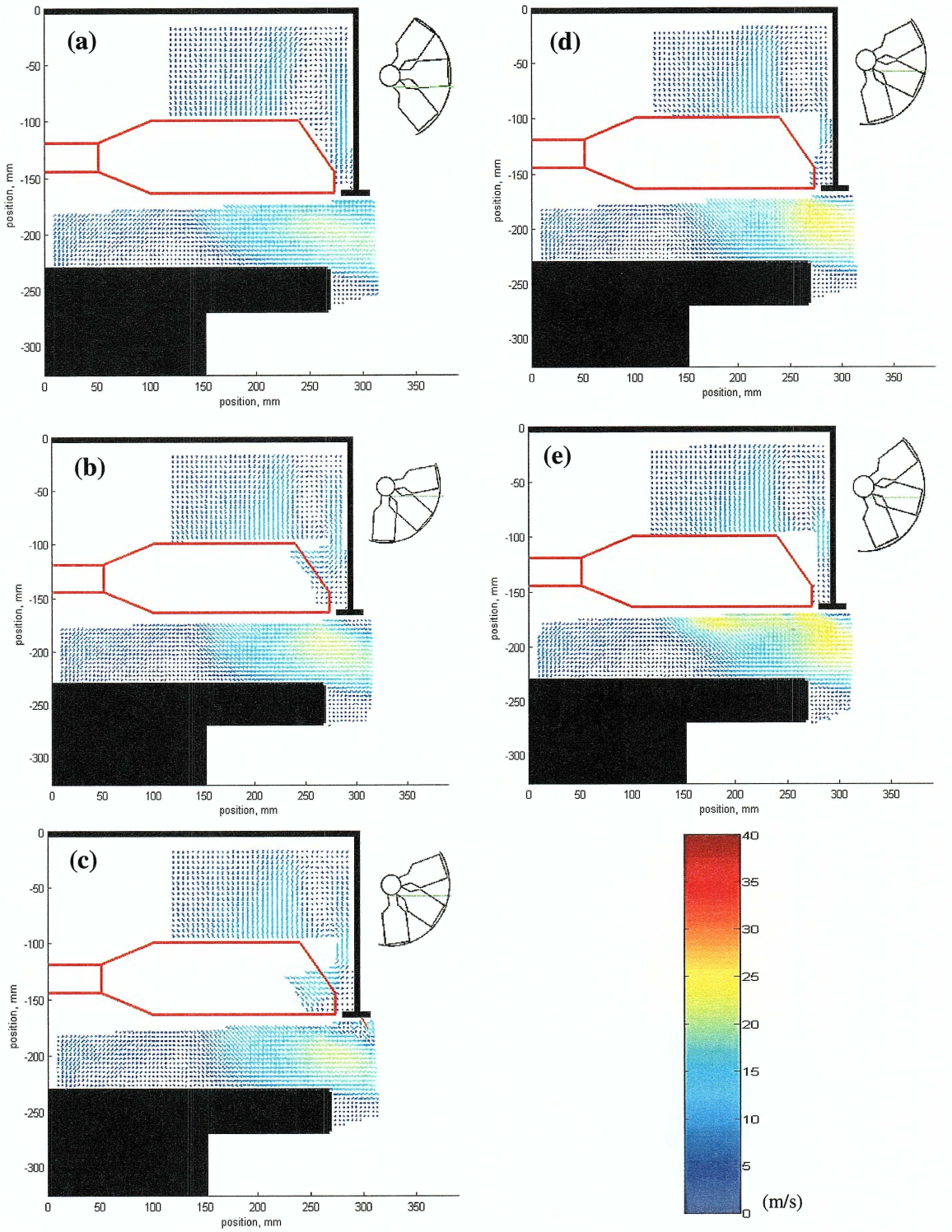

Figure 4.2 **(a)-(e)** Series of ensemble-averaged velocity fields at five different fan blade positions for 1800 rpm, 100% immersion, and 2.5 inch engine spacing; where (a) 3, (b) 11, (c) 20, (d) 28 and (e) 37.

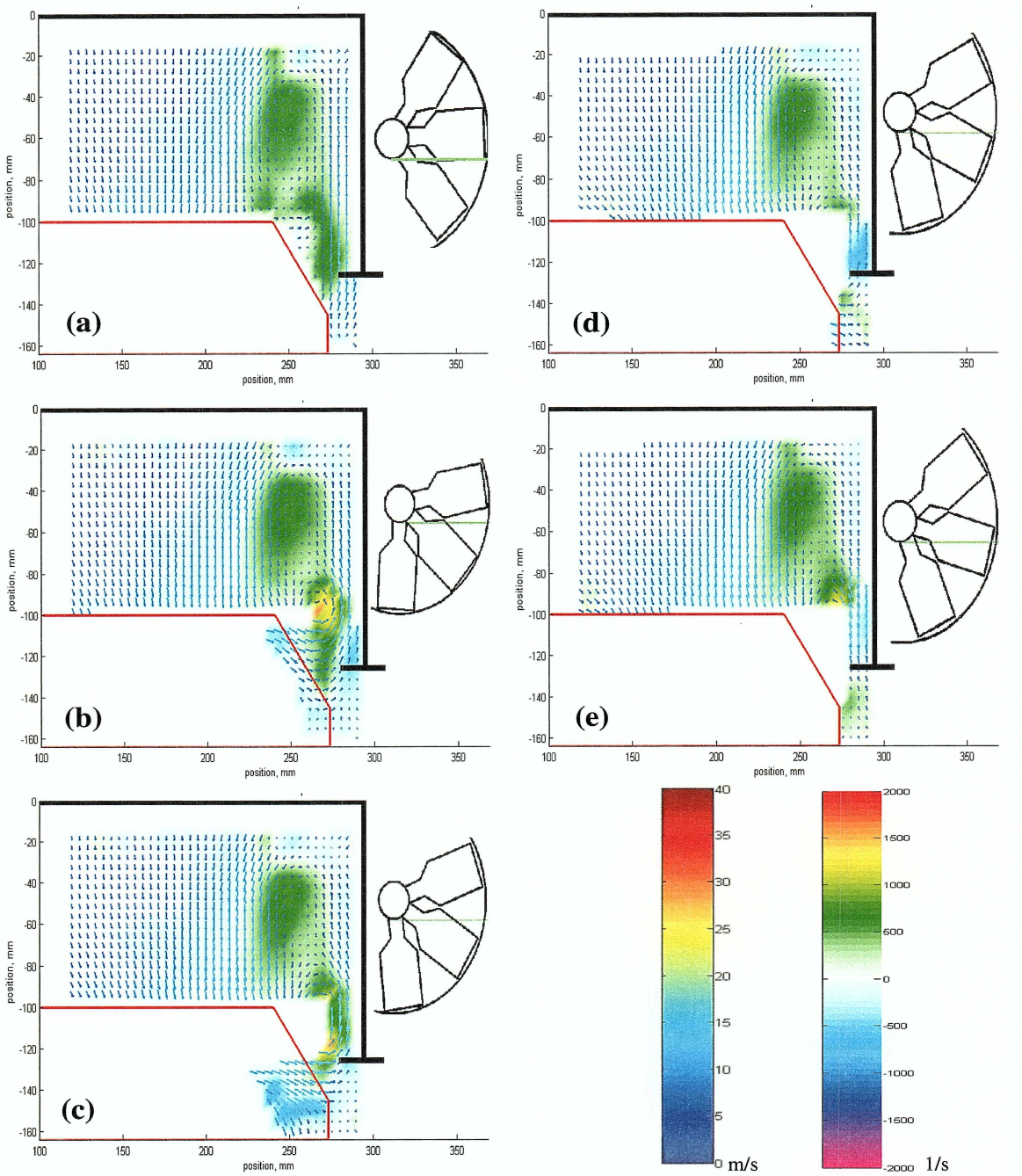

Figure 4.3 **(a)-(e)** Series of ensemble-averaged upstream velocity and vorticity fields at five different fan blade positions for 1800 rpm, 100% immersion, and 2.5 inch engine spacing; where (a) 3, (b) 11, (c) 20, (d) 28 and (e) 37.

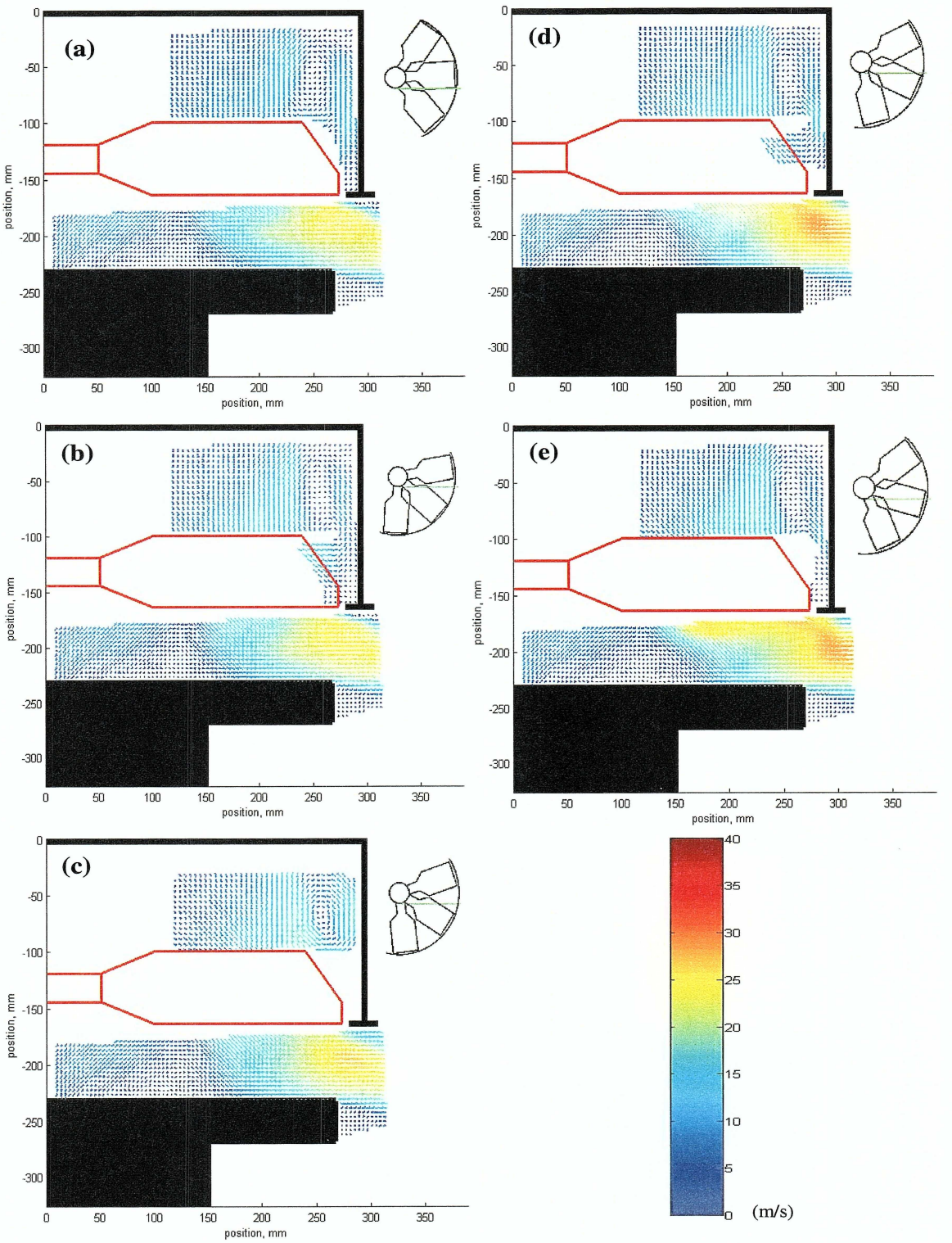

Figure 4.4 **(a)-(e)** Series of ensemble-averaged velocity fields at five different fan blade positions for 2200 rpm, 100% immersion, and 2.5 inch engine spacing; where (a) 5, (b) 14, (c) 22, (d) 31 and (e) 40.

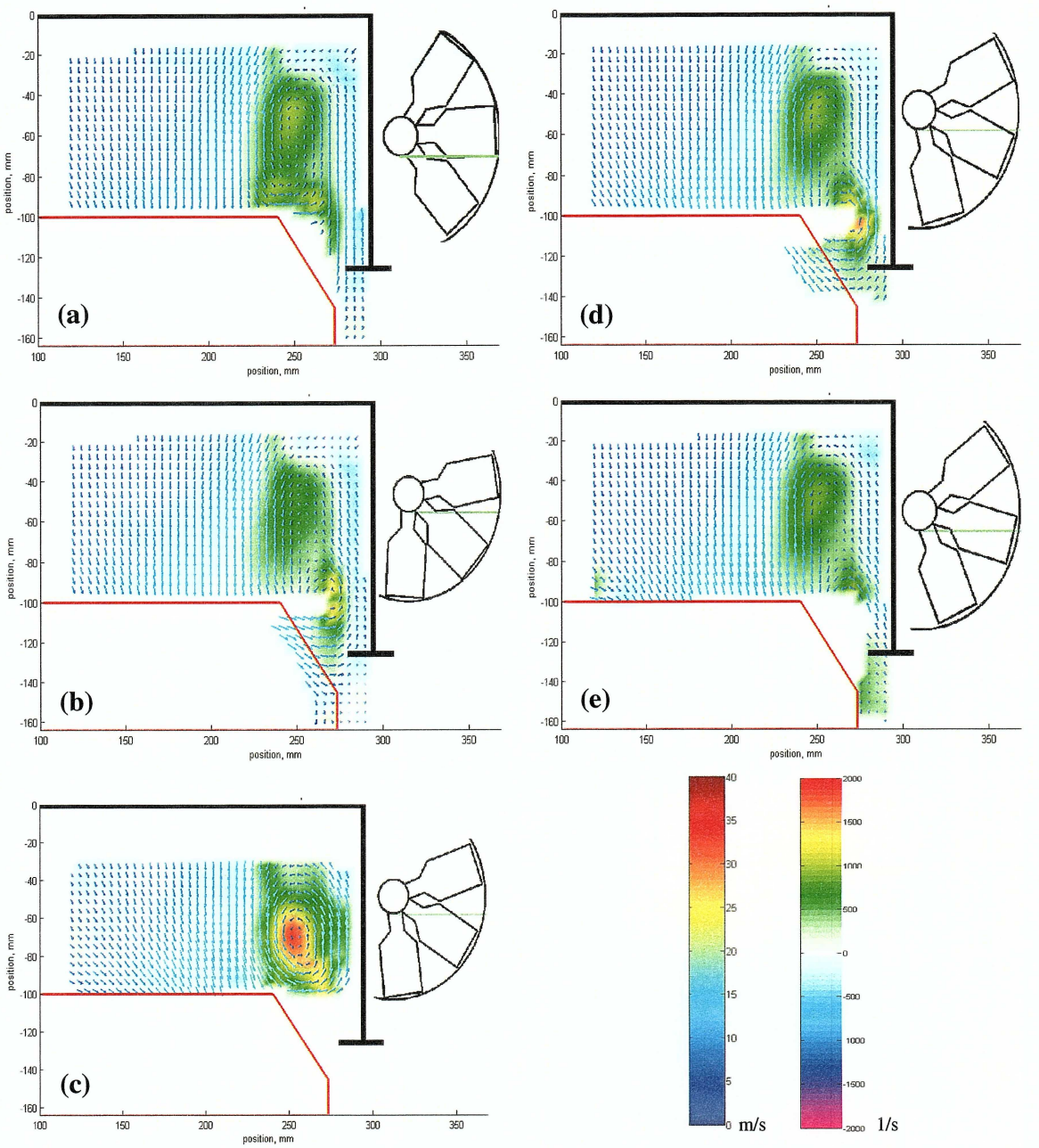

Figure 4.5 **(a)-(e)** Series of ensemble-averaged upstream velocity and vorticity fields at five different fan blade positions for 2200 rpm, 100% immersion, and 2.5 inch engine spacing; where (a) 5, (b) 14, (c) 22, (d) 31 and (e) 40.

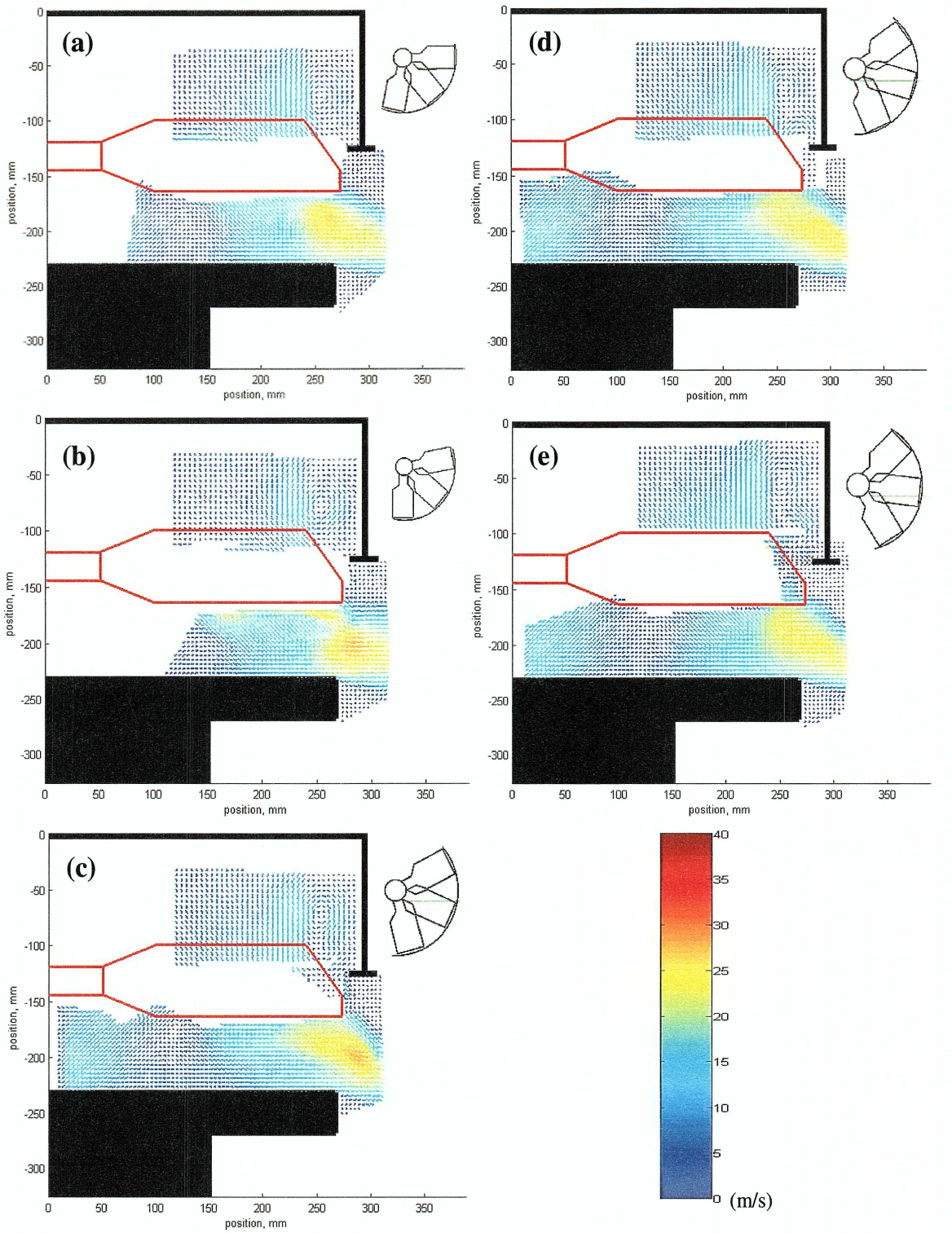

Figure 4.6 (a)-(e) Series of ensemble-averaged velocity fields at five different fan blade positions for 1800 rpm, 50% immersion, and 2.5 inch engine spacing; where (a) 28, (b) 37, (c) 3, (d) 11 and (e) 20.

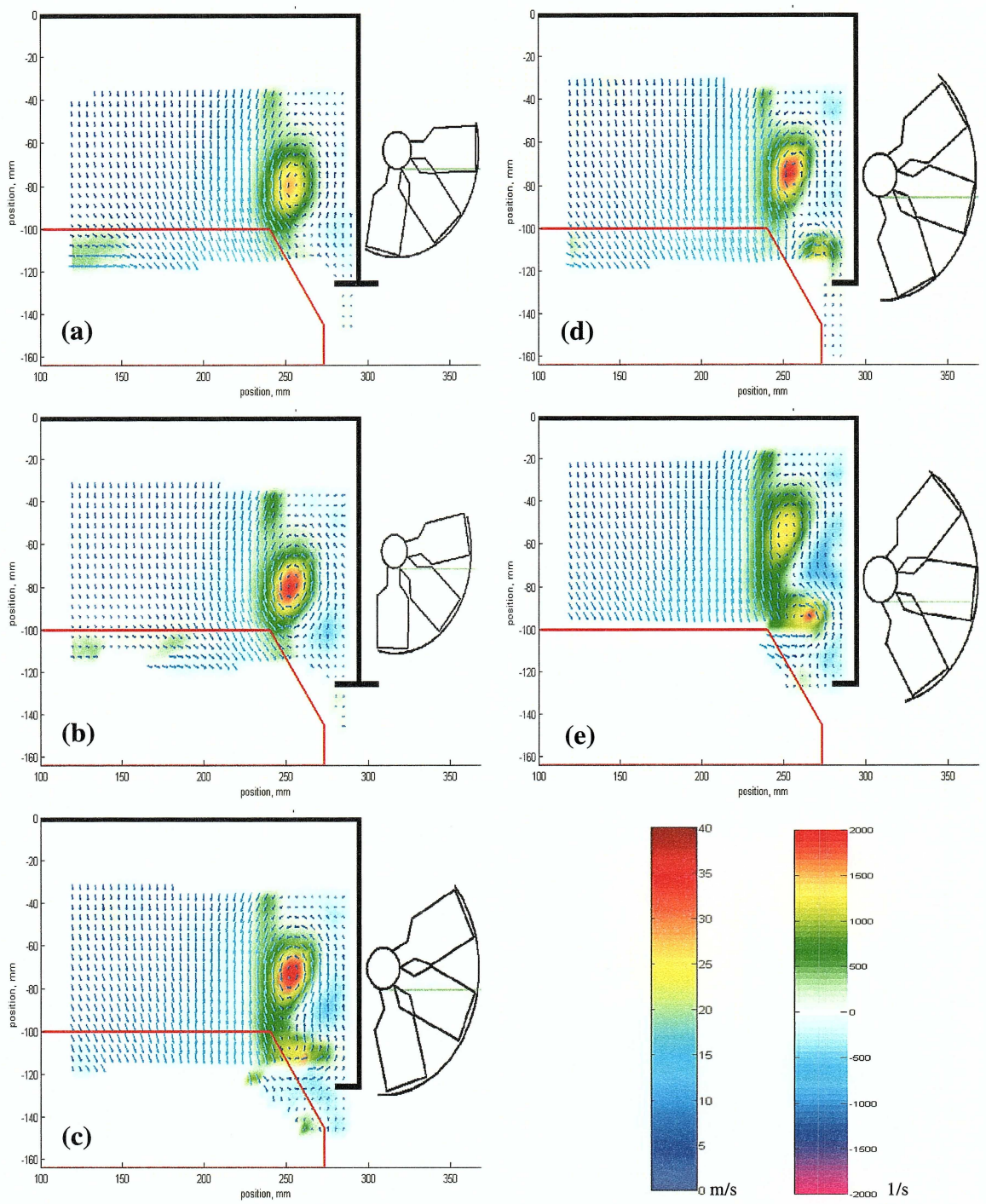

Figure 4.7 **(a)-(e)** Series of ensemble-averaged upstream velocity and vorticity fields at five different fan blade positions for 1800 rpm, 50% immersion, and 2.5 inch engine spacing; where (a) 28, (b) 37, (c) 3, (d) 11 and (e) 20.

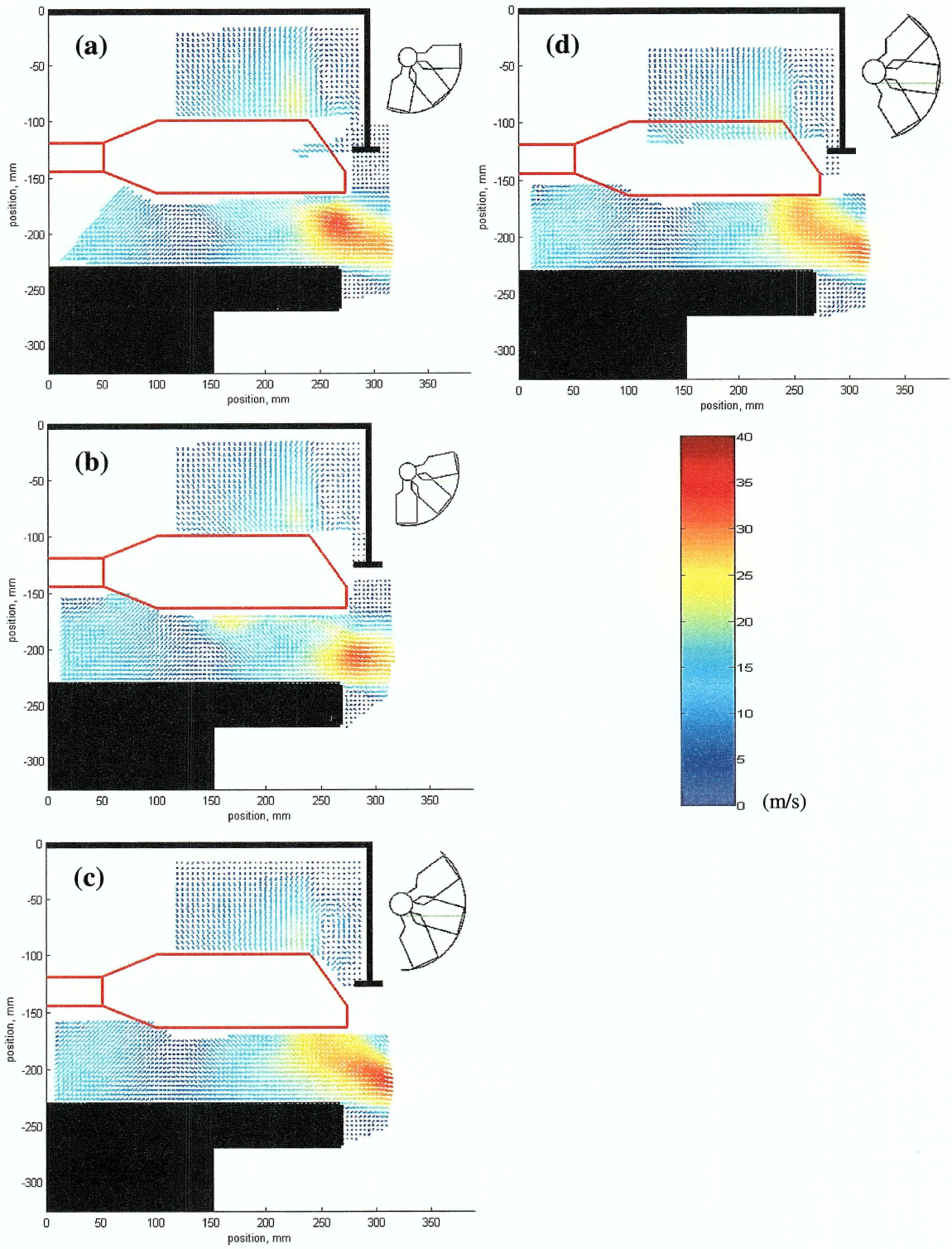

Figure 4.8 **(a)-(d)** Series of ensemble-averaged velocity fields at five different fan blade positions for 2200 rpm, 50% immersion, and 2.5 inch engine spacing; where (a) 31, (b) 40, (c) 14 and (d) 22.

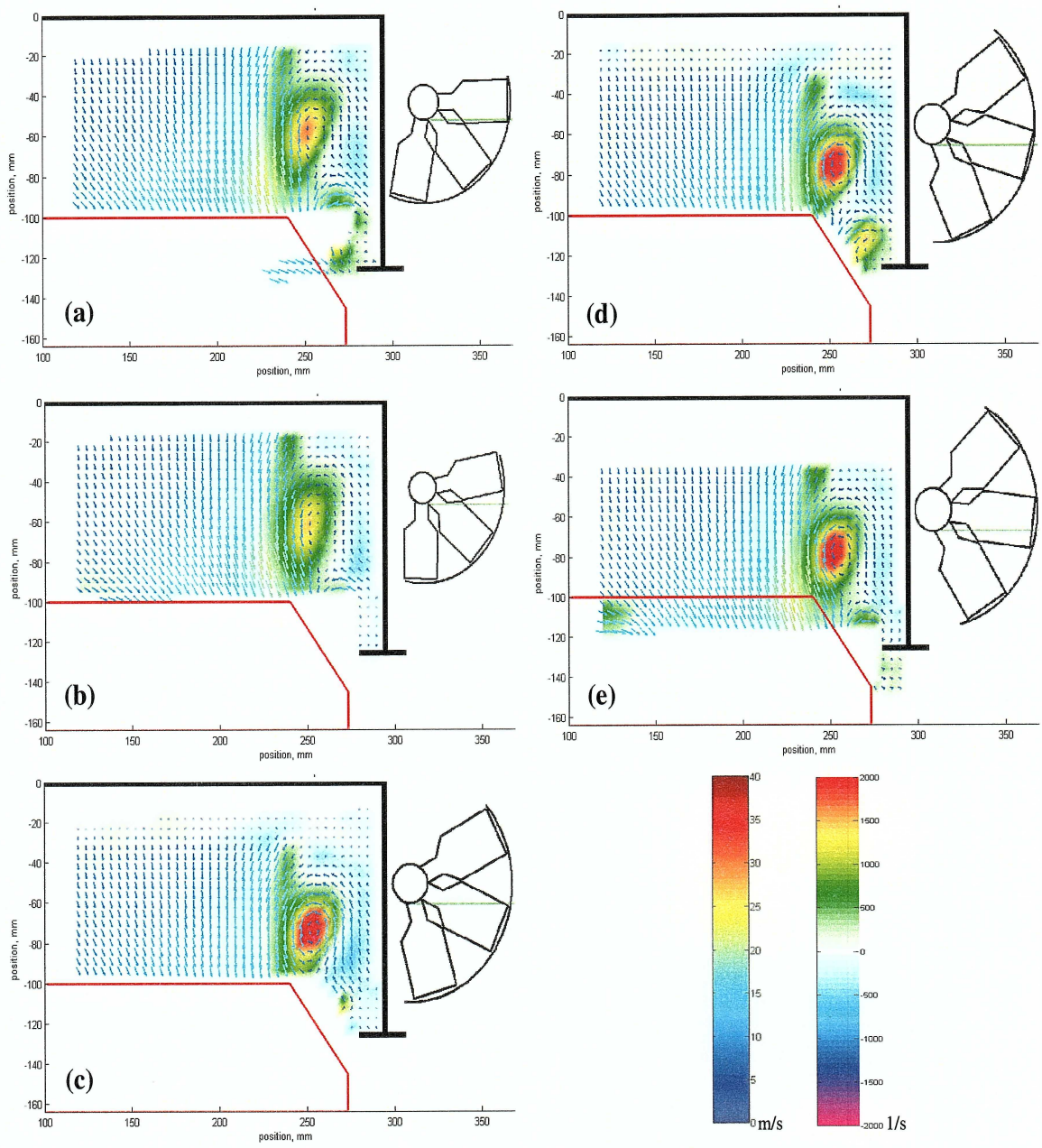

Figure 4.9 **(a)-(d)** Series of ensemble-averaged upstream velocity and vorticity fields at five different fan blade positions for 2200 rpm, 50% immersion, and 2.5 inch engine spacing; where (a) 31, (b) 40, (c) 14 and (d) 22.

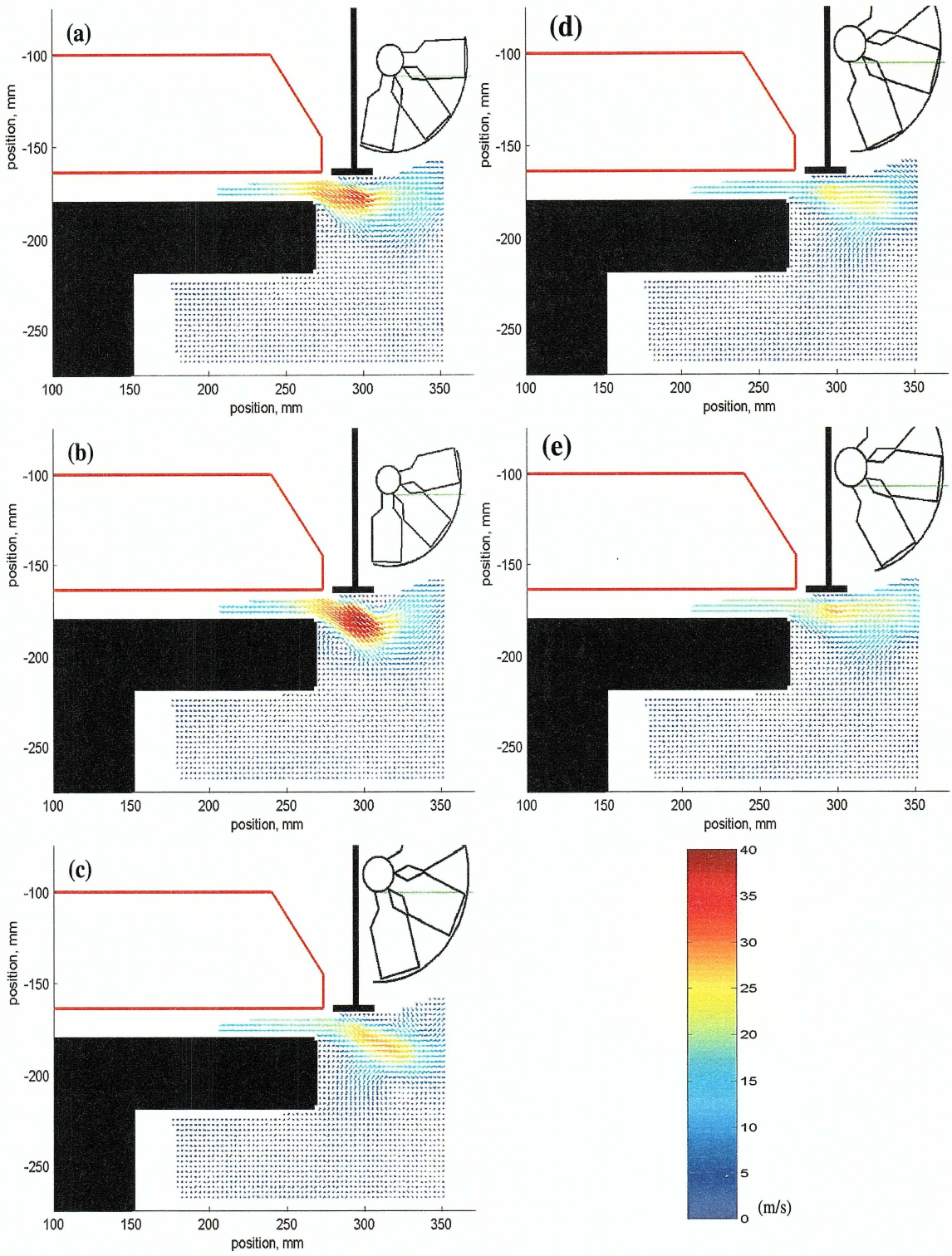

Figure 4.10 **(a)-(e)** Series of ensemble-averaged downstream velocity fields at five different fan blade positions for 1800 rpm, 100% immersion, and 0.5 inch engine spacing; where (a) 28, (b) 37, (c) 3, (d) 11 and (e) 20.

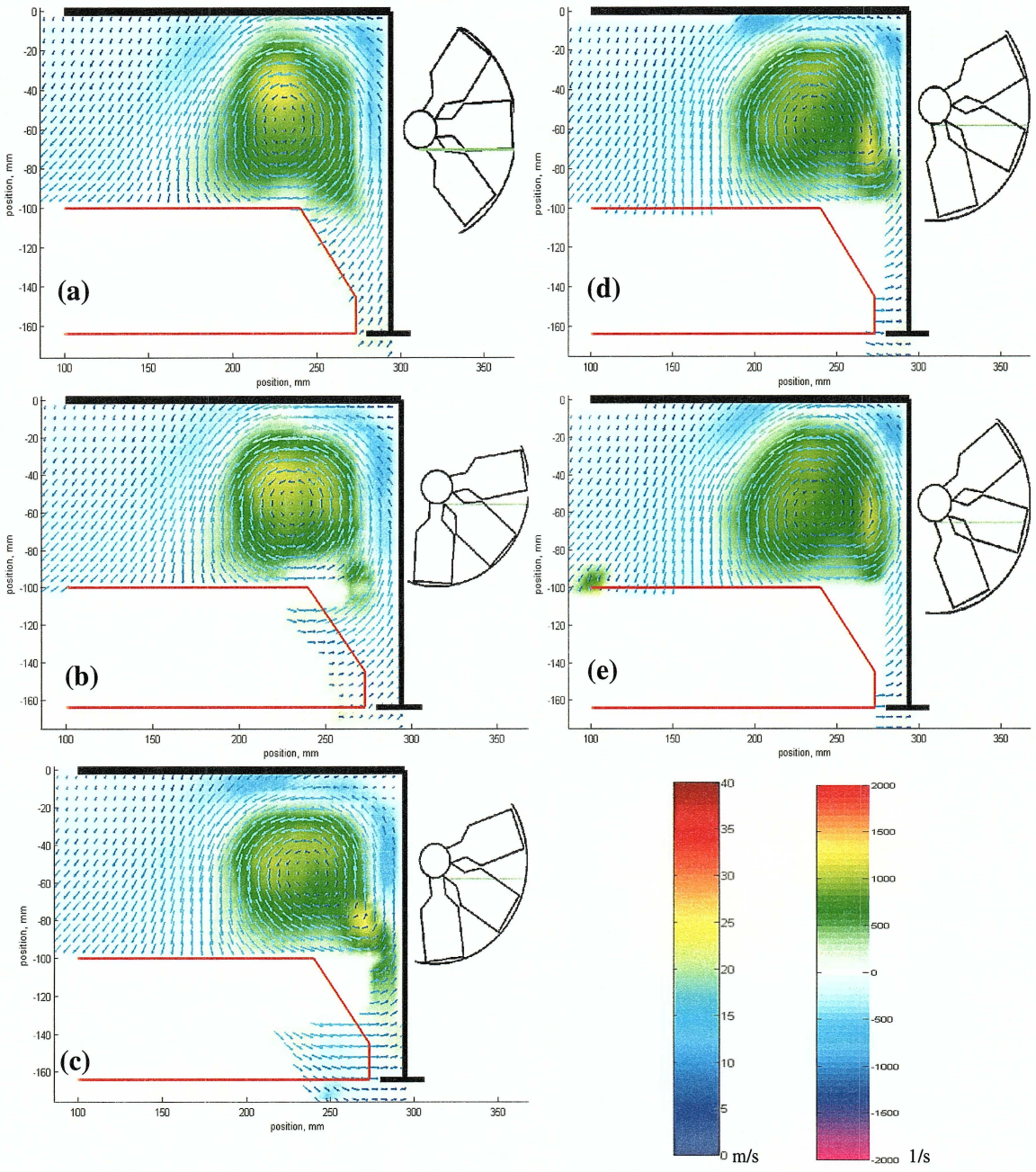

Figure 4.11 **(a)-(e)** Series of ensemble-averaged upstream velocity and vorticity fields at five different fan blade positions for 1800 rpm, 100% immersion, and 0.5 inch engine spacing; where (a) 3, (b) 11, (c) 20, (d) 28 and (e) 37.

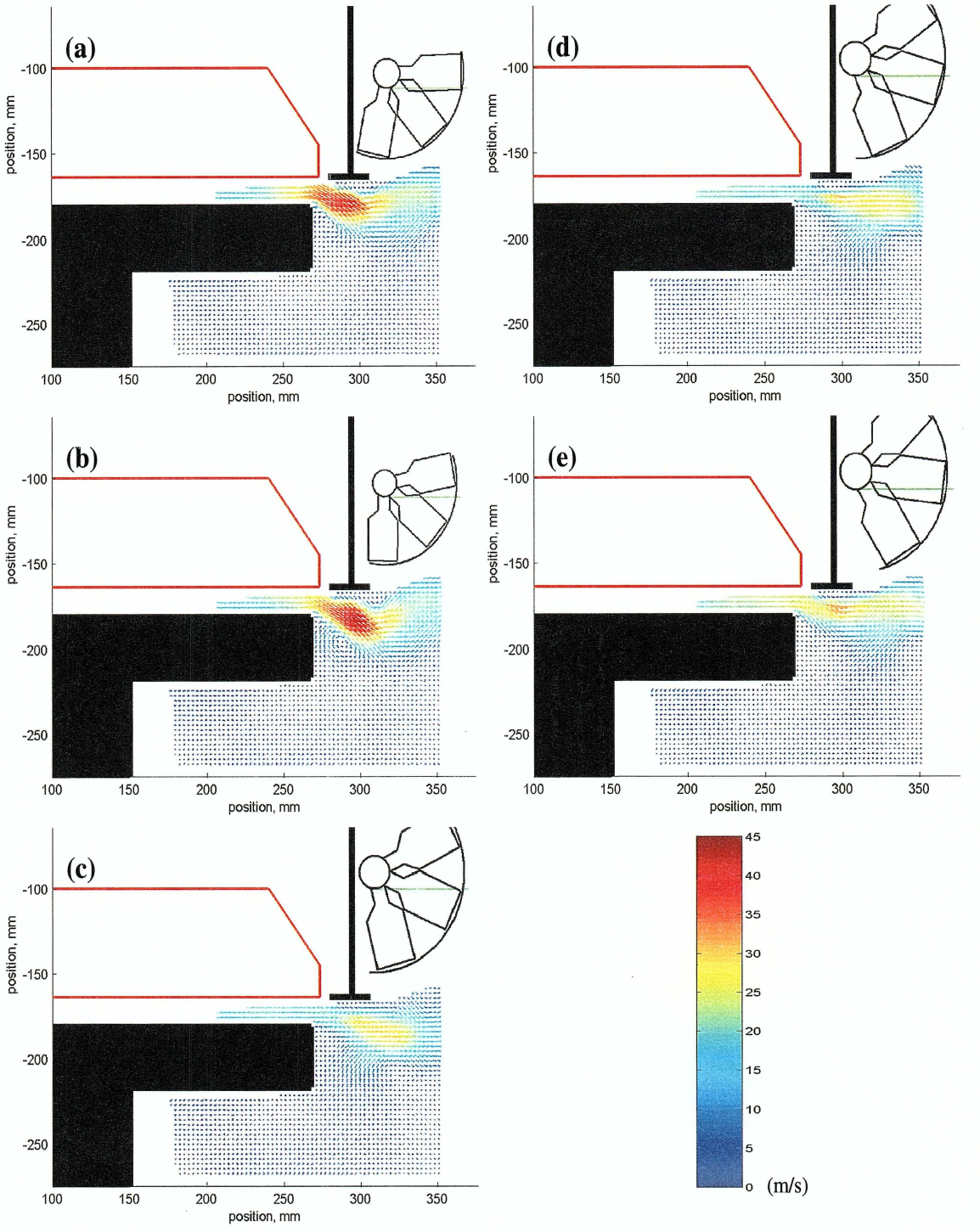

Figure 4.12 **(a)-(e)** Series of ensemble-averaged downstream velocity fields at five different fan blade positions for 2200 rpm, 100% immersion, and 0.5 inch engine spacing; where (a) 31, (b) 40, (c) 5, (d) 14 and (e) 22.

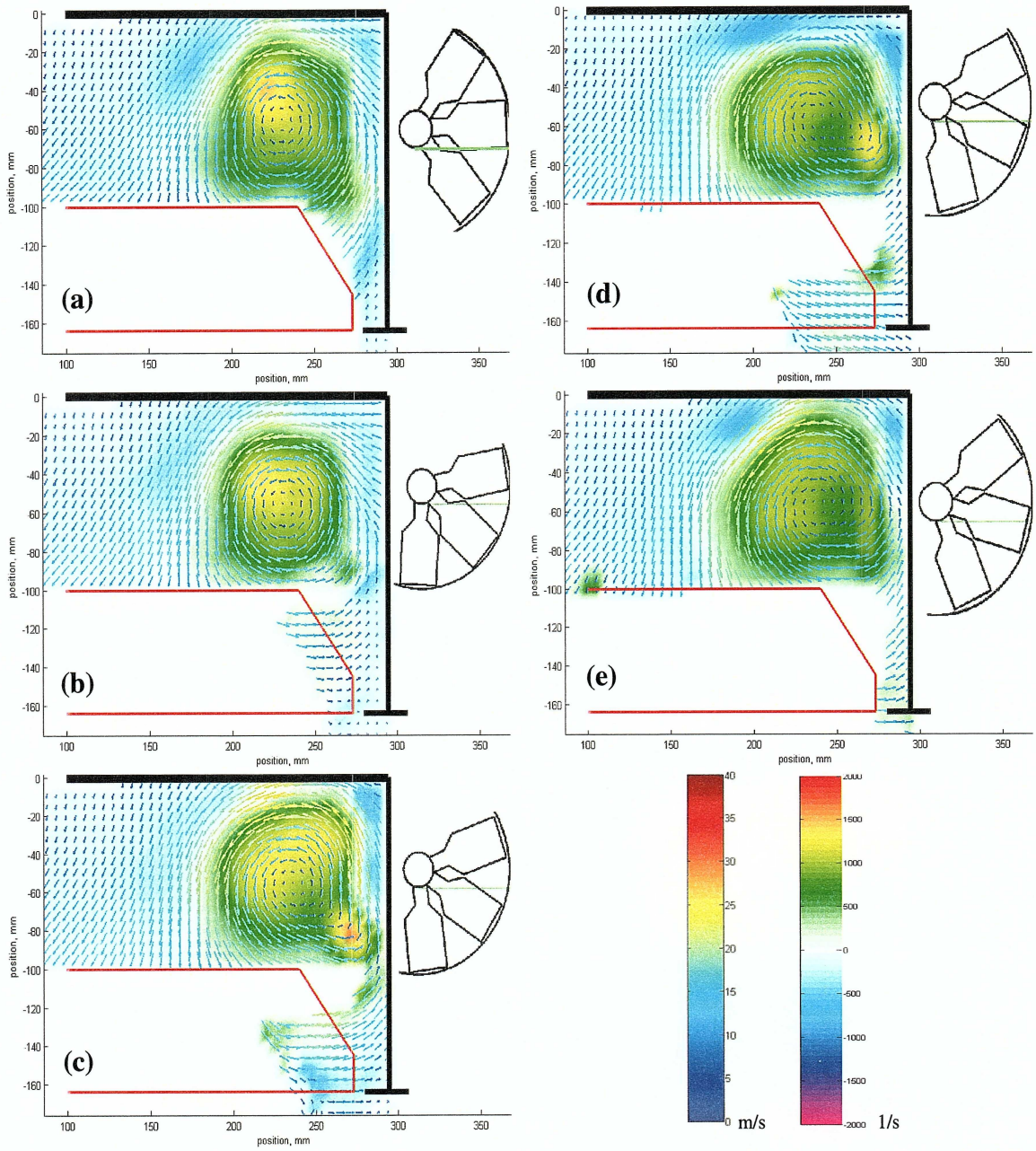

Figure 4.13 (a)-(e) Series of ensemble-averaged upstream velocity and vorticity fields at five different fan blade positions for 2200 rpm, 100% immersion, and 0.5 inch engine spacing; where (a) 5, (b) 14, (c) 22, (d) 31 and (e) 40.

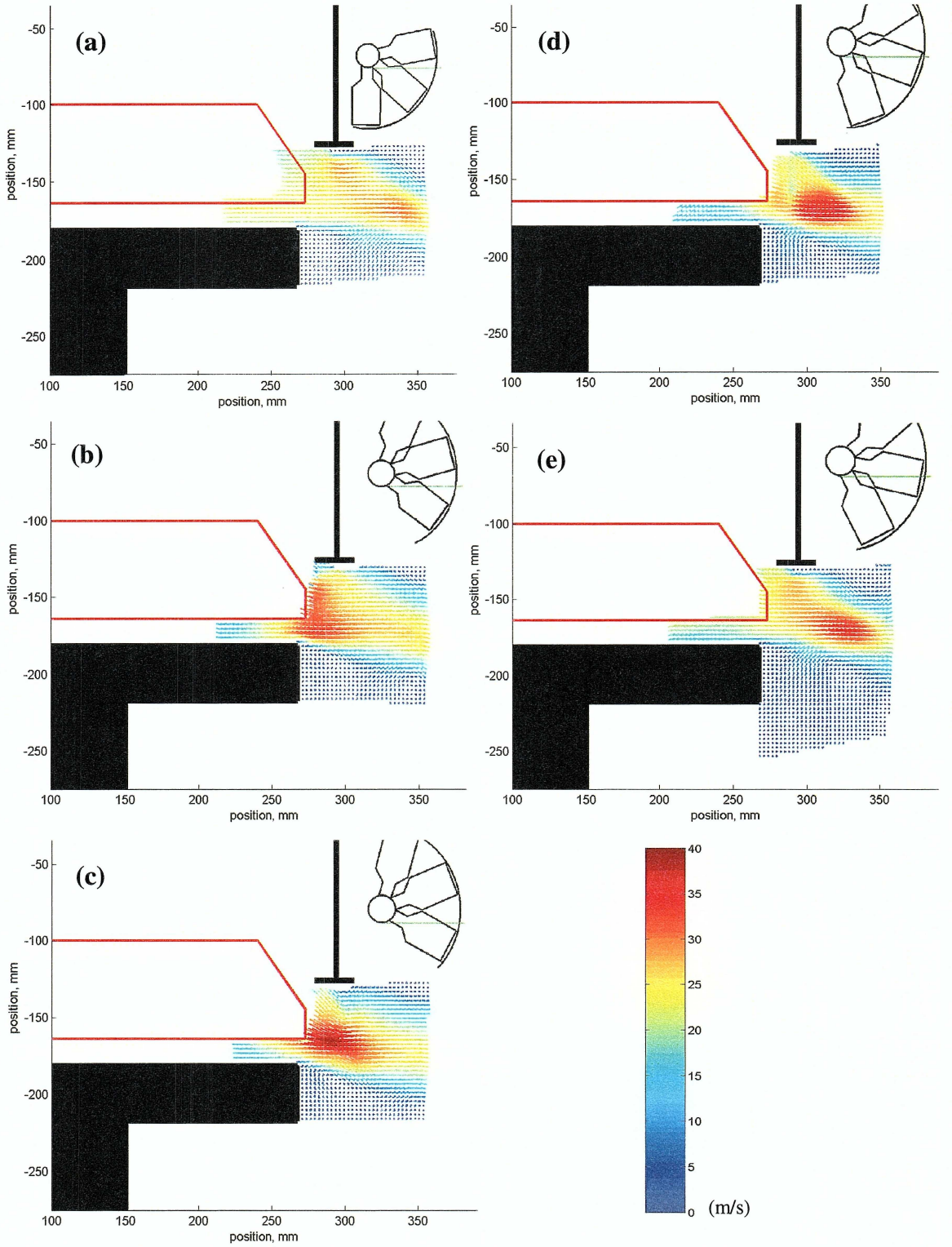

Figure 4.14 **(a)-(e)** Series of ensemble-averaged downstream velocity fields at five different fan blade positions for 1800 rpm, 50% immersion, and 0.5 inch engine spacing; where (a) 37, (b) 3, (c) 11, (d) 20, and (e) 28.

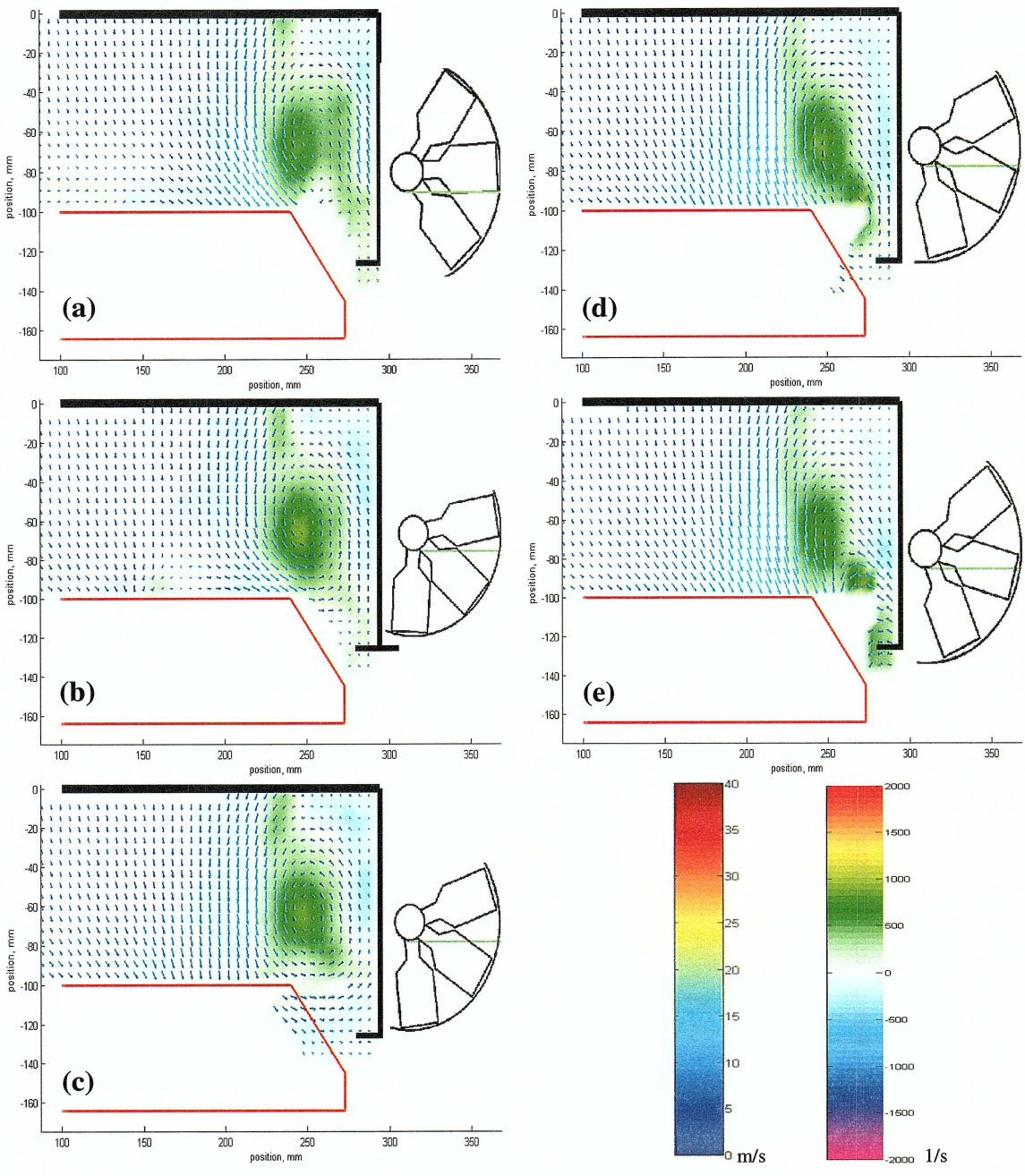

Figure 4.15 **(a)-(e)** Series of ensemble-averaged upstream velocity and vorticity fields at five different fan blade positions for 1800 rpm, 50% immersion, and 0.5 inch engine spacing; where (a) 3, (b) 11, (c) 20, (d) 28, and (e) 37.

4.3 Turbulent kinetic energy

In addition to providing information on instantaneous and mean velocity fields, PIV data can be analyzed to quantify the turbulence of the flowfield through such quantities as Reynolds stresses and turbulent kinetic energy. In the work presented here, turbulent kinetic energy was calculated using ensembles of instantaneous velocity field data. In a three-dimensional flow, the turbulent kinetic energy is defined as

$$TKE = u'^2 + v'^2 + w'^2$$

where u', v', and w' are the root mean square x, y, and z velocity fluctuations, respectively. However, in single camera PIV experiments like those presented here, only the x and y velocities are measured, and so the TKE cannot be calculated directly. Instead, an approximation must be made. In the present research, the TKE was calculated by assuming that the z velocity fluctuations were zero. Therefore, the turbulent kinetic energy equation for two-dimensional flow simply becomes

$$TKE = u'^2 + v'^2$$

Turbulent kinetic energy fields for the various geometries and fan speeds investigated are presented and discussed in the following section. However, the upstream region of flow had a TKE of about $1/10^{th}$ of the downstream values. This was to be expected, since the radiator acts as a flow straightening device. Because this happened in all cases, the upstream profiles will not be presented in the text below. Profiles were taken at 53, 124, 203, 262, and

309 mm from the axle for the engine spacing of 2.5" and at 225, 251, 274, 302, 325, and 351 mm from the axle for the engine spacing of 0.5". Figures 4.16 and 4.17 show the locations where the turbulent kinetic energy profiles were taken for Figures 4.18-4.25.

4.3.1 1800 rpm, 100% shroud and engine block 2.5" away from fan

The first case investigated was for 100% shroud immersion, 2.5" engine block spacing, and 1800 rpm and is shown in Figure 4.18 (a)-(e). The regions of high TKE were only near the edge of the shroud. This is also to be expected because the air leaving the fan blade should be highly turbulent. In the third image, a band of moderate TKE is seen leaving the fan at about a 30 degree angle.

Figure 4.19 (a)-(e) shows the TKE profiles calculated for this setup. The profiles taken at 53, 124, 203, and 262 mm all had low TKE values. This was expected because the velocity in that region was very low as well. However, in plot (c), there is an area of high TKE near the fan blade on the 262 mm profile. The profile at 309 mm was high near the fan blade and then decreased toward the engine block. This is also to be expected because the air leaving the fan blade should be highly turbulent.

4.3.2 2200 rpm, 100% shroud and engine block 2.5" away from fan

Figure 4.20 (a)-(e) shows the TKE images taken when the fan speed is increased to 2200 rpm for the same geometry as the previous setup. In the first two images, high TKE can be found leaving the fan tip at about a 30 degree angle downward. In the other images, the only regions of high TKE were near the edge of the shroud.

In Figure 4.21 (a)-(e), the profiles taken at 53, 124, and 203mm all had low TKE values. This was expected because the velocity in that region was very low as well. In the plots (a) and (b), high TKE can be found near the fan tip in the 262 and 309 mm profiles. In the other plots, the only regions of high TKE were further away from the axle, in only the 309 mm profile. This is to be expected because the air leaving the fan blade should be highly turbulent. Overall, the TKE seemed to be about 30% higher then in the 1800 rpm case.

4.3.3 1800 rpm, 50% shroud and engine block 2.5" away from fan

Next, TKE was calculated when the shroud immersion was changed to 50% with 2.5" engine block spacing and a fan speed of 1800 rpm. Figure 4.22 (a)-(e) shows the TKE images taken for this setup. Two of the images in this set show a lot of noise. This could be because there was an oil buildup on the Plexiglas and also serves as a reminder why it is important to keep the equipment clean. However, it is clear even in those images that there is a region of high TKE near the fan tip. This region extends up to the edge of the shroud. This is to be expected because the air leaving the fan blade should be highly turbulent. There is also a high TKE region near the edge of the image between the fan blade and the engine block.

In Figure 4.23 (a)-(e), the profiles taken at 53, 124, and 203 mm all had low TKE values, for the same reasons as in the previous cases. The TKE profile at 309 mm has a high point near the fan blade and near the engine block, with lower TKE values in the middle. These TKE values are much higher then those in the 100% shroud case. Plot 4.23 (b) shows a high TKE region in the 203 and 309 mm profiles, while 4.23 (e) shows the 262 mm profile is similar to the 309 mm profile near the fan tip until about halfway to the engine block.

4.3.4 2200 rpm, 50% shroud and engine block 2.5" away from fan

TKE was then measured for the same geometry for 2200 rpm fan speed and Figure 4.24 (a)-(d) shows the TKE images taken for this setup. In the first two images, the area near the tip of the fan blade was not usable. This is probably due to the fact the flow was so turbulent it was difficult to get accurate velocity readings there because of particles exiting the laser sheet in the time between the two laser pulses. In looking at the nearest usable part of the image, it shows a moderate increase in the TKE that would seem to support the previous sentence. The second two images show a high TKE region near the fan blade tip. In the last image, this region extends at a 45 degree angle downstream.

The TKE profiles that were calculated are shown in Figure 4.25 (a)-(d). Again, the profiles taken at 53, 124, and 203mm all had low TKE values. In plot 4.25 (a) the 309 mm profile shows a high region of TKE, again about 30% higher then the 1800 rpm case. Plot 4.25 (b) shows a high TKE region in the 203 and 309 mm profiles also about 30% higher then the 1800 rpm case. However, plot 4.25 (c) and (d) show lower TKE then in the 1800 rpm case. In all plots, the region of high TKE is only near the fan tip, not near the engine block.

4.3.5 1800 rpm, 100% shroud and engine block 0.5" away from fan

In the next case studied, the engine block spacing was reduced to 0.5" with 100% shroud immersion, with the images shown in Figure 4.26 (a)-(e). A small region of high TKE is seen moving away from the fan as the images progress. It moves almost entirely in the x- direction. The last image shows it reforming. There is also a region of moderate TKE

in the lower right corner of each image. This could be the region from the previous blade after it has reflected off the side of the compartment.

In Figure 4.27(a)-(e), the TKE profiles that were calculated are shown. Once again, the profiles taken at 225, 251, and 274 mm all had low TKE values. The profiles taken at 302, 325, and 351mm all showed the same trends. All of those profiles show a region of high TKE near the fan blade, then it decreases in the middle, and increases near the engine block. In plots (a) and (b), the highest TKE occurs in the 302 mm profile. In plot (c) the highest TKE is in profile 325 mm, and in plots (d) and (e) it occurs in the 351 mm profile. This movement means the region of high TKE is leaving the fan blade. Plot (b) shows an increase in overall TKE from plot (a). The TKE then decreases in plot (c) and continues to decrease in (d). Plots (d) and (e) are nearly identical.

4.3.6 2200 rpm, 100% shroud and engine block 0.5" away from fan

Next, the fan speed was increased to 2200 for the previous geometry and Figure 4.28 (a)-(e) shows the TKE profiles taken for this setup. Again, a small region of high TKE is seen moving away from the fan as the images progress. It moves almost entirely in the radial direction. As expected, this region is bigger then in the 1800 rpm case. The region looks like it is pinched through the area between the shroud and the engine block, because after it passes, it expands. Again there is a region of moderate TKE in the lower right corner of each image. This could be the region from the previous blade after it has bounced off the side of the compartment. The fourth image seems to have all its values shifted high because instead of no TKE in most of the image, it shows moderate levels of TKE in the whole image, an

indication of noisier velocity fields than in the other cases investigated. The reason for this discrepancy from the other cases is unknown.

Figure 4.29(a)-(e) shows the TKE profiles that were calculated for this case. The profiles taken at 225, 251, and 274 mm all had low TKE values. Again, the overall TKE was higher then in the 1800 rpm case. The profiles taken at 302, 325, and 351 mm all showed the same trends. All of those profiles show a region of high TKE near the fan blade, then it decreases in the middle, but only in plots (c), (d), and (e) did it increases near the engine block. In plots (a) and (b), the highest TKE occurs in the 302 mm profile. In plot (c) the highest TKE is in profile 325 mm, and in plots (d) and (e) it occurs in the 351 mm profile. This movement means the region of high TKE is leaving the fan blade. Plot (b) shows a decrease in overall TKE from plot (a). The TKE then decreases in plot (c) but increased in (d). Plots (d) and (e) are nearly identical.

4.3.7 1800 rpm, 50% shroud and engine block 0.5" away from fan

The final geometry investigated was 50% shroud immersion with an engine spacing of 0.5" and 2200 rpm with the TKE images shown in Figure 4.30 (a)-(e). A small region of high TKE is seen moving away from the fan as the images progress. It forms on the corner of the fan blade and moves mostly in the radial direction, only moving in the axial direction 0.5" by the time it reaches the edge of the image.

Finally, Figure 4.31 (a)-(e) shows the TKE profiles that were calculated from this image set. Again, the profiles taken at 225, 251, and 274 mm all had low TKE values. For the other profiles, the maximum value of TKE occurs in the middle, between the fan blade and engine block, which is different from all previous cases. Plot (b) shows all profiles with

very low TKE. In plot (c), the TKE in profile 302mm is high near the middle. Moving to plot (d), the high TKE is in the 325 mm profile. Plots (e) and (a) then show the high TKE in the 351 mm profile. Again, this movement means the region of high TKE is leaving the fan blade.

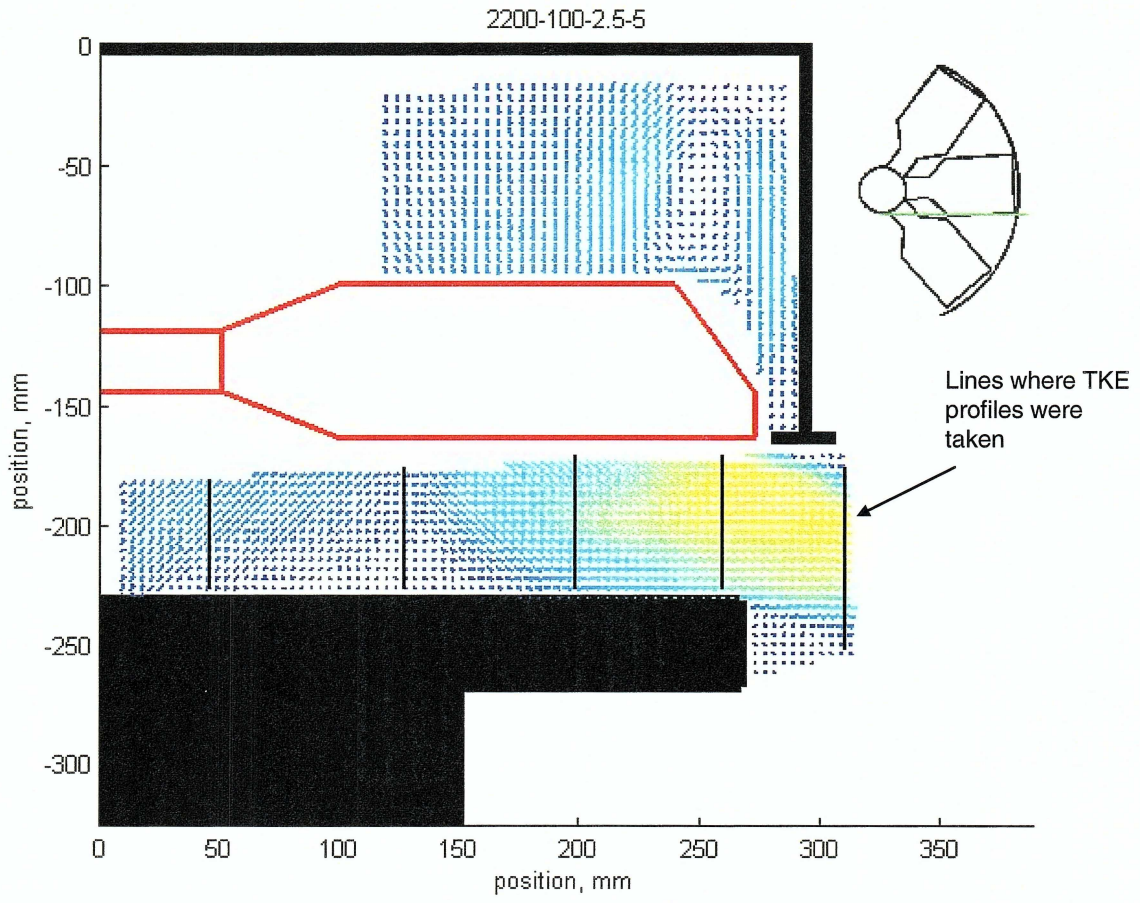

Figure 4.16 Position of lines where TKE profiles were taken.

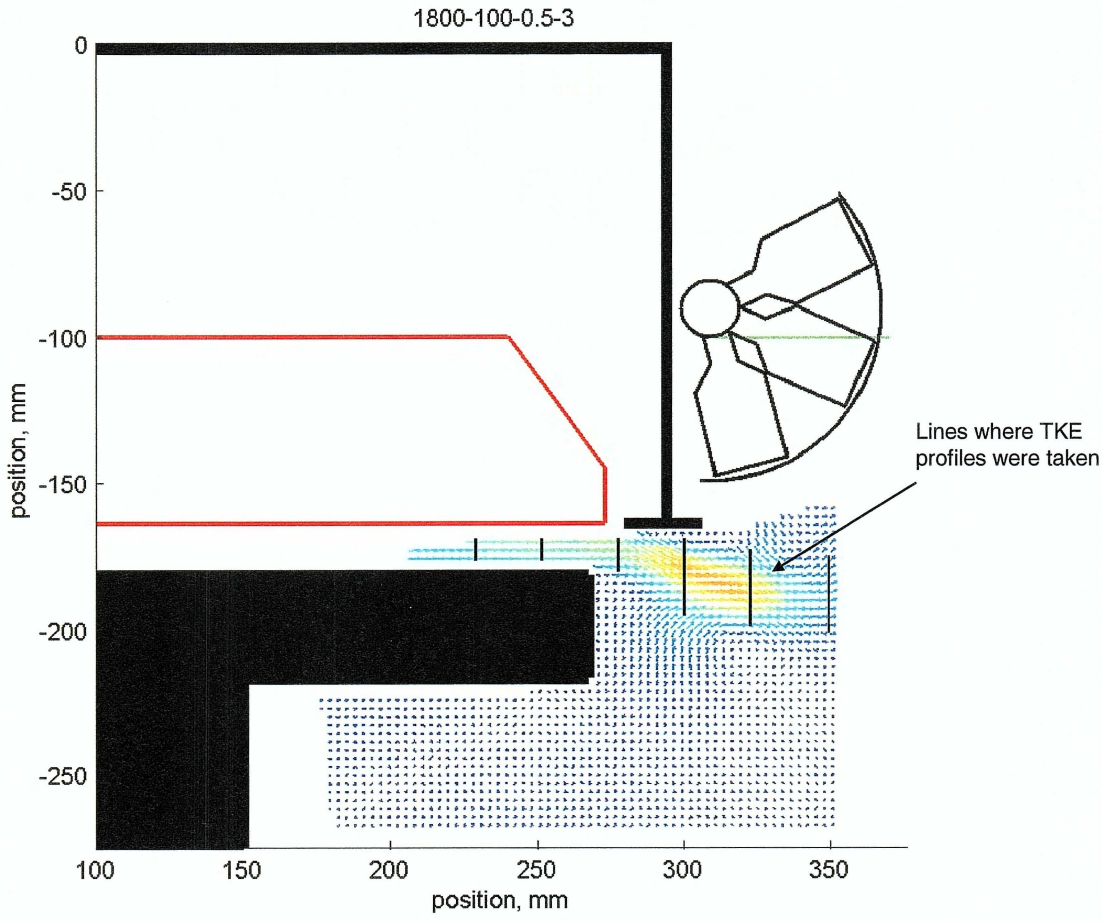

Figure 4.17 Position of lines where TKE profiles were taken.

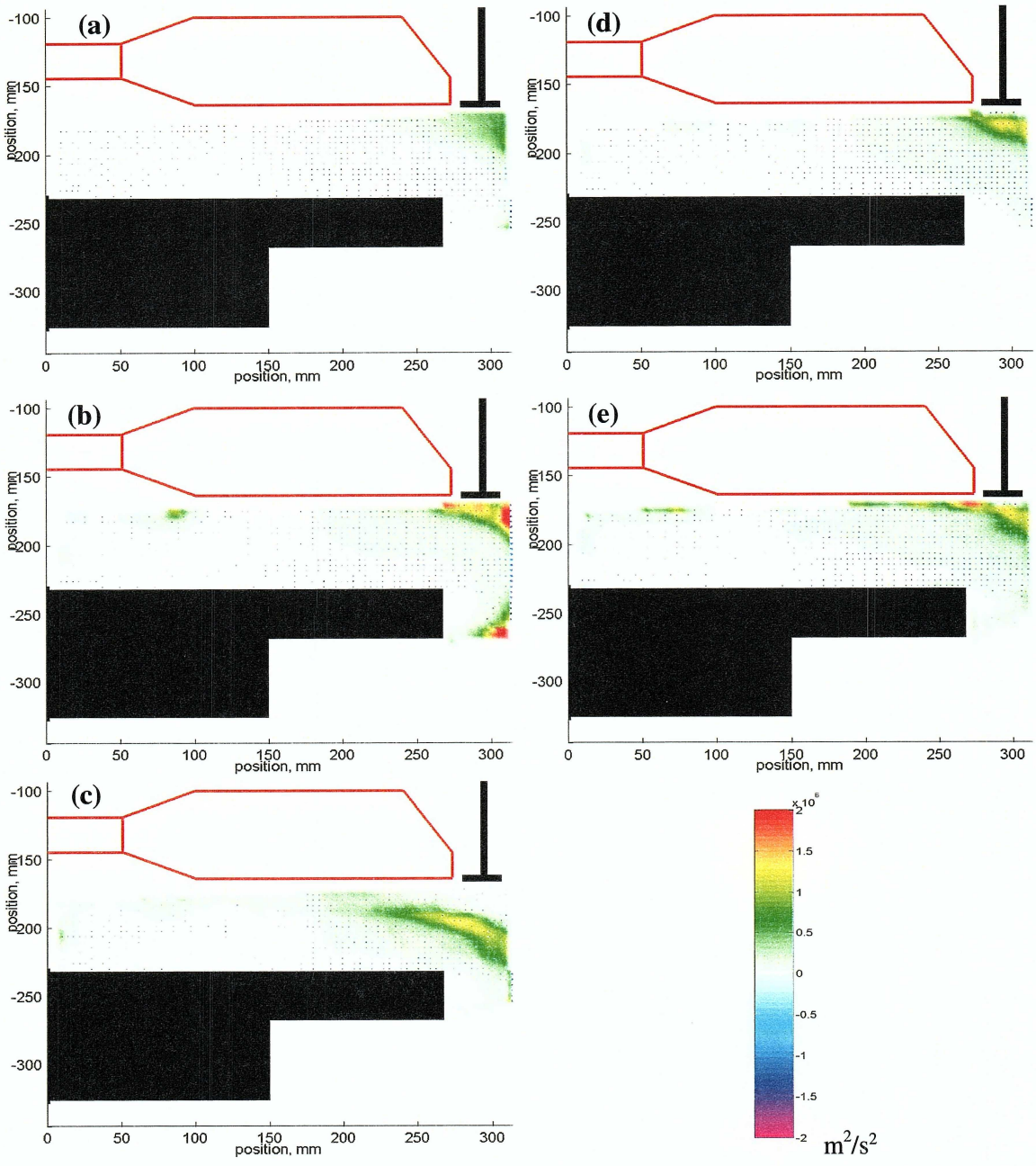

Figure 4.18 (a)-(e) Series of turbulent kinetic energy (TKE) images at a constant fan blade positions for 1800 rpm, 100% immersion, and 2.5 inch engine spacing; where (a) 3°, (b) 11°, (c) 20°, (d) 28°, and (e) 37°

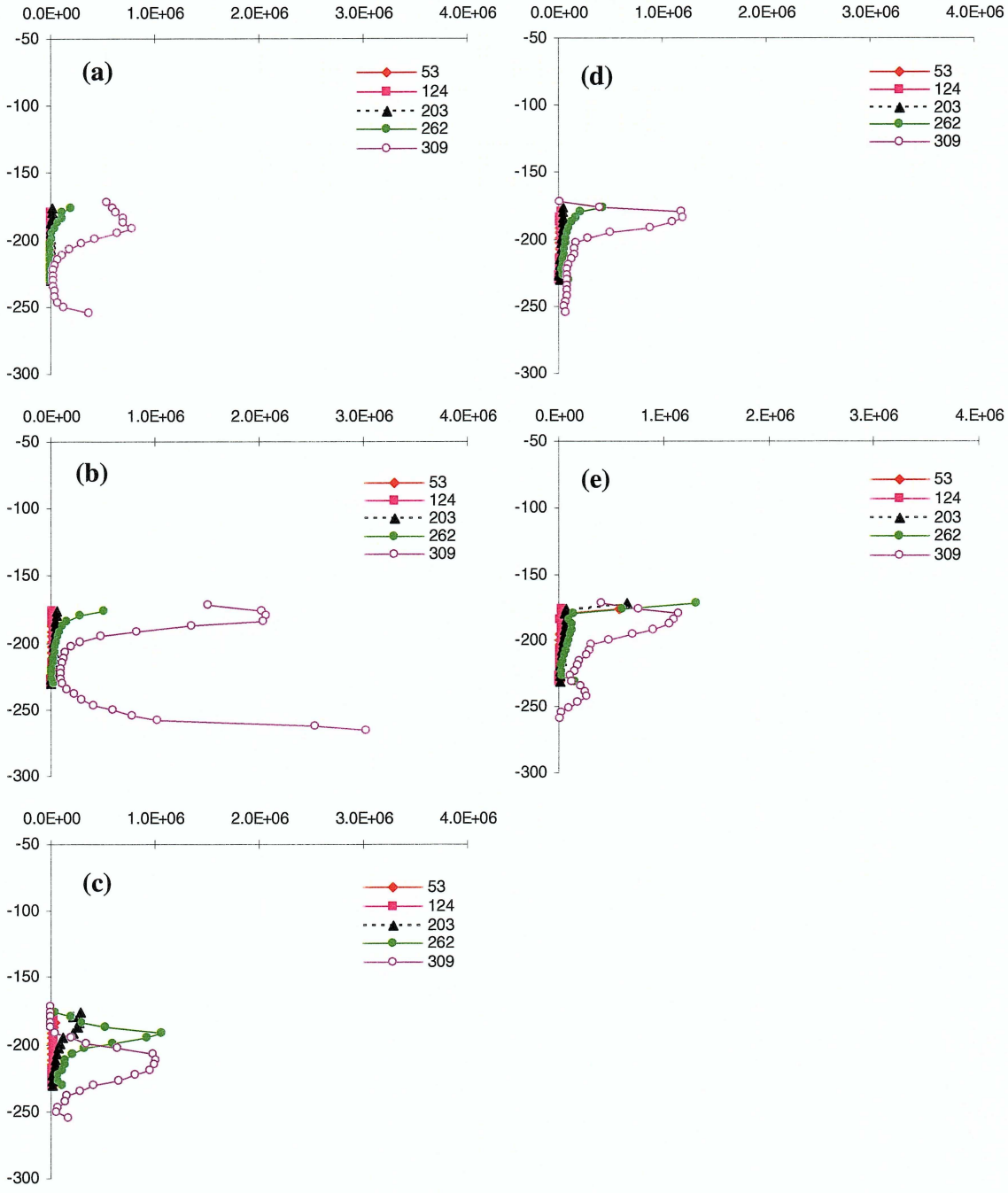

Figure 4.19 (a)-(e) Series of turbulent kinetic energy (TKE) profiles at a constant fan blade positions for 1800 rpm, 100% immersion, and 2.5 inch engine spacing; where (a) 3°, (b) 11°, (c) 20°, (d) 28°, and (e) 37°.

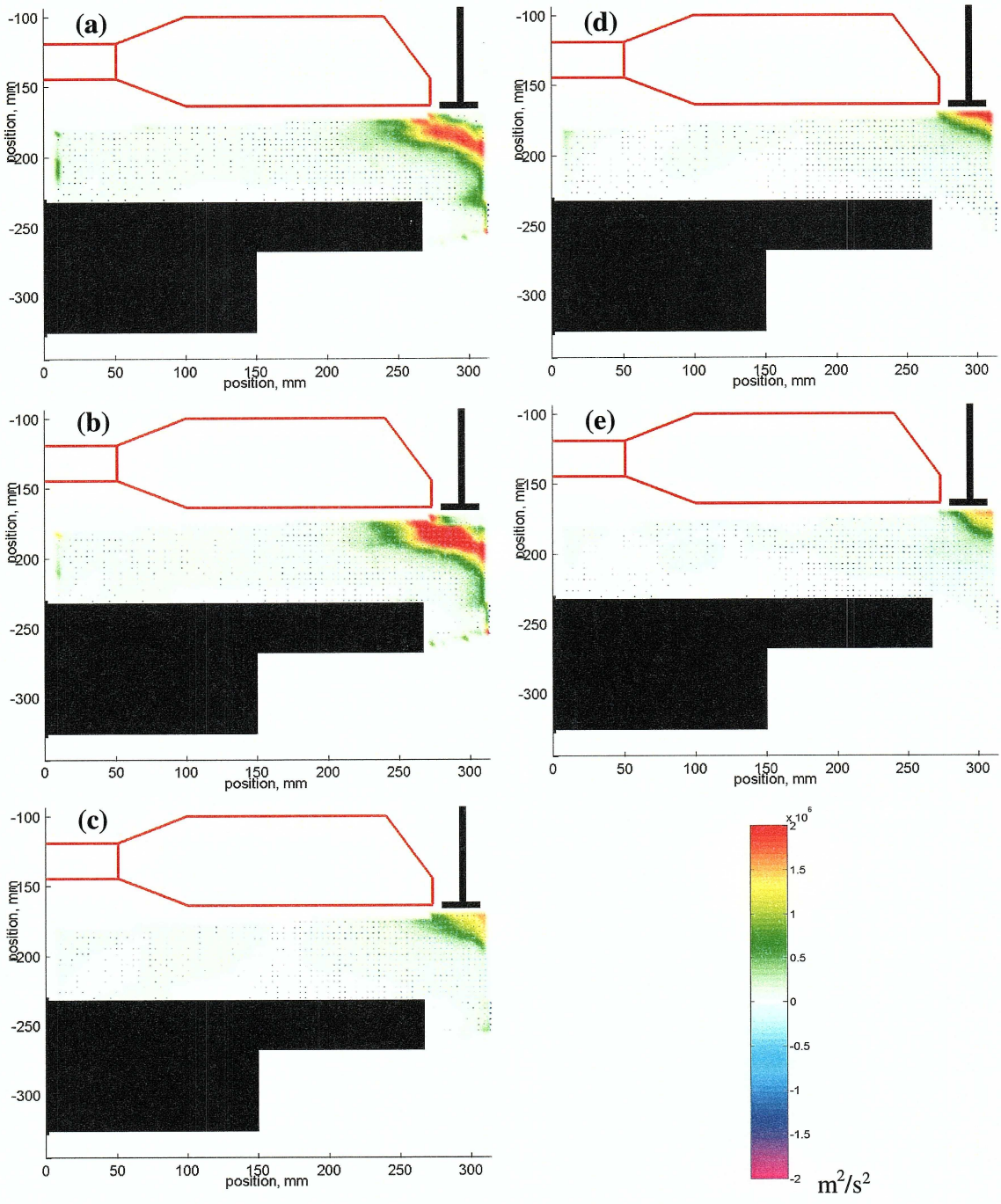

Figure 4.20 (a)-(e) Series of turbulent kinetic energy (TKE) images at a constant fan blade positions for 2200 rpm, 100% immersion, and 2.5 inch engine spacing; where (a) 5°, (b) 14°, (c) 22°, (d) 31°, and (e) 40°.

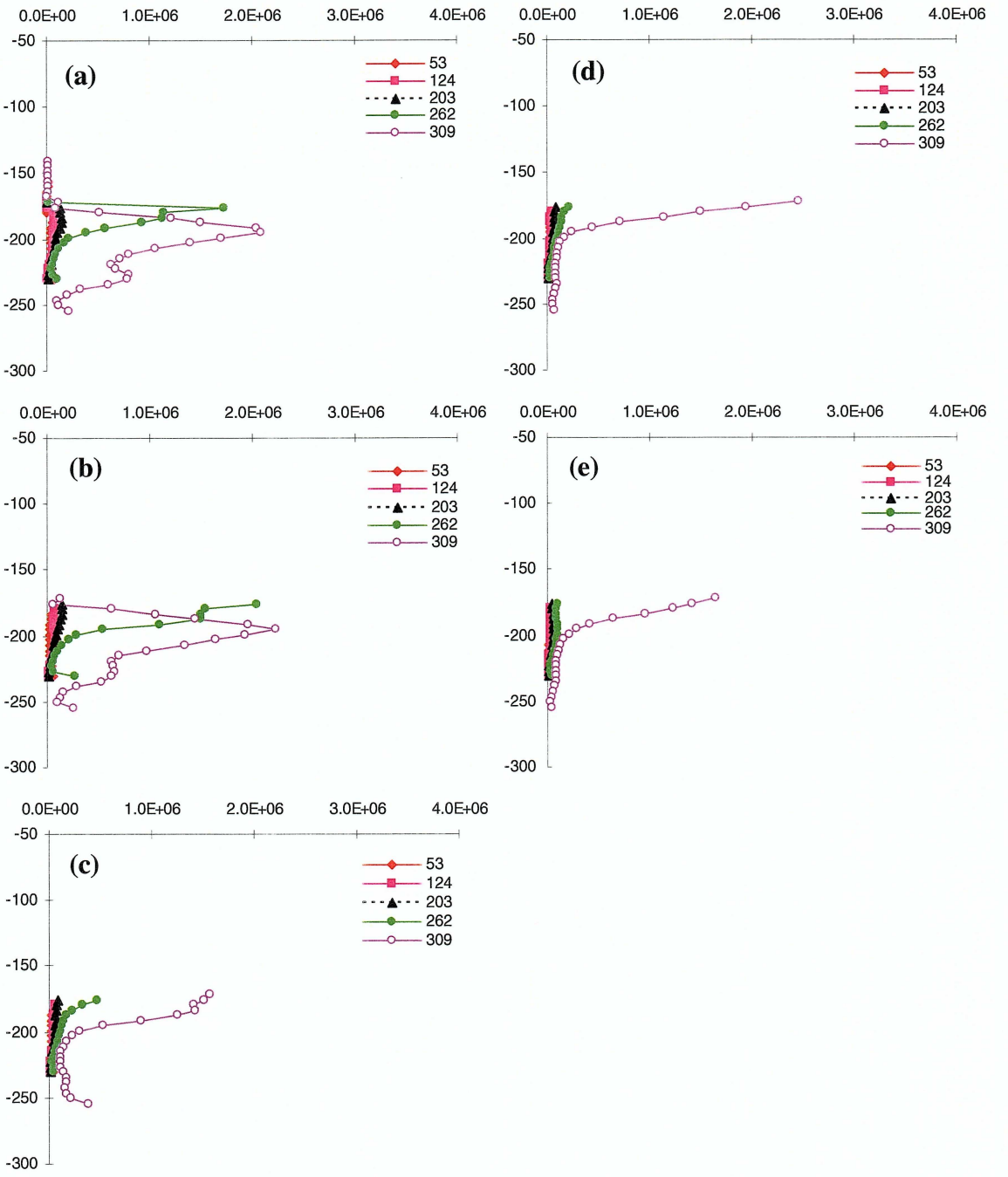

Figure 4.21 (a)-(e) Series of turbulent kinetic energy (TKE) profiles at a constant fan blade positions for 2200 rpm, 100% immersion, and 2.5 inch engine spacing; where (a) 5°, (b) 14°, (c) 22°, (d) 31°, and (e) 40°.

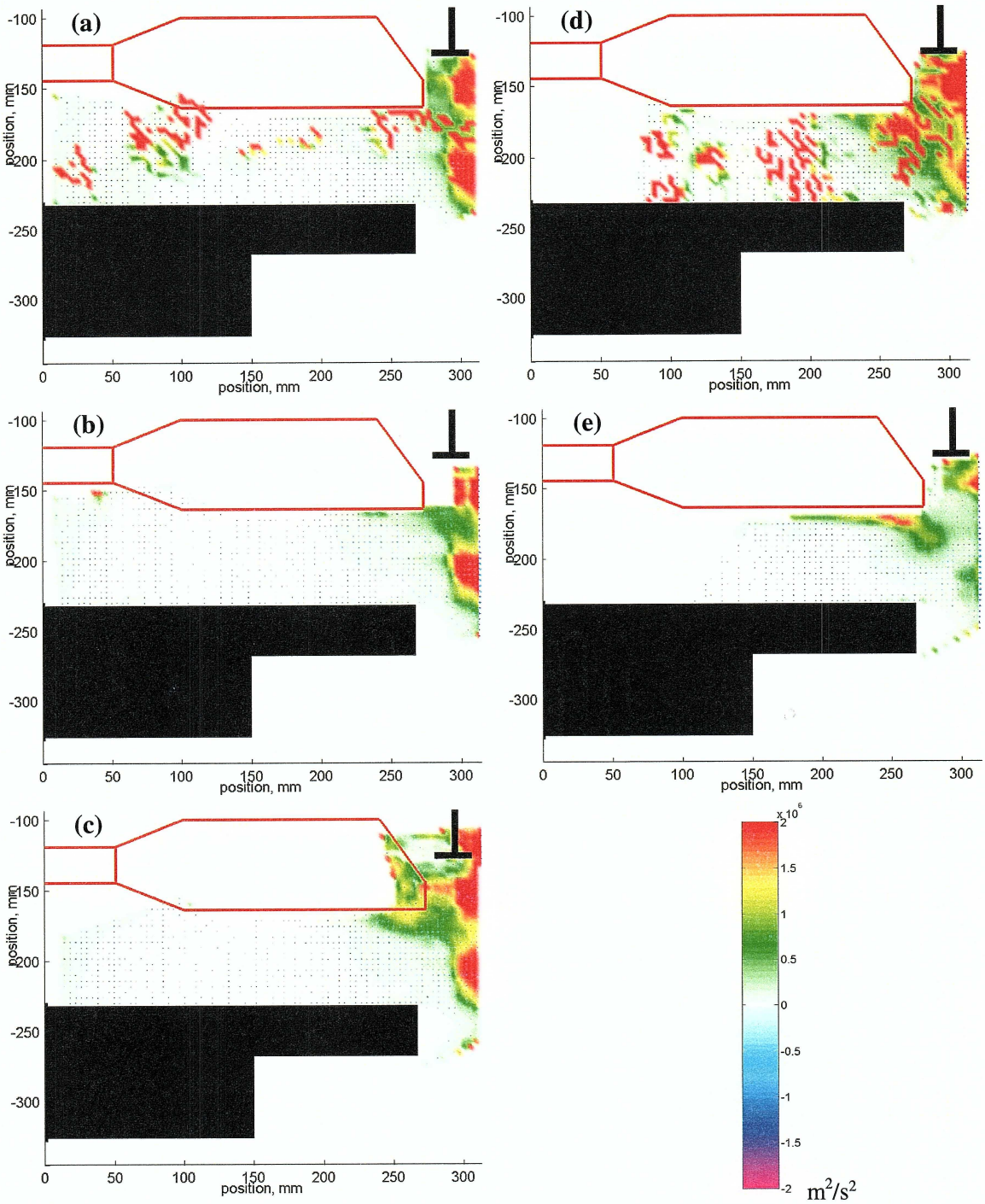

Figure 4.22 (a)-(e) Series of turbulent kinetic energy (TKE) images at a constant fan blade positions for 1800 rpm, 50% immersion, and 2.5 inch engine spacing; where (a) 28°, (b) 37°, (c) 3°, (d) 11°, and (e) 20°.

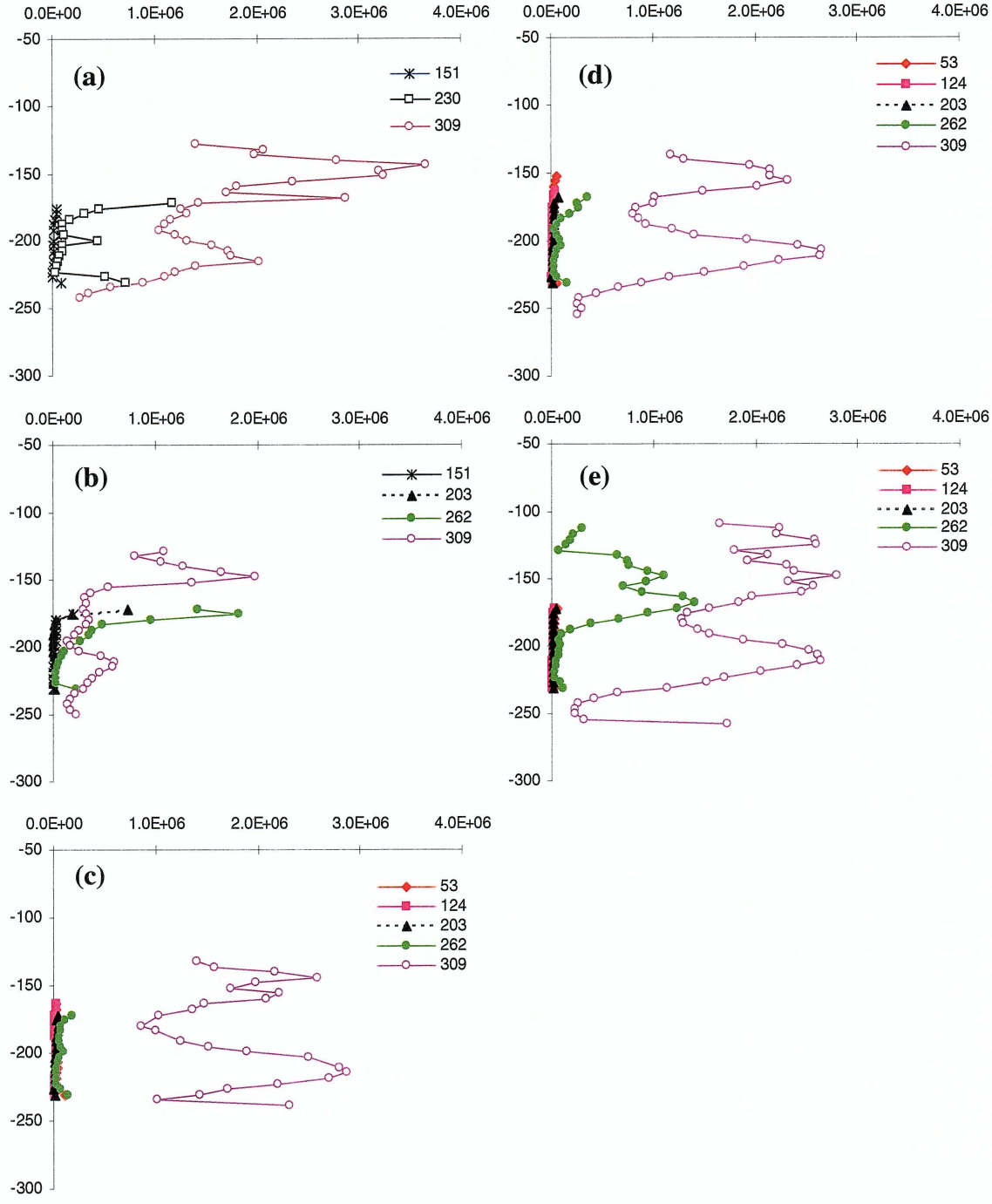

Figure 4.23 (a)-(e) Series of turbulent kinetic energy (TKE) profiles at a constant fan blade positions for 1800 rpm, 50% immersion, and 2.5 inch engine spacing; where (a) 28°, (b) 37°, (c) 3°, (d) 11°, and (e) 20°.

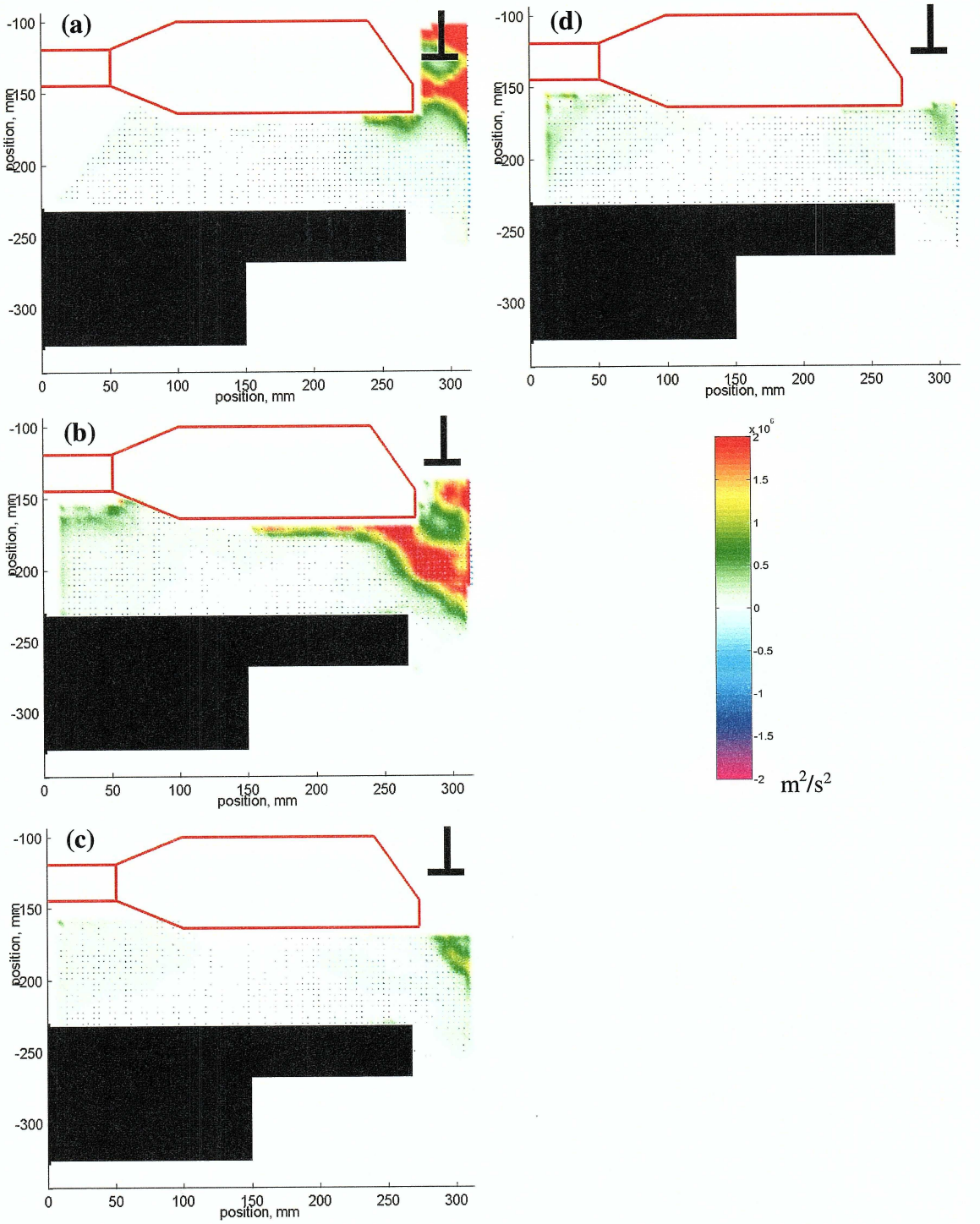

Figure 4.24 (a)-(d) Series of turbulent kinetic energy (TKE) images at a constant fan blade positions for 2200 rpm, 50% immersion, and 2.5 inch engine spacing; where (a) 31°, (b) 40°, (c) 14° and (e) 22°.

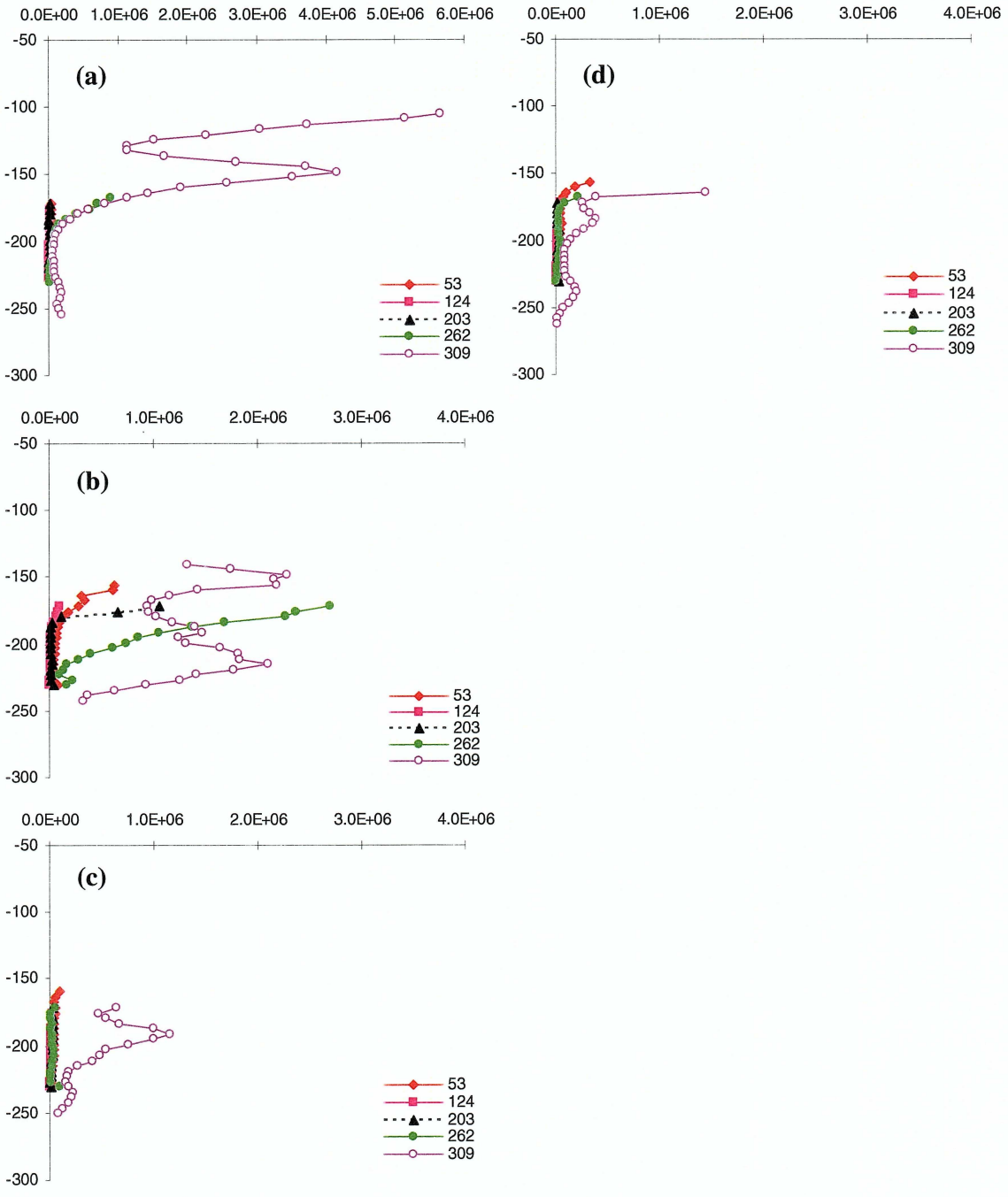

Figure 4.25 (a)-(d) Series of turbulent kinetic energy (TKE) profiles at a constant fan blade positions for 2200 rpm, 50% immersion, and 2.5 inch engine spacing; where (a) 31°, (b) 40°, (c) 14° and (e) 22°.

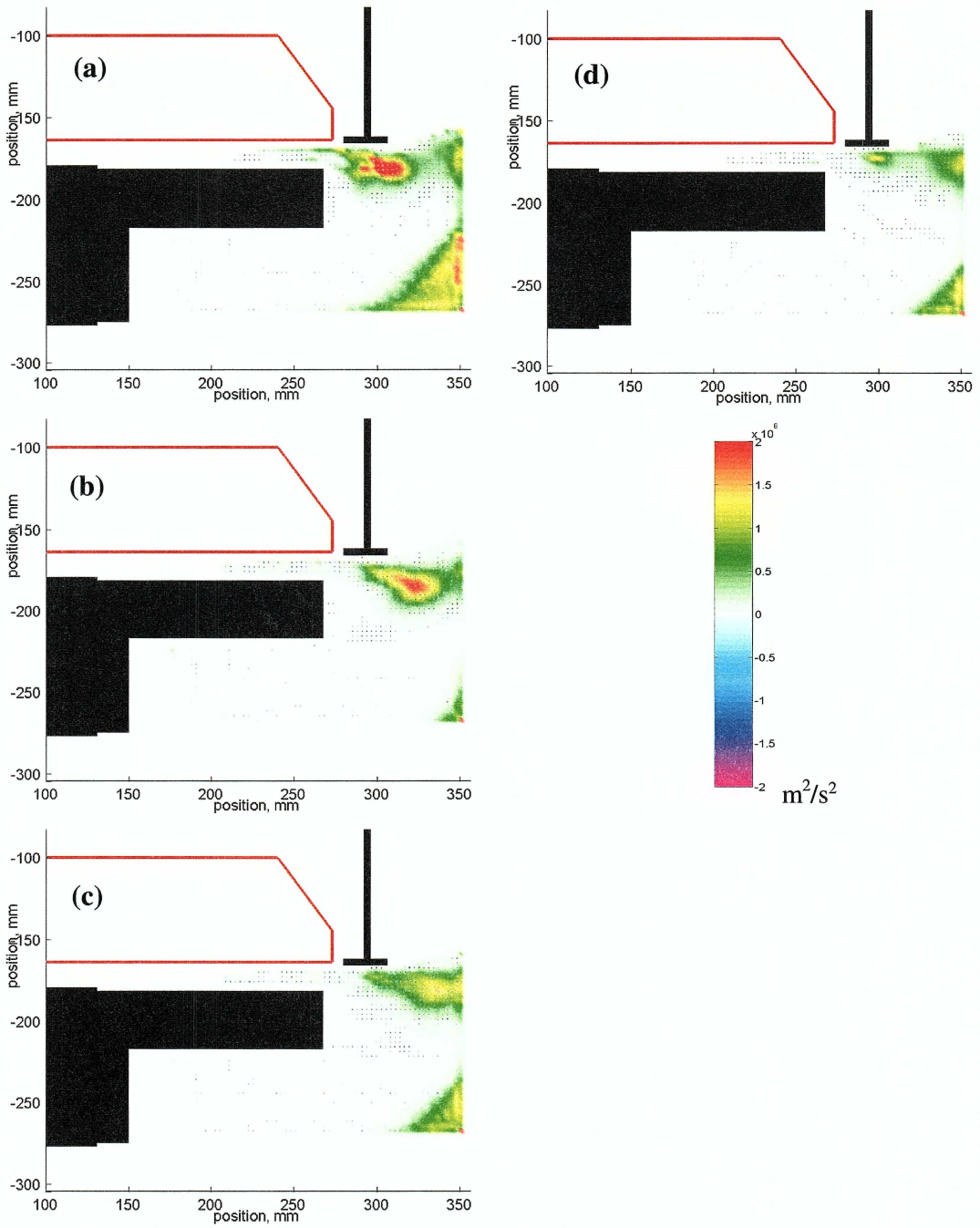

Figure 4.26 (a)-(d) Series of turbulent kinetic energy (TKE) images at a constant fan blade positions for 1800 rpm, 100% immersion, and 0.5 inch engine spacing; where (a) 37°, (b) 3°, (c) 11°, and (d) 20°.

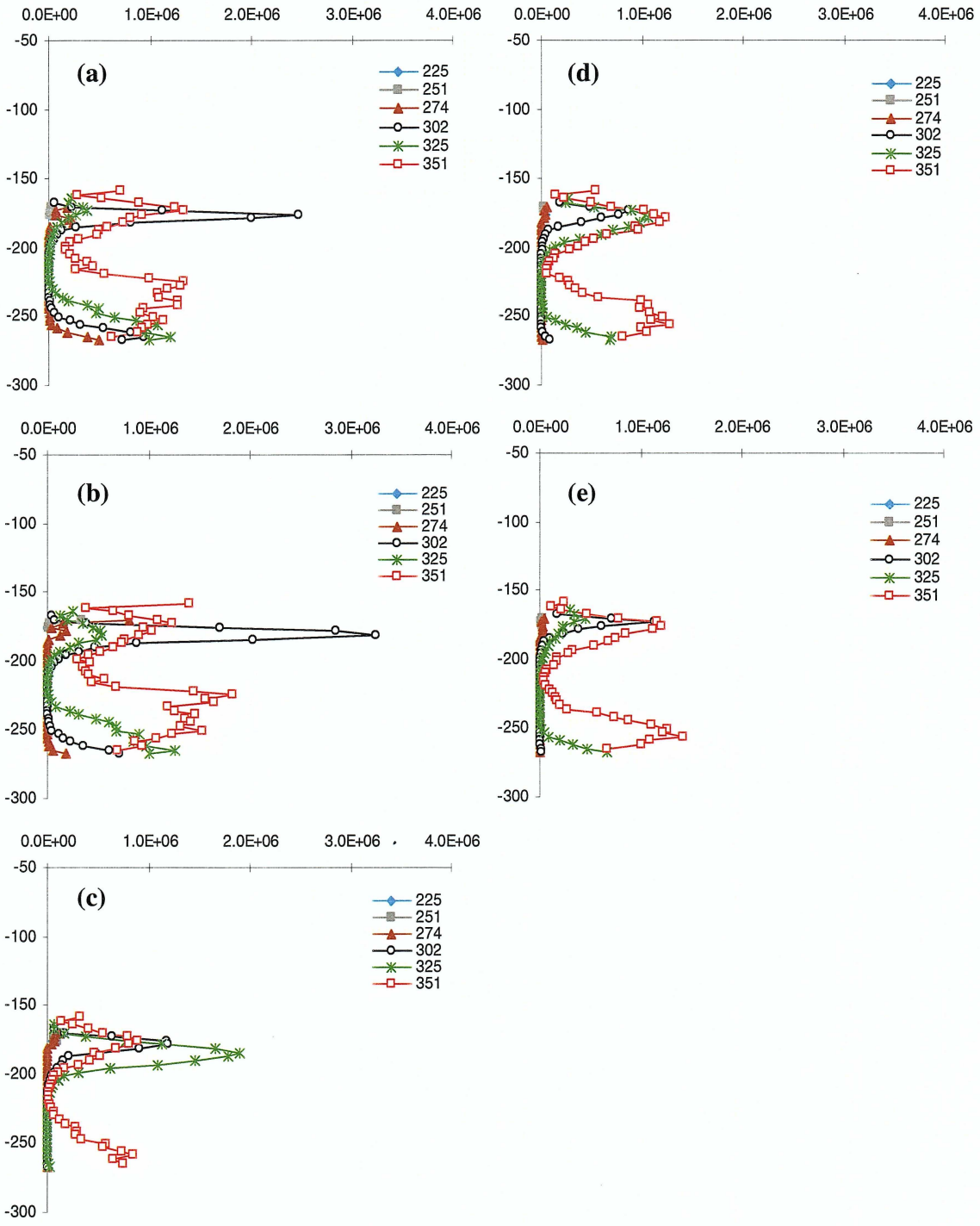

Figure 4.27 (a)-(e) Series of turbulent kinetic energy (TKE) profiles at a constant fan blade positions for 1800 rpm, 100% immersion, and 0.5 inch engine spacing; where (a) 28°, (b) 37°, (c) 3°, (d) 11°, and (e) 20°.

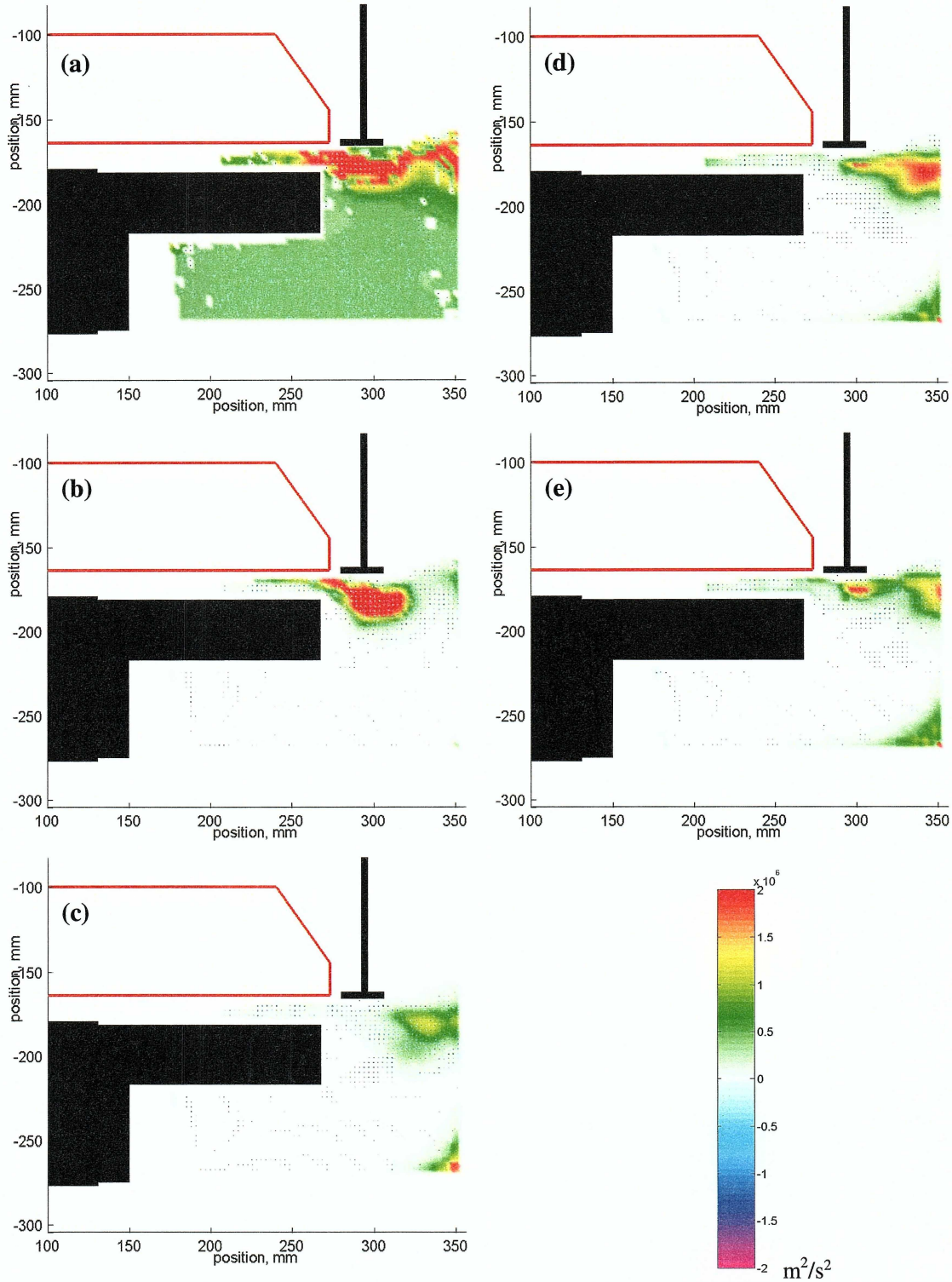

Figure 4.28 (a)-(e) Series of turbulent kinetic energy (TKE) images at a constant fan blade positions for 2200 rpm, 100% immersion, and 0.5 inch engine spacing; where (a) 31°, (b) 40°, (c) 5°, (d) 14°, and (e) 22°.

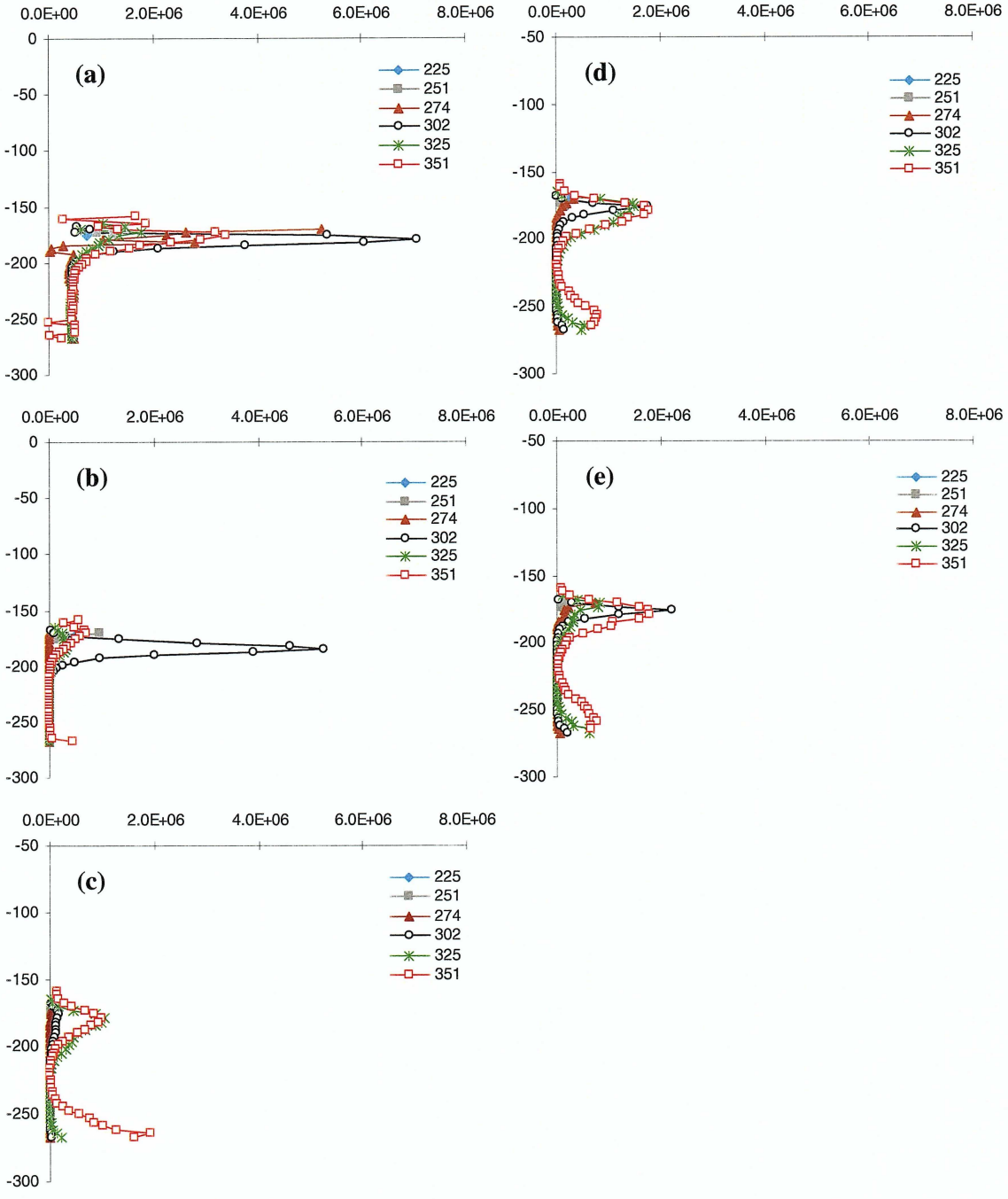

Figure 4.29 (a)-(e) Series of turbulent kinetic energy (TKE) profiles at a constant fan blade positions for 2200 rpm, 100% immersion, and 0.5 inch engine spacing; where (a) 31°, (b) 40°, (c) 5°, (d) 14°, and (e) 22°.

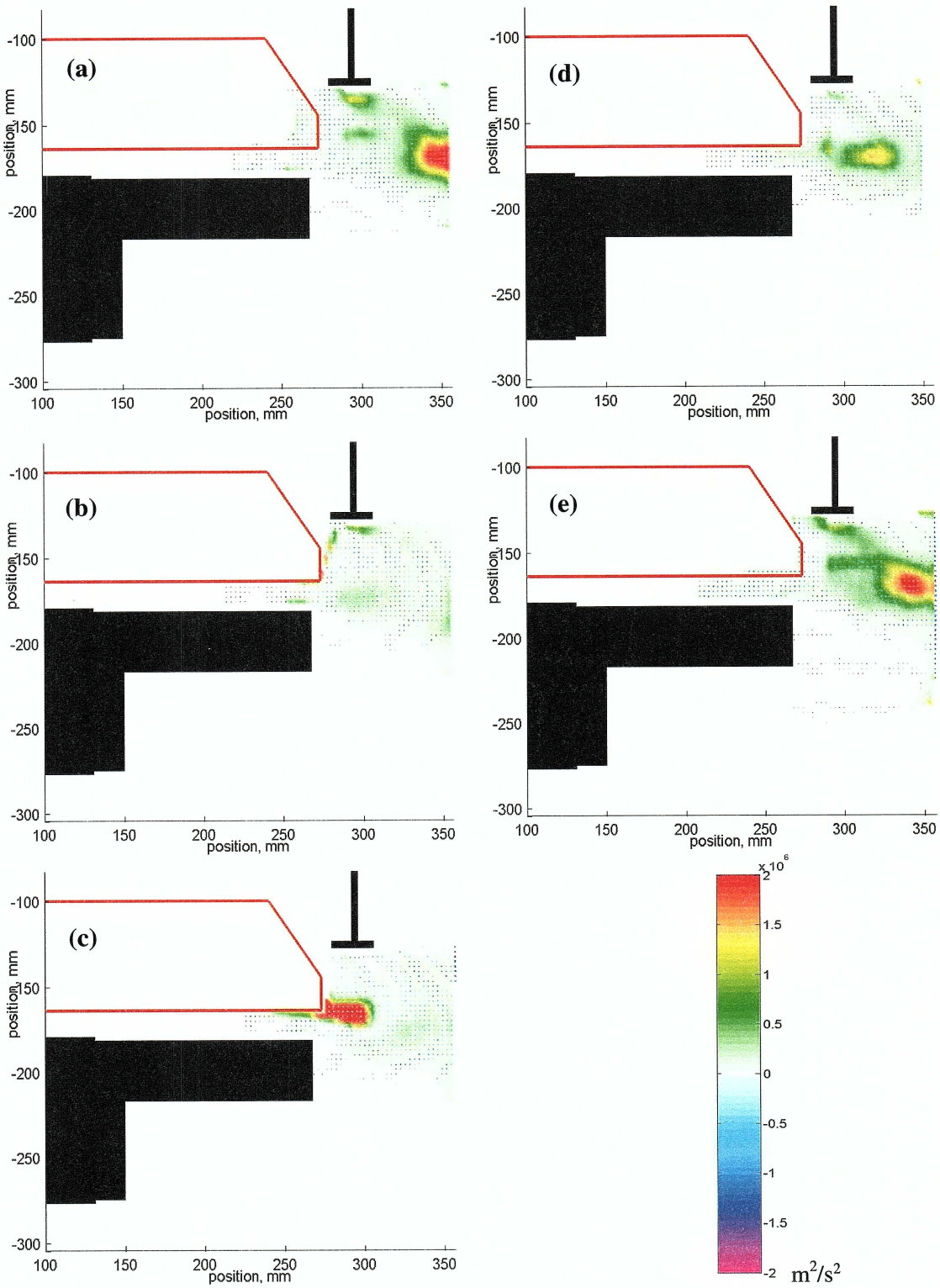

Figure 4.30 (a)-(e) Series of turbulent kinetic energy (TKE) images at a constant fan blade positions for 1800 rpm, 50% immersion, and 0.5 inch engine spacing; where (a) 37°, (b) 3°, (c) 11°, (d) 20°, and (e) 28°.

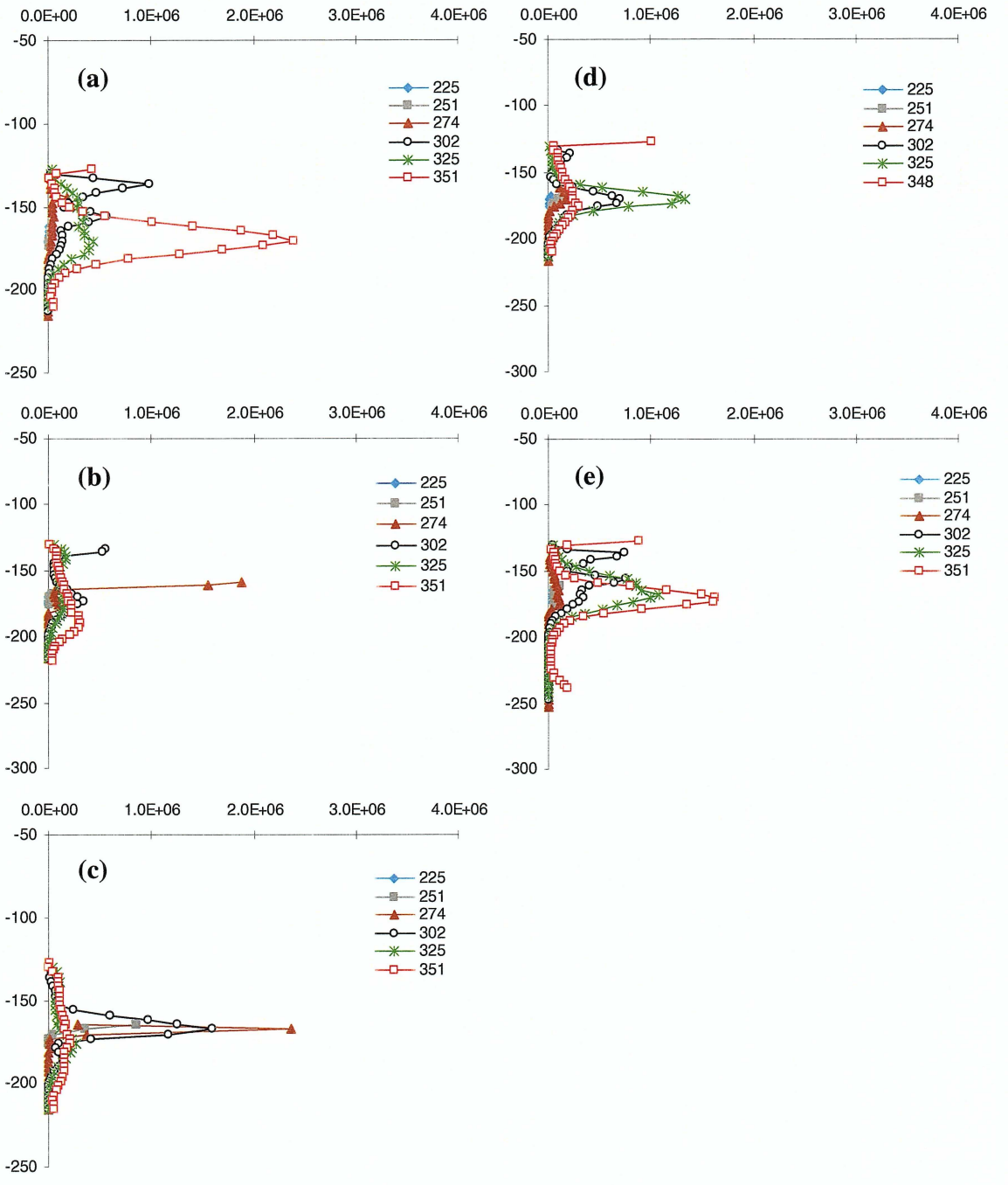

Figure 4.31 (a)-(e) Series of turbulent kinetic energy (TKE) profiles at a constant fan blade positions for 1800 rpm, 50% immersion, and 0.5 inch engine spacing; where (a) 37°, (b) 3°, (c) 11°, (d) 20°, and (e) 28°.

4.4 Momentum plots

The air leaving the fan blades resembles an unsteady jet (at least within the two-dimensional region captured in the PIV velocity fields). To describe the time varying behavior of this jet-like region, jet momentum was calculated from the mean velocity fields using the relationship shown below:

$$Momentum = \rho \times v^2 \times A$$

Where ρ is the density of the air, v is the velocity, and A is the area. The area was calculated by using distance between velocity vectors as on side and a unit depth as the other side.

Momentum profiles for the jet were calculated at different distances away from the axle. These profiles were then compared at constant fan positions and at constant distances. Figures 4.32 and 4.33 show the positions of the lines were the momentum was calculated.

4.4.1 Constant fan position

These sets of momentum profiles presented below depict the structure of the jet at a given fan position.

4.4.1.1 1800 rpm, 100% shroud and engine block 2.5" away from fan

Momentum profile plots for 100% shroud immersion and 2.5" engine block spacing for a fan speed of 2200 rpm are shown in Fig. 4.34 (a)-(e). The momentum lines at 150 mm and 200 mm are between the fan blade and the engine block. Their momentum is lower near the edges and higher in the middle of the jet as expected. As the distance from the axle

increases, so does the overall momentum. In the last fan position, the momentum is very high near the fan blade at 150 mm and 200 mm but near zero at the engine block. This could be because the bottom of the fan blade is passing that point, as shown in the velocity figures.

4.4.1.2 2200 rpm, 100% shroud and engine block 2.5" away from fan

Figure 4.35 (a)-(e) show the momentum profile plots taken when the fan speed is increased to 2200 rpm for the same geometry as the previous setup. The plots in of this setup look nearly identical to the previous setup, the only difference being the momentum is shifted higher, as expected because the speed is higher. The momentum lines at 150 mm and 200 mm are between the fan blade and the engine block. Their momentum is lower near the edges and higher in the middle of the jet as expected. As the distance from the axle increases, so does the overall momentum. In the last fan position, the momentum is very high near the fan blade at 150 mm and 200 mm but near zero at the engine block. This could be because the bottom of the fan blade is passing that point, as shown in the velocity figures.

4.4.1.3 1800 rpm, 50% shroud and engine block 2.5" away from fan

In this setup, the 100% shroud was removed and replaced with a 50% shroud. Figure 4.36 (a)-(e) show the momentum profiles taken at this setup. Again, the momentum lines at 150 mm and 200 mm are between the fan blade and the engine block. Their momentum is lower near the edges and higher in the middle of the jet as expected. As the distance from the axle increases, so does the overall momentum. At the 250 mm line, the momentum is high near the fan and lower near the engine block. At the 300 mm line, this changes, with a very low momentum level near the fan and a higher momentum level toward the engine block.

This is probably due to the different type of shroud. As noted previously, this setup makes the jet move more in the axial direction instead of only in the radial direction. Again in the last fan position, the momentum is very high near the fan blade at 150 mm and 200 mm.

4.4.1.4 2200 rpm, 50% shroud and engine block 2.5" away from fan

The fan speed for this setup was increased to 2200 rpm for the same geometry as the previous setup. The plots of this setup (Figure 4.37(a)-(d)) reflected that, in that they look nearly identical to the previous setup, the only difference being the momentum is shifted higher, as expected because the speed is higher. The momentum lines at 150 mm and 200 mm are between the fan blade and the engine block. Their momentum is lower near the edges and higher in the middle of the jet as expected. As the distance from the axle increases, so does the overall momentum. At the 250 mm line, the momentum is high near the fan and lower near the engine block. At the 300 mm line, this changes, with a very low momentum level near the fan and a higher momentum level toward the engine block. This is probably due to the different type of shroud. As noted previously, this setup makes the jet move more in the axial direction instead of only in the radial direction. Again in the last fan position, the momentum is very high near the fan blade at 150 mm and 200 mm.

4.4.1.5 1800 rpm, 100% shroud and engine block 0.5" away from fan

In this setup, the 100% shroud is placed back on, and the engine block is moved to within 0.5" of the fan blade. Figure 4.38(a)-(e) shows the plots for this setup. Because the space between the fan blade and engine block was so small, it was necessary to start the momentum lines at the 225 mm mark instead of the 150 mm mark as done with the previous

setups. The first 3 lines show very little momentum although it does increase slightly the closer to the edge of the fan blade the jet gets. Once the jet passes the edge of the engine block, there is a sharp increase in momentum. The highest region is on the fan blade side of the jet.

4.4.1.6 2200 rpm, 100% shroud and engine block 0.5" away from fan

This had the same geometry as the previous setup, but the fan speed was increased to 2200 rpm. The plots of this setup (Figure 4.39(a)-(e)) look nearly identical to the previous setup, the only difference being the momentum is shifted higher, as expected because the speed is higher. The first 3 lines show very little momentum although it does increase slightly the closer to the edge of the fan blade the jet gets. Once the jet passes the edge of the engine block, there is a sharp increase in momentum. The highest region is on the fan blade side of the jet.

4.4.1.7 1800 rpm, 50% shroud and engine block 0.5" away from fan

Finally, the 50% shroud is placed examined again in this setup. Figure 4.40(a)-(e) shows the plots for this setup. The first 2 lines show very little momentum although it does increase slightly the closer to the edge of the fan blade the jet gets. The 275 mm line shows some increase in momentum as this is near the edge of the engine block. The 300 mm line shows a curved profile of the jet, lower momentum near the edges and higher in the middle. The highest reading is in the plot (b) with not much change in the plot (c). After the plot (c), the jet begins to decay, with the momentum becoming lower and the profile flattening out in the middle.

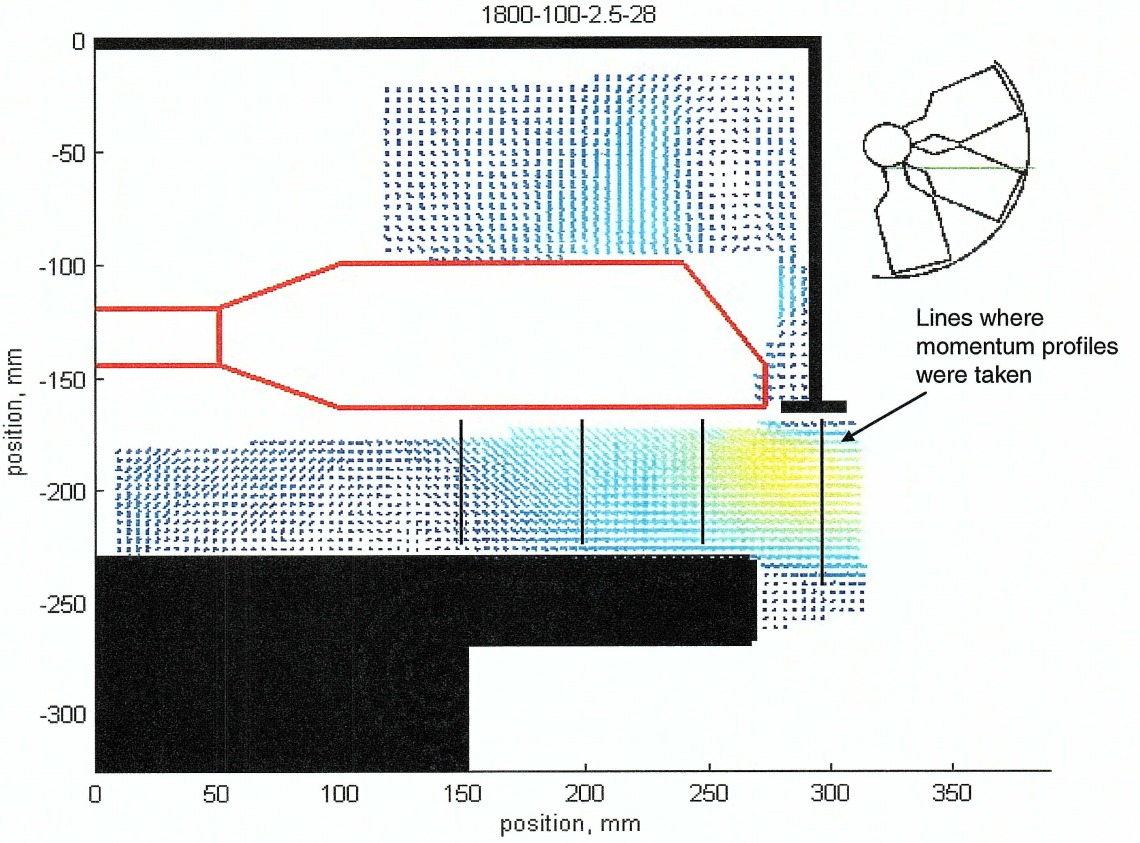

Figure 4.32 Position of lines where momentum profiles were taken.

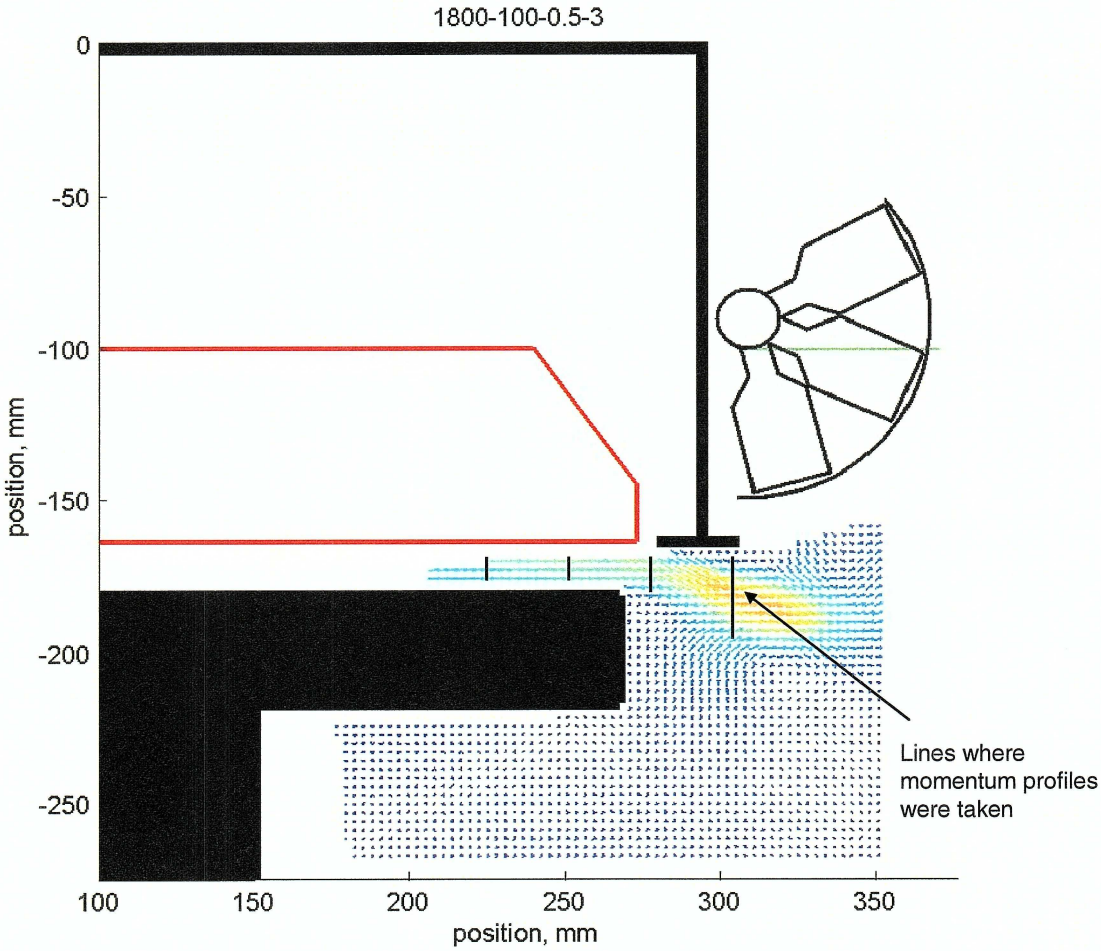

Figure 4.33 Position of lines where momentum profiles were taken.

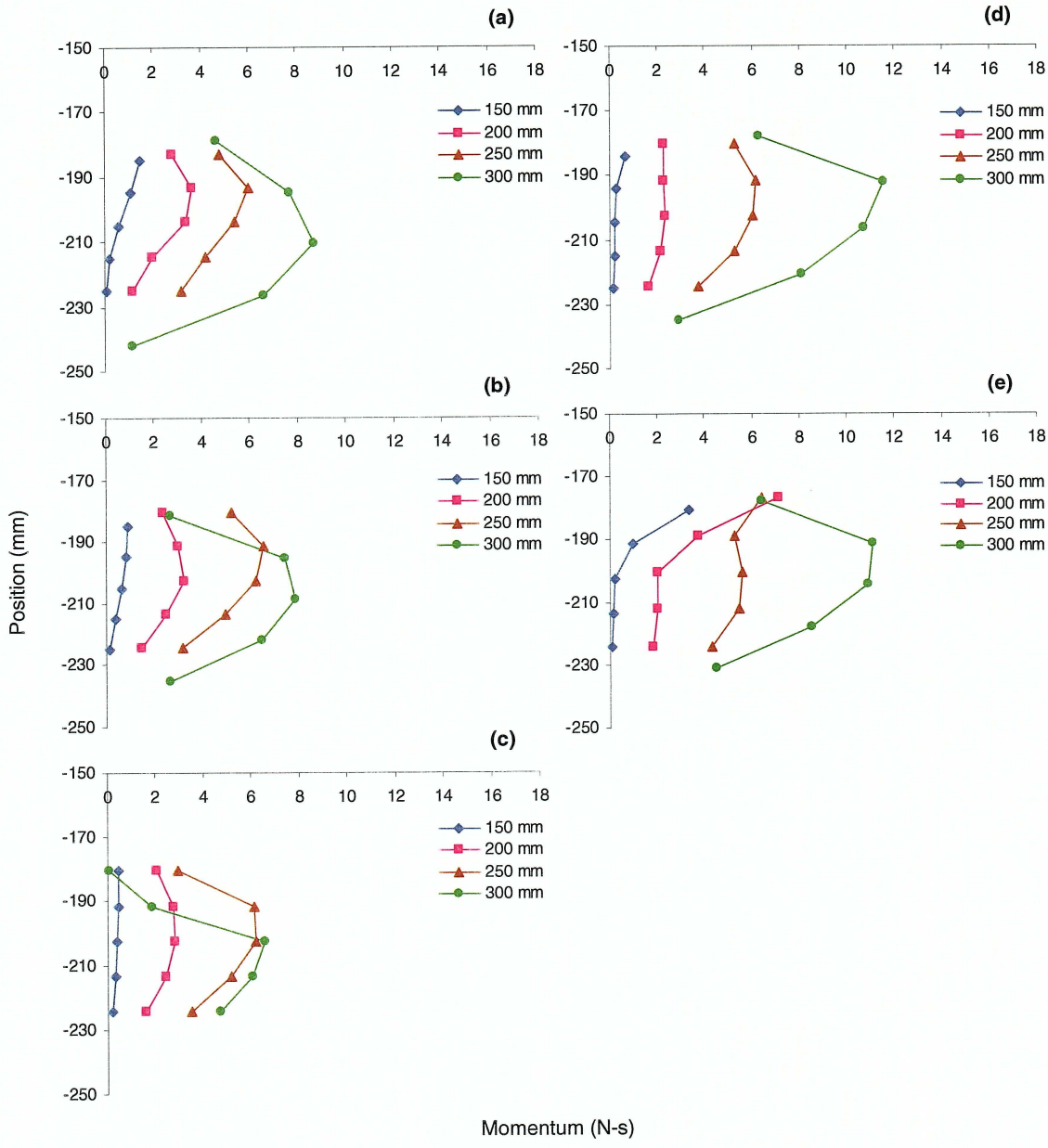

Figure 4.34 (a)-(e) Series momentum plots at a constant fan blade positions for 1800 rpm, 100% immersion, and 2.5 inch engine spacing; where (a) 3°, (b) 11°, (c) 20°, (d) 28°, and (e) 37°.

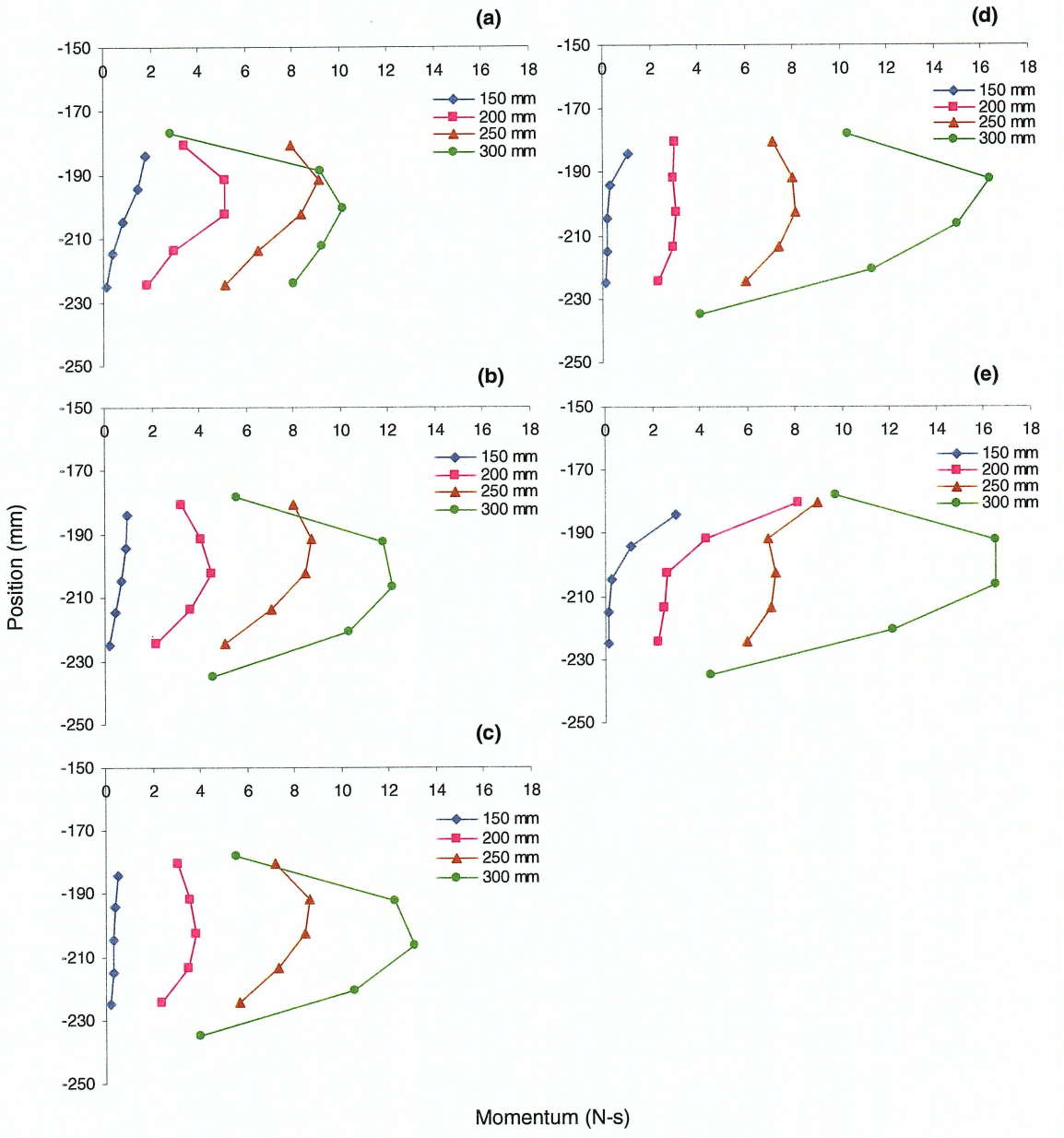

Figure 4.35 (a)-(e) Series momentum plots at a constant fan blade positions for 2200 rpm, 100% immersion, and 2.5 inch engine spacing; where (a) 5°, (b) 14°, (c) 22°, (d) 31°, and (e) 40°.

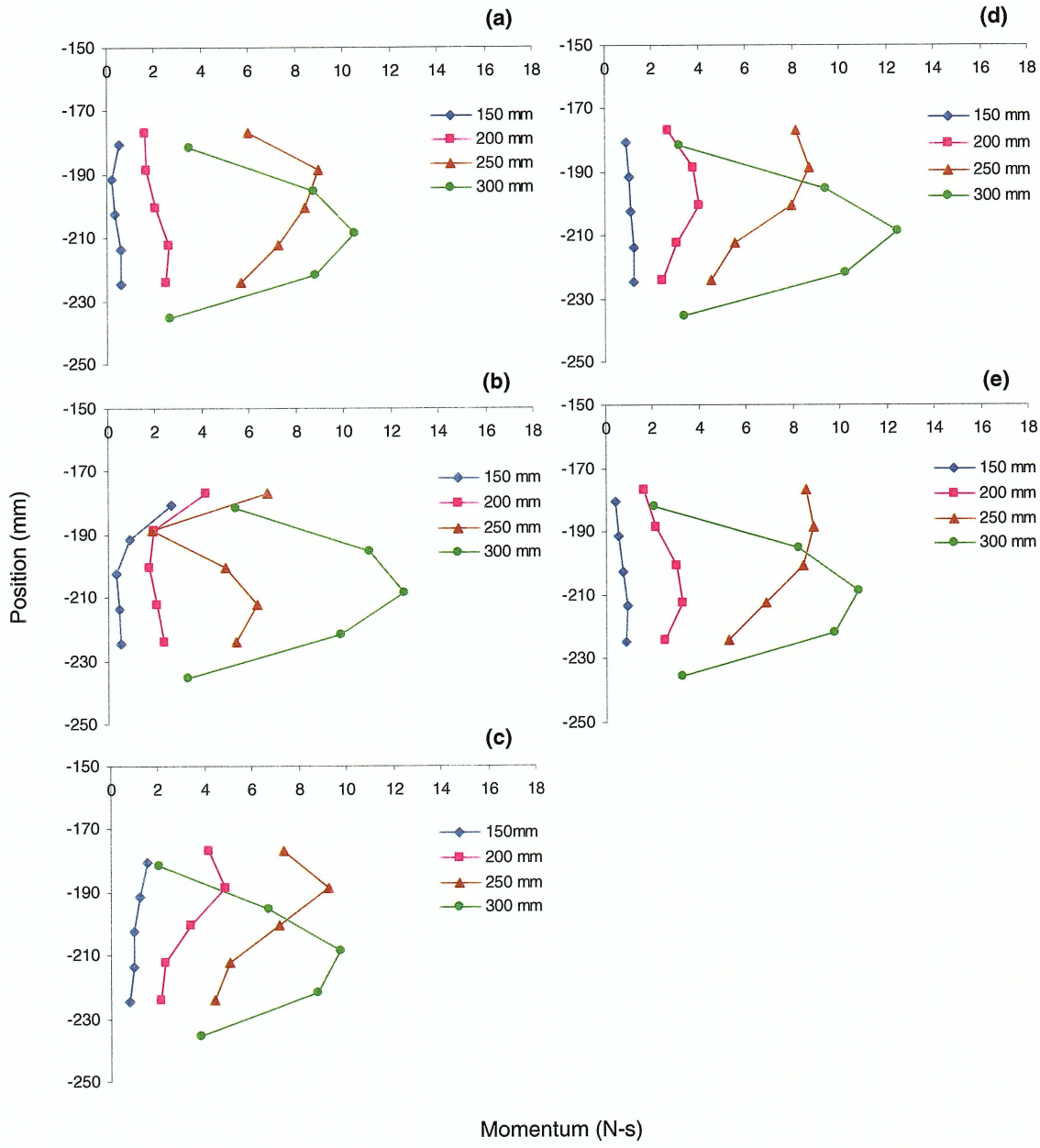

Figure 4.36 (a)-(e) Series momentum plots at a constant fan blade positions for 1800 rpm, 50% immersion, and 2.5 inch engine spacing; where (a) 28°, (b) 37°, (c) 3°, (d) 11°, and (e) 20°.

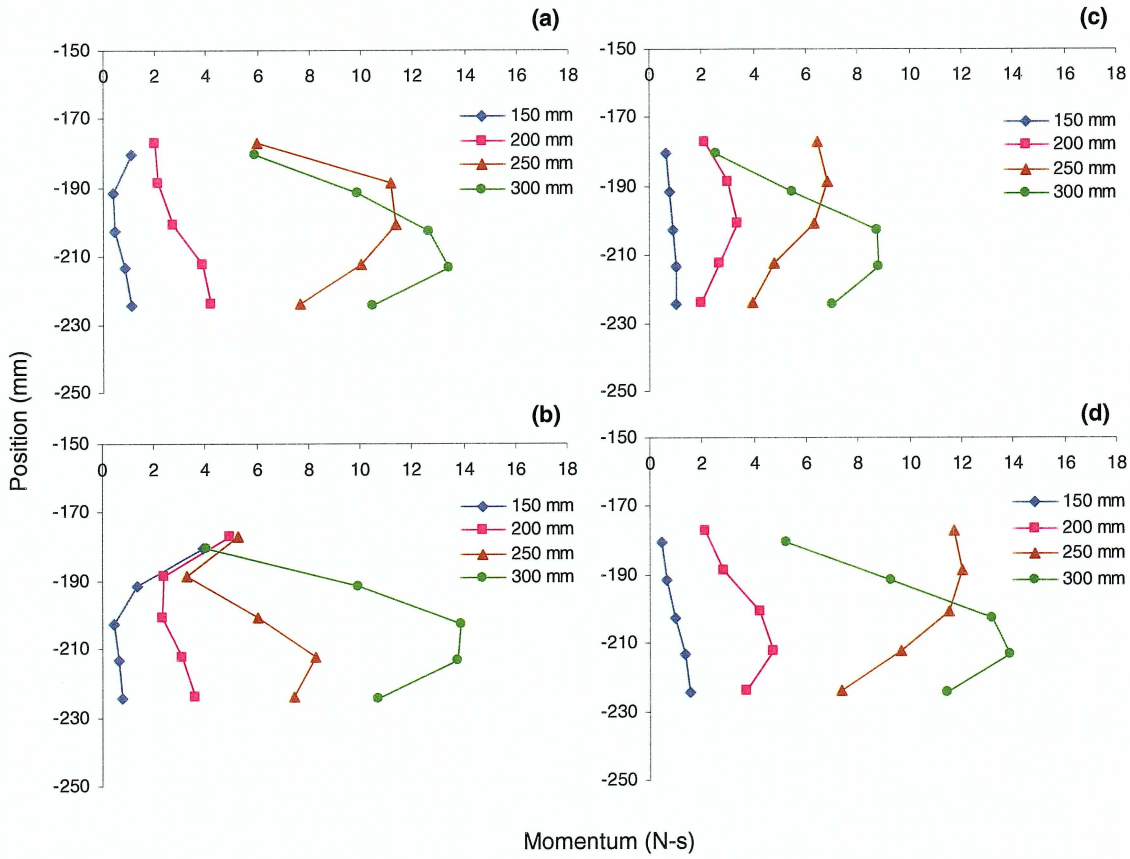

Figure 4.37 (a)-(d) Series momentum plots at a constant fan blade positions for 2200 rpm, 50% immersion, and 2.5 inch engine spacing; where (a) 31°, (b) 40°, (c) 14° and (e) 22°.

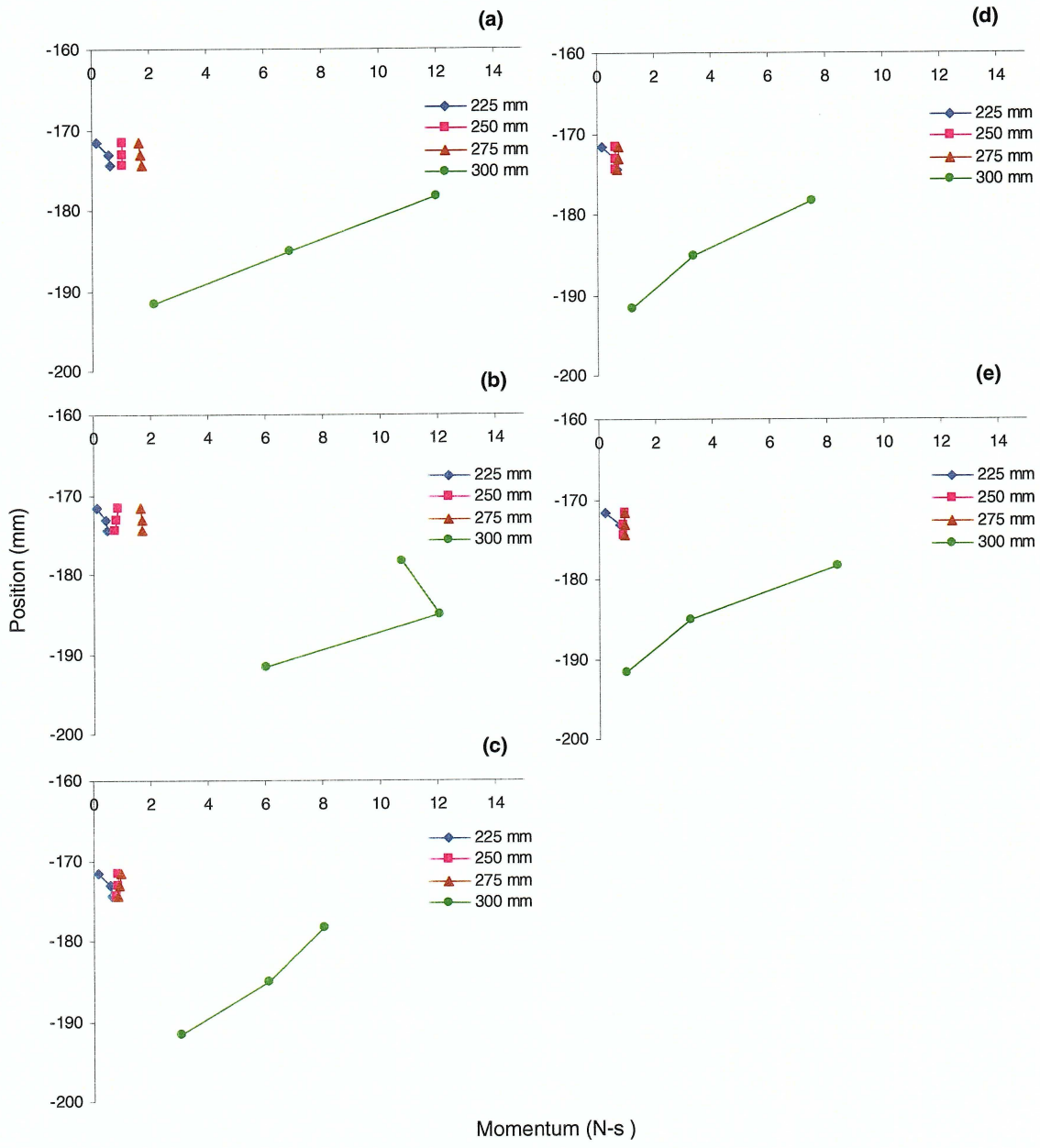

Figure 4.38 (a)-(e) Series momentum plots at a constant fan blade positions for 1800 rpm, 100% immersion, and 0.5 inch engine spacing; where (a) 28°, (b) 37°, (c) 3°, (d) 11°, and (e) 20°.

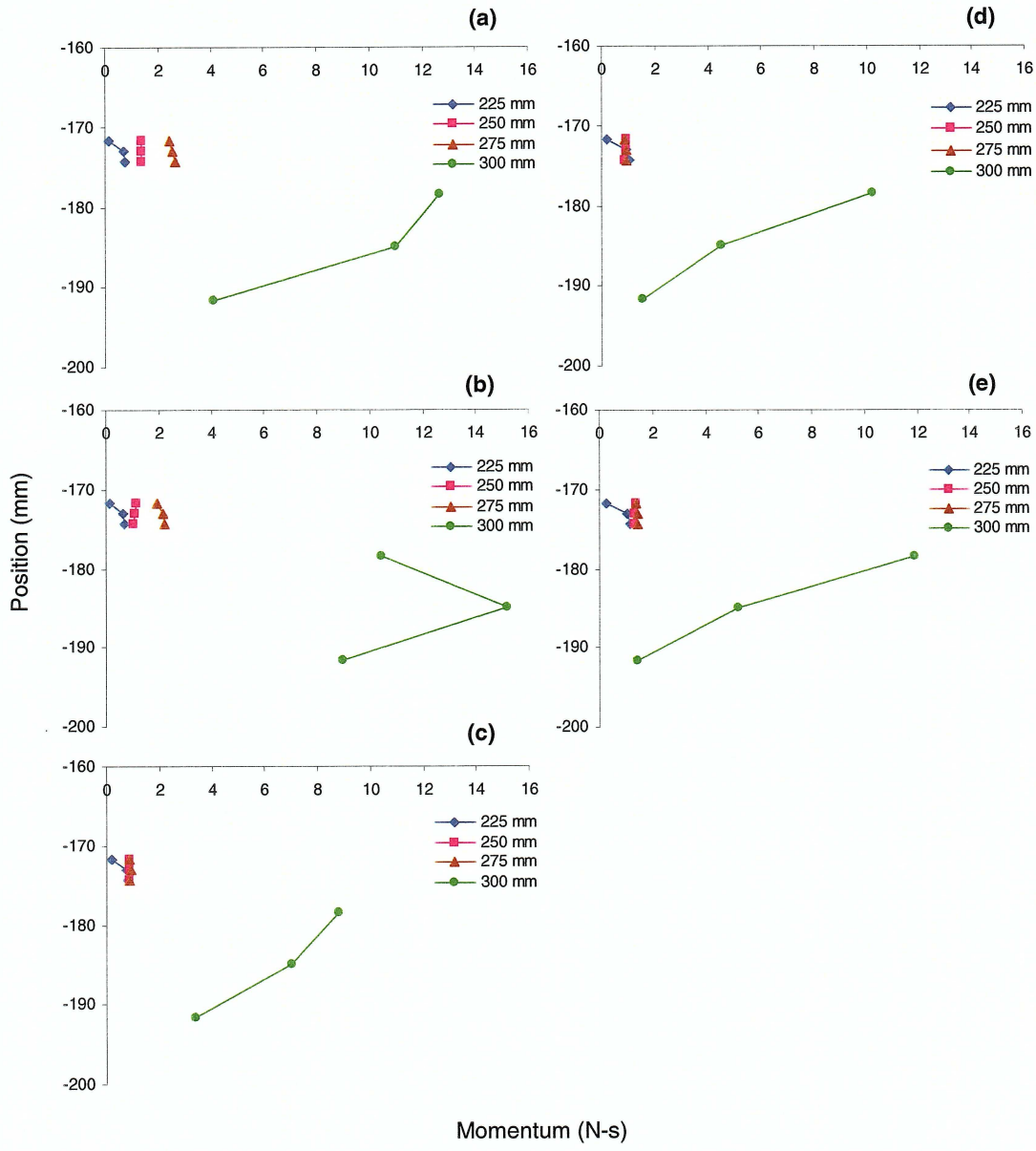

Figure 4.39 (a)-(e) Series momentum plots at a constant fan blade positions for 2200 rpm, 100% immersion, and 0.5 inch engine spacing; where (a) 31°, (b) 40°, (c) 5°, (d) 14°, and (e) 22°.

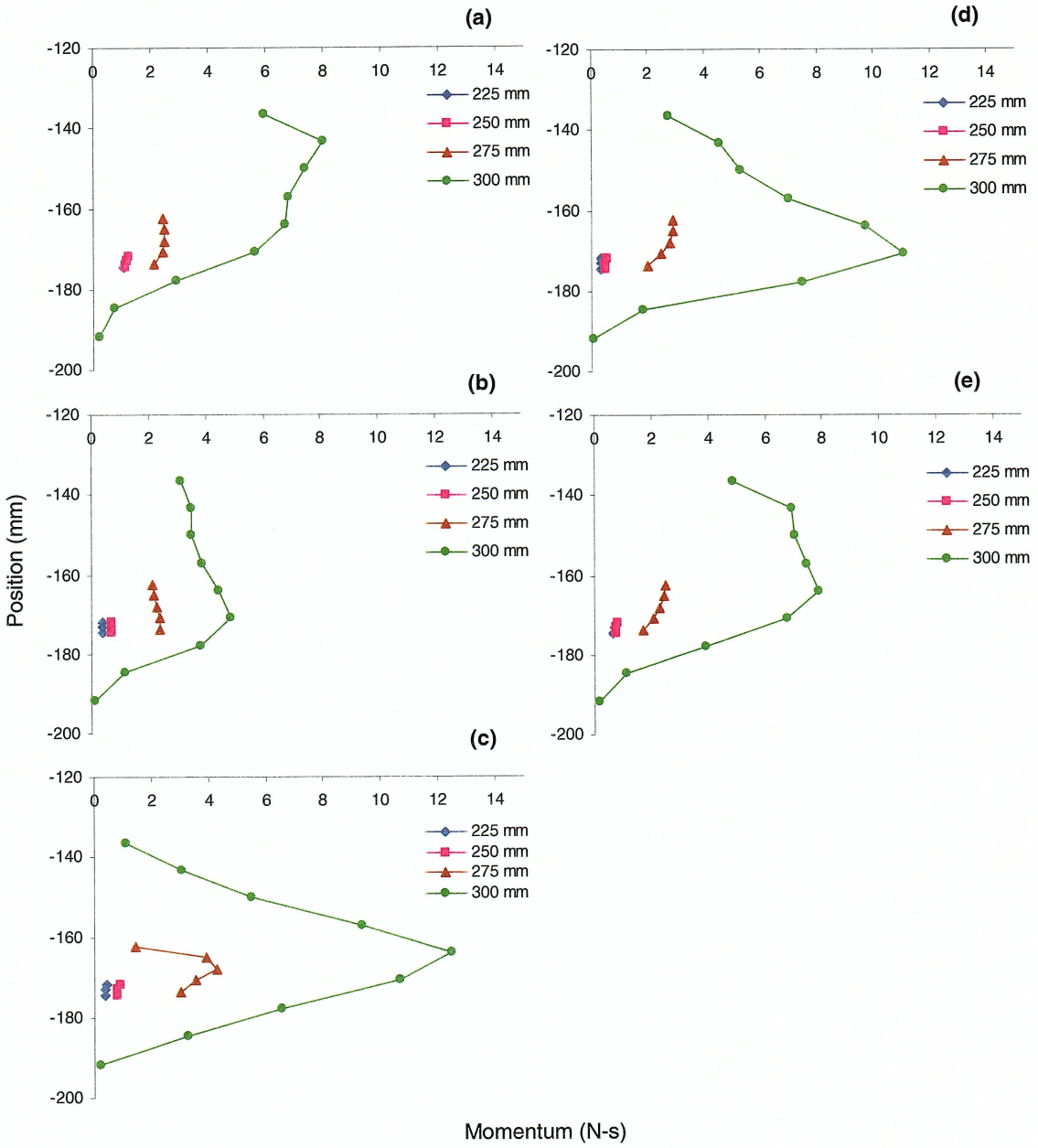

Figure 4.40 (a)-(e) Series momentum plots at a constant fan blade positions for 1800 rpm, 50% immersion, and 0.5 inch engine spacing; where (a) 37°, (b) 3°, (c) 11°, (d) 20°, and (e) 28°.

4.4.2 Constant distance

These sets of momentum profiles presented below depict the structure of the jet at a given distance as the fan is rotated. The angles given are the amount the fan has been rotated.

4.4.2.1 1800 rpm, 100% shroud and engine block 2.5" away from fan

Figure 4.41 (a)-(d) shows a gradual increase in momentum as the distance from the fan axle. The lines near the axle show a nearly uniform momentum which is under 2 N-s. As the profiles get further from the axle, the lines begin to develop more momentum in the middle of the jet and less momentum on the ends, as expected. One point of interest occurs on the 150 mm and 200 mm lines, with the fan blade rotated to 37° the point closest to the fan blade, the momentum was about twice the value of the other points at those positions. At the 300 mm line, the lowest overall momentum occurs at 20° and the highest at 28° and 37°, which have nearly identical profiles.

4.4.2.2 2200 rpm, 100% shroud and engine block 2.5" away from fan

Next the fan speed was increased while the geometry remained the same. This plot (Figure 4.42 (a)-(d)) is nearly identical to the previous plot, the difference being that the momentum values were about 33% higher then the 1800 rpm case. This shows that the momentum increases at a faster rate then the speed, since the difference in speed is only 22% higher.

4.4.2.3 1800 rpm, 50% shroud and engine block 2.5" away from fan

Figure 4.43 (a)-(d) shows a gradual increase in momentum as the distance from the fan axle. Again, the line near the axle shows a nearly uniform momentum which is under 2 N-s. As the profiles get further from the axle, the lines begin to develop more momentum in the middle of the jet and less momentum on the ends, as expected. However, on the 250 mm line, at 37°, the momentum in the middle of the jet is only 2 N-s instead of nearly 9 N-s like in the other fan positions.

4.4.2.4 2200 rpm, 50% shroud and engine block 2.5" away from fan

This setup is identical to the previous setup, but the fan speed has been increased. Figure 4.44 (a)-(d) is similar to the previous setup; however, there are some differences in the 250 mm and 300 mm lines. There is a bigger range between the momentum values between fan positions at these points. The low point of 2 N-s is still seen at 40° on the 250 mm line.

4.4.2.5 1800 rpm, 100% shroud and engine block 0.5" away from fan

In Figure 4.45 (a)-(d), the 225 mm, 250 mm and 275 mm lines, the momentum was below 2 N-s and the profiles were nearly straight. At 300 mm however, the profiles were very different from all the previous plots. Lower momentum was seen near the engine block and higher momentum was seen near the fan. Instead of the profiles being curved, they were all increasing as they got close to the fan. The only profile that was curved was the one at 37°.

4.4.2.6 2200 rpm, 100% shroud and engine block 0.5" away from fan

This plot (Figure 4.46 (a)-(d)) is nearly identical to the previous plot. Again, at the 225 mm, 250 mm and 275 mm lines, the momentum was below 2 N-s and the profiles were nearly straight. At 300 mm however, the profiles were very different from all the previous plots. Lower momentum was seen near the engine block and higher momentum was seen near the fan. Instead of the profiles being curved, they were all increasing as they got close to the fan. The only profile that was curved was the one at 40°.

4.4.2.7 1800 rpm, 50% shroud and engine block 0.5" away from fan

Finally, in Figure 4.47(a)-(d)) the 225 mm, 250 mm and 275 mm lines, the momentum was below 2 N-s and the profiles were nearly straight. At 300 mm however, the profiles were very different from all the previous plots. All the profiles showed curves as expected in a jet. The momentum intensities varied greatly by fan position. At 3° the maximum momentum was 5 N-s while at 11° it was 13 N-s. Also the peak momentum from each blade position was located in a different vertical position. This means that the jet is moving as the fan blade passes by.

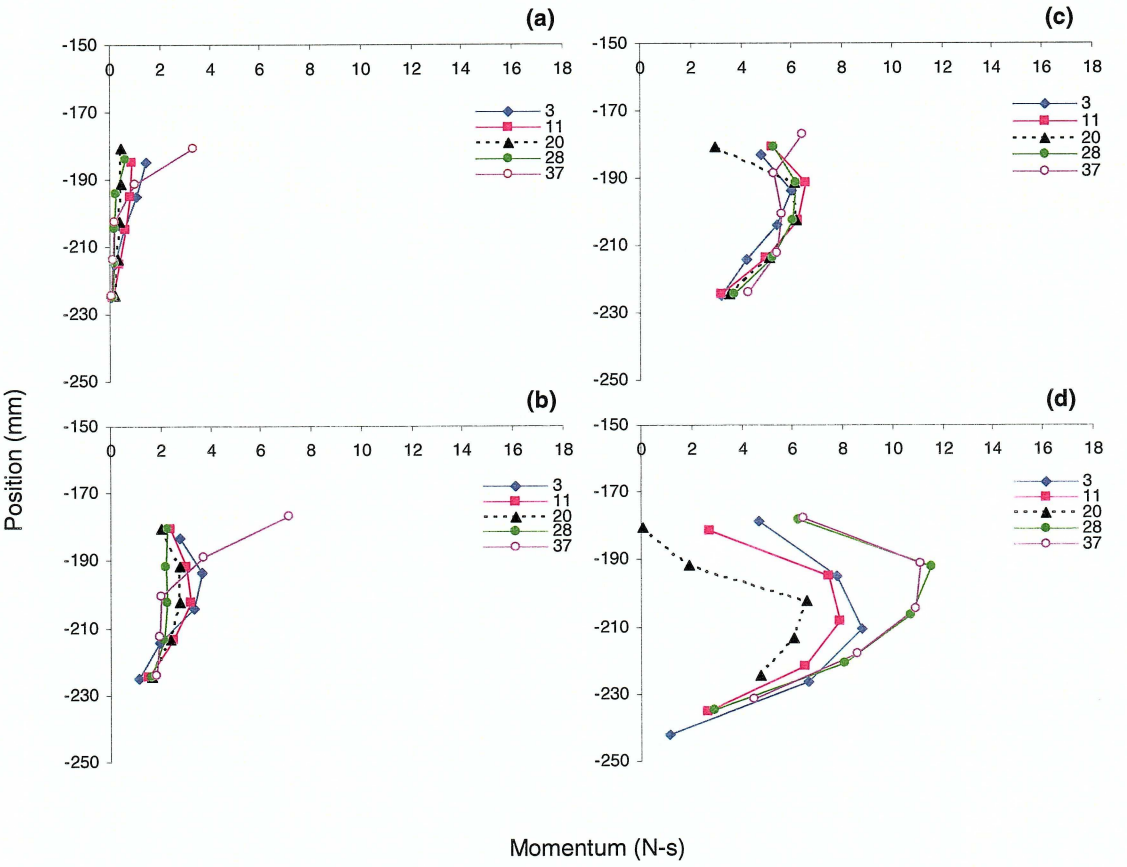

Figure 4.41(a)-(d) Series momentum plots at a constant distance from the fan axle for 1800 rpm, 100% immersion, and 2.5 inch engine spacing; where (a) 150 mm, (b) 200 mm, (c) 250 and (d) 300 mm.

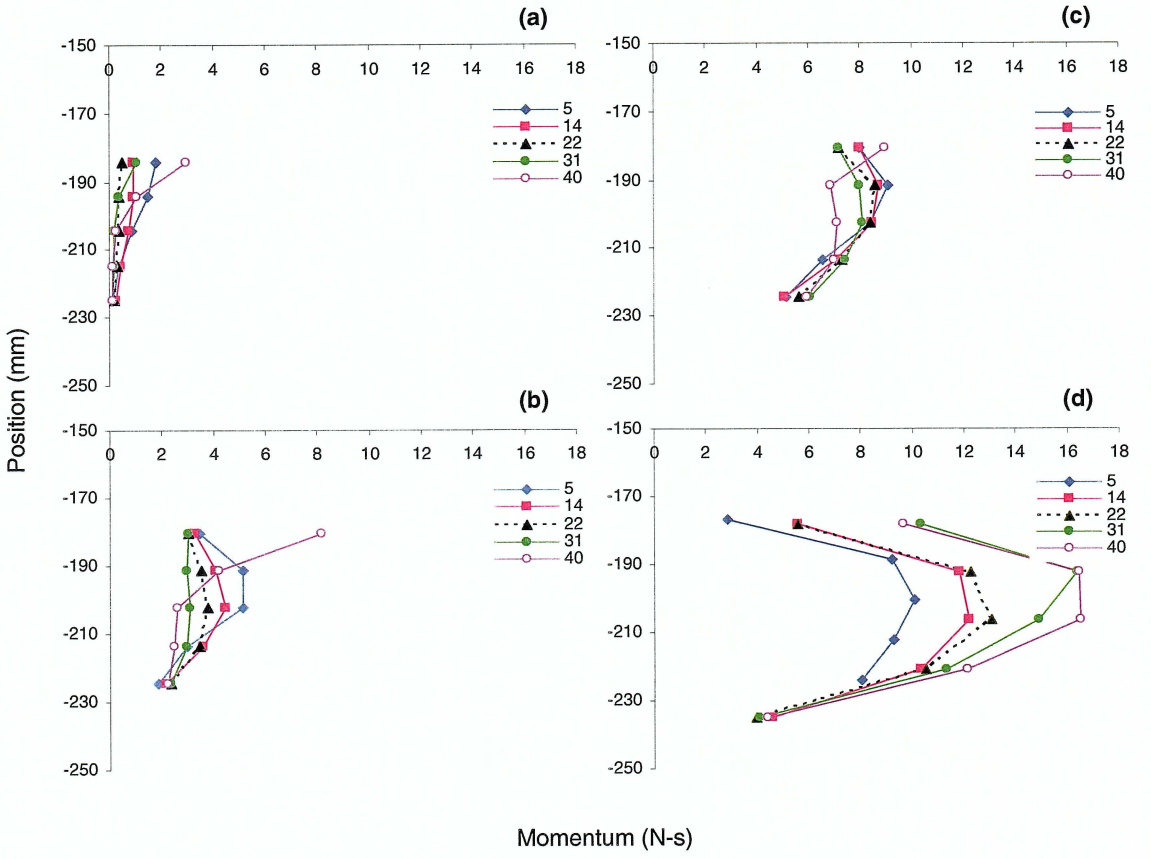

Figure 4.42 (a)-(d) Series momentum plots at a constant distance from the fan axle for 2200 rpm, 100% immersion, and 2.5 inch engine spacing; where (a) 150 mm, (b) 200 mm, (c) 250 and (d) 300 mm.

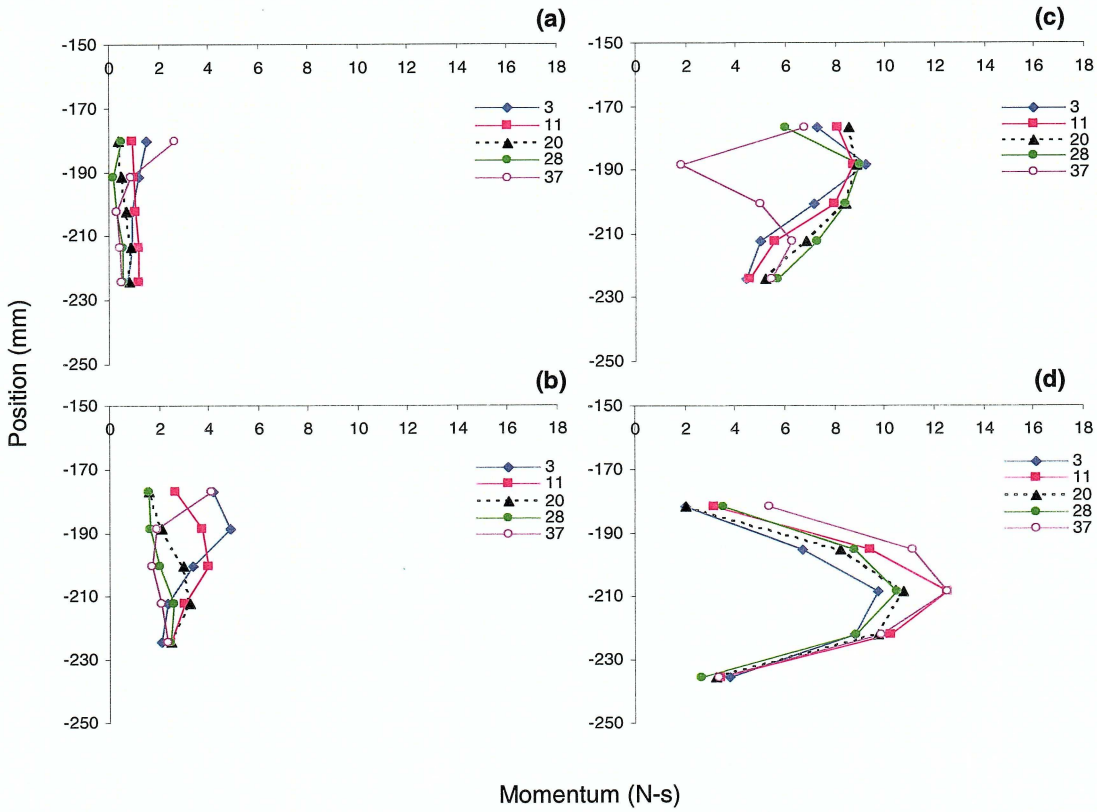

Figure 4.43 (a)-(d) Series momentum plots at a constant distance from the fan axle for 1800 rpm, 50% immersion, and 2.5 inch engine spacing; where (a) 150 mm, (b) 200 mm, (c) 250 and (d) 300 mm.

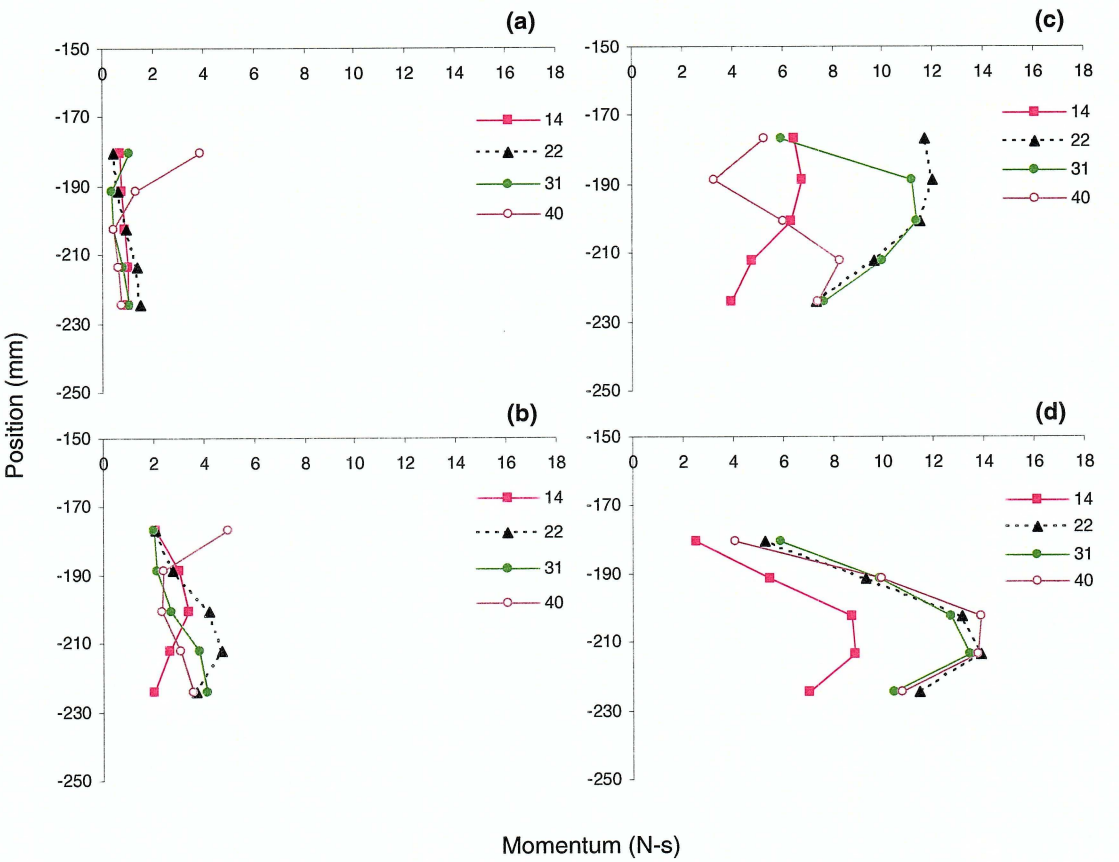

Figure 4.44 (a)-(d) Series momentum plots at a constant distance from the fan axle for 2200 rpm, 50% immersion, and 2.5 inch engine spacing; where (a) 150 mm, (b) 200 mm, (c) 250 and (d) 300 mm.

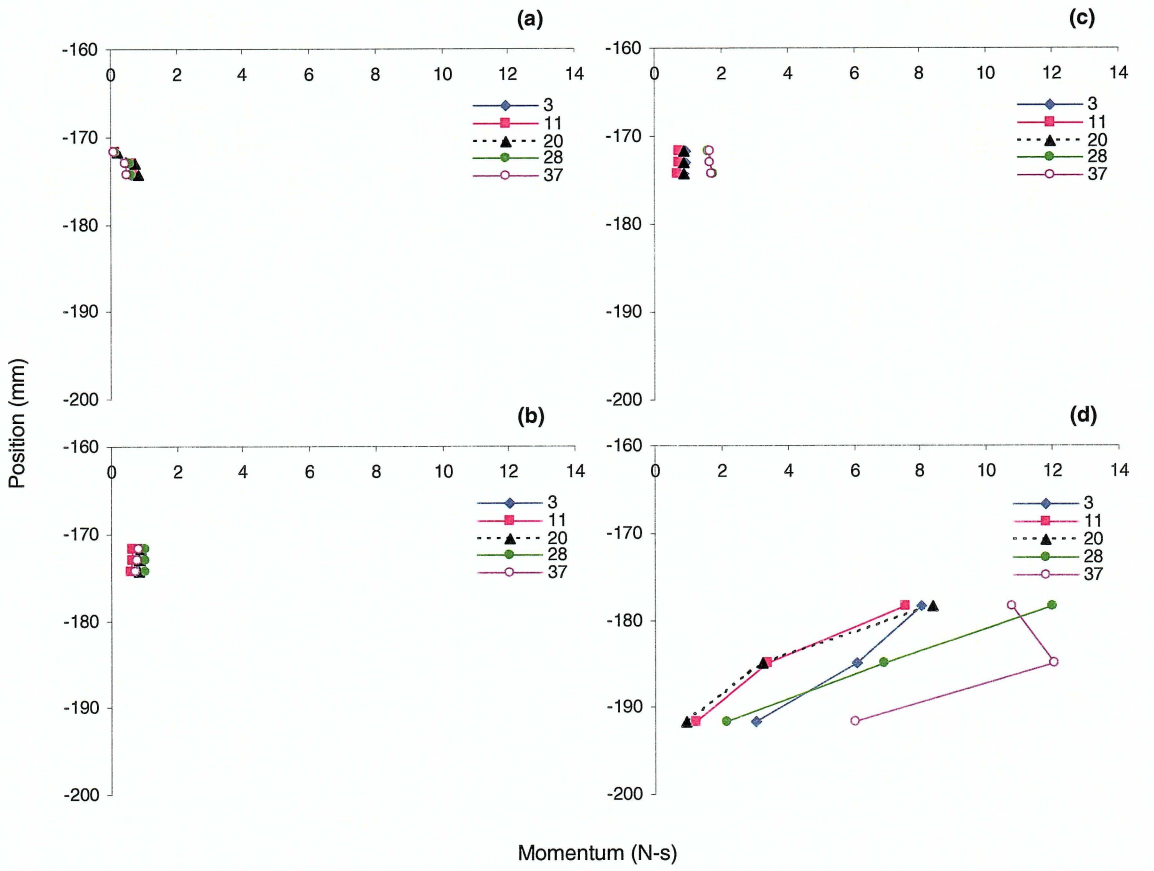

Figure 4.45 (a)-(d) Series momentum plots at a constant distance from the fan axle for 1800 rpm, 100% immersion, and 0.5 inch engine spacing; where (a) 225 mm, (b) 250 mm, (c) 275 and (d) 300 mm.

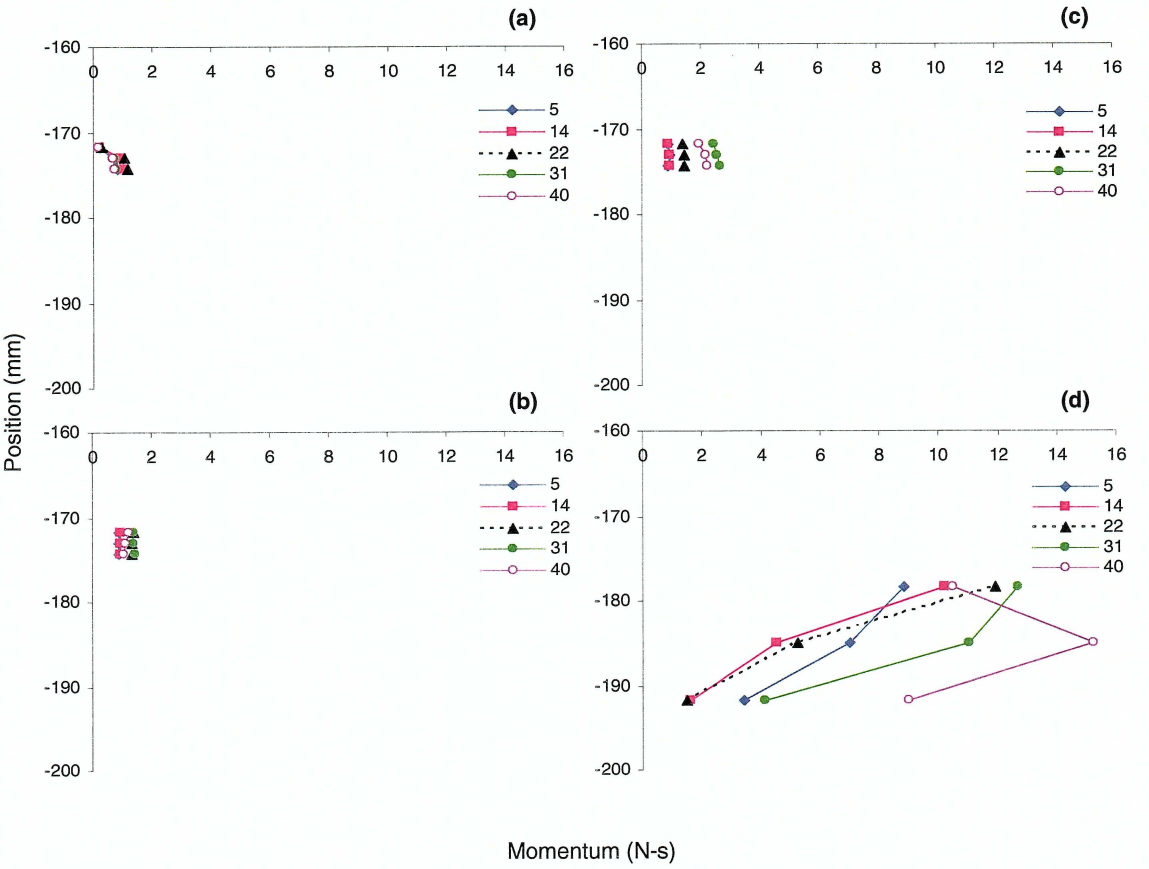

Figure 4.46 (a)-(d) Series momentum plots at a constant distance from the fan axle for 2200 rpm, 100% immersion, and 0.5 inch engine spacing; where (a) 225 mm, (b) 250 mm, (c) 275 and (d) 300 mm.

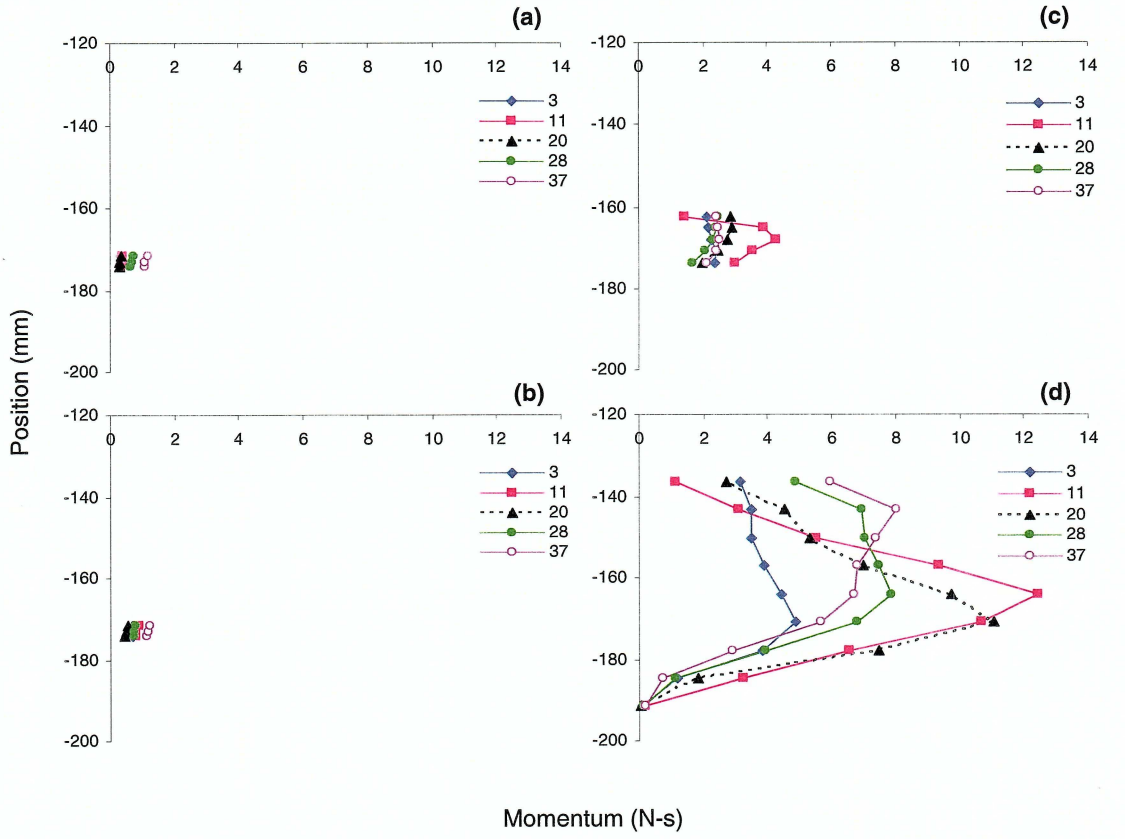

Figure 4.47 (a)-(d) Series momentum plots at a constant distance from the fan axle for 1800 rpm, 50% immersion, and 0.5 inch engine spacing; where (a) 225 mm, (b) 250 mm, (c) 275 and (d) 300 mm.

CHAPTER 5. CONCLUSIONS AND RECOMMENDATIONS

Modifications were done to the anechoic chamber to allow for PIV experiments. A shaft encoder was added to allow the collection of images at a specified point in the fan cycle. Data were collected in a plane just below the fan axle both upstream and downstream of the fan blade. Data were collected at 5 points as one fan blade moved through the plane.

The largest impact on the upstream flow field happened when the engine block was moved from 2.5" to 0.5" from the fan blade. This movement created a much larger vortex to form between the fan blade and radiator. This large vortex eliminated the smaller vortex near the fan blade tip.

A smaller change in the upstream flow occurred when the 100% shroud was replaced with the 50% shroud. This change caused the upstream vortex to move in the axial direction. It also caused the small vortex near the fan blade to increase in strength.

The downstream flow field showed the pulsing nature of the flow coming off the fan blade. The downstream jet was contained by the engine block on one side and the shroud on the other. As the fan blade passed, the jet's strength changed, based on the fan position and speed.

The turbulent kinetic energy profiles showed that near the middle of the fan there was little turbulence. Near the edge of the fan blade, the flow was highly turbulent. Decreasing the engine block distance increased the turbulent nature of the flow near the fan blade tip.

The momentum profiles showed low momentum near the middle of the fan. The momentum increased towards the fan blade tip. Past the fan blade tip, the momentum was low near the engine block and shroud, and higher between the two.

Further work could be done on different planes in the test section. This would give a more overall view of what is happening in the entire engine housing. Three dimensional PIV could also be used to find the out of plane component of the velocity, which in turn would further aid in the understanding of the flow.

Finally, the PIV data from this and future studies could be used to aid in the development of CFD models of an axial fan. This would be of great use since once developed, these CFD models would provide accurate flow predictions on different setups without the time consuming research on physical prototypes.

REFERENCES

1. Roth, D., Periyathamby, H.K., Gallivan, W., and To, C.W.S., "Modification and Evaluation of an Automotive Cooling Axial Flow Fan Noise Prediction Model," *Canadian Acoustics,* Vol. 24, pp. 3-9, 1996.

2. Howe, M.S., *Acoustics of Fluid-Structure Interactions,* Cambridge University Press, New York, pp.101-156, 1998.

3. Maaloum, A., Kouidri, S., Bakir, F. and Rey, R., "Effect of Inlet Duct Contour and Lack Thereof on the Noise Generated of an Axial Flow Fan," *Applied Acoustics,* Vol. 64, pp. 999-1010, 2003.

4. Maaloum, A., Kouidri, S., and Rey, R., "Aeroacoustic Performance Evaluation of Axial Flow Fans Based on the Unsteady Pressure Field on the Blade Surface," *Applied Acoustics,* Vol. 65, pp. 367-384, 2004.

5. Adrian, R.J., "Particle-Imaging Techniques for Experimental Fluid Mechanics," *Annu. Rev. Fluid Mech.,* Vol. 23, pp. 261-304, 1991.

6. Lawson, N. J., "The Application of Laser Measurement Techniques to Aerospace Flows," *Proc. Instn Mech. Engrs*, Vol. 218, pp. 33-57, 2004.

7. Kawaguchi, K., and Matsui, K., "Flow Visualization Around Axial Flow Fan Blades," *Bulletin of JSME,* Vol. 29, pp. 466-475, 1986.

8. Morris, S.C., Good, J.J., and Foss, J.F., "Velocity Measurements in the Wake of an Automotive Cooling Fan," *Exp. Thermal Fluid Sc.,* Vol. 17, pp. 100-106, 1998.

9. Zahn, H., Seyler, A., and Hinrichs, H., "Particle Image Velocimetry (PIV) as a Tool in Optimization of Fan Based Cooling Systems in Cars," *Proceedings of the International Society for Optical Engineering,* Vol. 3824, pp. 287-296, 1999.

10. Estevadeordal, J., Gogineni, S., Copenhaver, W., Bloch, G., and Brendel, M., "Flow Field in a Low-Speed Axial Fan: a DPIV Investigation," *Exp. Thermal Fluid Sc.,* Vol. 23, pp. 11-21, 2000.

11. Du, Z., Lin, W., Zhu, X., and Zhao, Y., "The Measurement of Three-Dimensional Flow Flied in an Axial Flow Fan Using PDA," *Proceedings of AME Joint U.S.-European Fluids Engineering Conference,* Québec, Montreal, pp. 1231-1237, 2002.

12. Lee, G.H., Baek, J.H. and Myung, H.J., "Structure of Tip Leakage Flow in a Forward-Swept Axial-Flow Fan," *Flow, Turbulence and Combustion,* Vol. 70, pp. 241-265, 2003.

13. Yoon, J.H., and Lee, S.J.," Stereoscopic PIV Measurements of Flow Behind an Isolated Low-Speed Axial-Fan," *Exp. Thermal Fluid Sc.,* Vol. , pp. 1-12, 2003.

14. Lee, S.J., Choi, J., and Yoon, J.H., "Phase-Averaged Velocity Field Measurements of Flow Around an Isolated Axial-Fan Model," *J. Fluids Eng.,* Vol. 125, pp. 1067-1072, 2003.

15. Yu, Chen, "An experimental study of the noise radiation from a construction vehicle cooling package," Iowa State University, 2004.

ACKNOWLEDGMENTS

I would like to thank my major professor, Dr. Michael Olsen for all his advice and support throughout my graduate and undergraduate career here at Iowa State. I would also like to thank Dr. Adin Mann and Dr. Olsen for their patience throughout the research and writing of this thesis.

I would also like to thank Dan Eiler, Feng Hua, and John Laage for their help throughout the experimental process.

Additionally I would like to thank the John Deere Corporation for the funding and equipment for this project.

I would also like to thank my family for believing in me, even when it looked like this thesis would never be finished.

Lastly I would like to thank Nela, who has poured countless hours into making sure I finished this thesis. Without the help of these people, this thesis would not have been possible.